KARADENİZ TECHNICAL UNIVERSITY
THE GRADUATE SCHOOL OF NATURAL AND APPLIED SCIENCE

ELECTRICAL-ELECTRONICS ENGINEERING GRADUATE PROGRAM

DESIGN AND IMPLEMENTATION OF SINGLE- INPUT MULTIPLE-OUTPUT (SIMO) DC-DC BUCK CONVERTER FOR SOLAR ENERGY APPLICATION

MASTER THESIS

Electrical-Electronics Eng. Ilyass Abdillahi ADEN

JUNE 2018
TRABZON

KARADENİZ TECHNICAL UNIVRSITY
THE GRADUATE SCHOOL OF NATURAL AND APPLIED SCIENCE

ELECTRICAL-ELECTRONICS ENGINEERING GRADUATE PROGRAM

DESIGN AND IMPLEMENTATION OF SINGLE INPUT MULTIPLE OUTPUT (SIMO) DC-DC BUCK CONVERTER FOR SOLAR ENERGY APPLICATION

Electrical-Electronics Eng. Ilyass Abdillahi ADEN

This Thesis is Accepted to Give The Degree of
"MASTER OF SCIENCE IN ELECTRICAL-ELECTRONICS ENGINEERING"
By
The Graduate School of Natural and Applied Science
at KARADENIZ Technical University

The date of Submission: 22.05.2018
The date of Examination: 07.06.2018

Thesis Supervisor: Asst. Prof. Dr. Hakan KAHVECI

Co-supervisor: Asst. Prof. Dr. Mustafa Ergin ŞAHIN

Trabzon 2018

KARADENİZ TECHNICAL UNIVERSITY

THE GRADUATE SCHOOL OF NATURAL AND APPLIED SCIENCES

DEPARTMENT OF ELECTRICAL-ELECTRONICS ENGINEERING

Ilyas Abdillahi ADEN

DESIGN AND IMPLEMENTATION OF NON-ISOLATED SINGLE INPUT MULTIPLE OUTPUT DC-DC BUCK CONVERTER FOR SOLAR ENERGY APPLICATION

Has been accepted as a thesis of

MASTER OF SCIENCE

after the Examination by the Jury Assigned by the Administrative Board of the Graduate School of Natural and Applied Sciences with the Decision Number 1754 dated 22 /05 / 2018

Approved By

Chairman	: **Prof. Dr. Hasan KÜRÜM**	....
Member	: **Assoc. Prof. Dr. Halil İbrahim OKUMUŞ**	....
Member	: **Assist. Prof. Dr. Hakan KAHVECİ**	....

Prof. Dr. Sadettin KORKMAZ

Director of Graduate School

FOREWORD

This thesis is written as completion to the master of Electrical-Electronics Engineering, at Karadeniz Technical University. I would like to thank all those who, directly or indirectly, have contributed to realization of this study. Firstly my gratitude to my supervisor, Assist.Prof.Dr Hakan KAHVECI and Assist.Prof.Dr. Mustafa Ergin ŞAHIN for their judicious advice and for giving me the opportunity to conduct this research. Their availability and encouragements enabled me to work in an enjoyable and dynamic atmosphere. It was a pleasure working with them and their advice and comments were of tremendous help in my daily work. Lastly, I would like to express my thankfulness to my dear mother, who have brought me to the present. She has always encouraged and inspired me all my life.

Ilyass Abdillahi ADEN

Trabzon 2018

THESIS STATEMENT

I declare that, this Master Thesis, I have submitted with the tittle “Design and Implementation of Non-Isolated Single Input Multiple Output (SIMO) DC-DC Buck Converter for Solar Energy Application” has been completed under the guidance of my Master supervisors, Assist.Prof.Dr Hakan Kahveci and Assist.Prof.Dr. Mustafa Ergin ŞAHIN. All the data used in this thesis are obtained by simulation and experimental works done as part of this work in our research labs. All referred information used in thesis has been indicated in the text and cited in reference list. I have obeyed all research and ethical rules during my research during my research and i accept all responsibility if proven otherwise. 07/06/2018.

Ilyass ABDILLAHI ADEN

TABLE OF CONTENTS

Page No

Master Thesis

SUMMARY

DESIGN AND IMPLEMENTATION OF SINGLE INPUT MULTIPLE OUTPUT (SIMO) DC-DC BUCK CONVERTER FOR SOLAR ENERGY APPLICATION

Ilyass ABDILLAHI ADEN

Karadeniz Technical University
The Graduate School of Natural and Applied Sciences
Electrical-Electronics Engineering Graduate Program
Supervisor: Asst. Prof. Dr. Hakan KAHVECI
Asst. Prof. Dr. Mustafa Ergin ŞAHIN
2018, 77 Pages, 14 APPENDIX

Development of renewable energy sources seem inevitable to face the energy challenge of today and tomorrow. However, the power generation using promising renewable energy sources such as solar or wind power is intermittent and unpredictable due to the weather conditions. In order to provide the energy coming from these sources to the different components of the electric installation a power converters connect components to the grid. In the case of the transformerless conversion system introduce here, a high efficiency DC -DC converter is required. In this study, we have presented a non-isolated DC-DC buck converter with one input voltage coming from the photovoltaic source. This input will provide dual output voltages. An exhaustive control strategies and small signal modeling for the proposed converter will be presented. The simulation of the system is performed using Matlab Simulink and the experimental results are presented.

Keywords: SIMO DC-DC converters, Buck converters, Solar volatge, PID controller, Small signal analyses.

Yüksek Lisans Tezi

ÖZET

GÜNEŞ ENERJİ UYGULAMASI İÇİN TEK GİRİŞ ÇOKLU ÇIKIŞ (SIMO) DA-DA BUCK CONVERTERÜN TASARIMI VE UYGULANMASI

Ilyass ABDILLAHI ADEN

Karadeniz Teknik Üniversitesi
Fen Bilimleri Enstitüsü
Elektrik-Elektronik Mühendisliği Anabilim Dalı
Danışman: Yrd. Doç. Dr. Hakan Kahveci, Yrd. Doç. Dr. Mustafa Ergin Şahin,
2017, 77 Sayfa, 14 Ekler

Yenilenebilir enerjinin geliştirilmesi, bugünün ve yarının enerji sorunuyla yüzleşmek için kaçınılmaz görünüyor. Bununla birlikte, güneş enerjisi veya rüzgar enerjisi gibi umut verici yenilenebilir enerji kaynaklarından enerji üretim durumu hava koşullarına bağlı olması nedeniyle öngörülememektedir. Bu kaynaklardan üretilen enerjinin şebekeye aktarılabilmesi için elektrik enerjisi dönüştürücü devrelere ihtiyaç vardır. Transformatörsüz dönüştürme sisteminin dahil edilmesi durumunda yüksek verimli bir DA-DA dönüştürücü gereklidir. Bu çalışmada, fotovoltaik kaynaktan beslenen, izole edilmemiş tek girişli-çok çıkışlı bir DA-DA azaltan dönüştürücü tasarlanmış ve gerçeklenmiştir. Önerilen dönüştürücü için denetim stratejileri geliştirilerek küçük işaret modellemesi yapılmıştır. Sistemin benzetimi Matlab/Simulink kullanılarak gerçekleştirilmiş ve deneysel sonuçlarla karşılaştırılmıştır.

Anahtar Kelimeler: Tek girişli çok çıkışlı (SIMO), Azaltan dönüştürücüler, Fotovoltaik enerji, Güneş enerjisi, PI denetleyicisi, Küçük işaret analizi.

LIST OF FIGURES

Page No

LIST OF TABLES

Page No

LIST OF ABBREVIATIONS

MPPT	Maximum Power Point Tracker
AC	Alternating Current
DC	Direct Current
PO	Perturb and Observe
V	Voltage
PV	Photovoltaic
P-V	Power versus Voltage
PWM	Pulse Width Modulation
dI	Derivative of current
I_0	Saturation current
VC	Cell voltage
SIMO	Single Input Multiple Output
kWh	kilo Watt-hours
DC	Direct Current
Voc	Open circuit voltage
Pmax	Maximum power
Vmpp	Voltage at maximum power point
Imp	Current at maximum power point
I_{PV}	Cell current
V_{PV}	Cell voltage
I_R	Load current
V_R	Load voltage
R	Resistance
D	Duty cycle

PPV	Cell power
dPPV	Derivative of cell power
ESR	Equivalent Series Resistance
Δt	Variation of time
e(t)	Error

1. GENERAL INFORMATION

1.1. Introduction

Electricity is taking more important role in the embedded systems such as cell phones, computers and electronics systems and it is a very adaptable form of energy. It is easy to transport and adjustable with a very low losses. The electrical energy, associated with power converters is easier to control than pneumatic or hydraulic energies, for example providing a finer regulation and a low cost of maintenance [1].

Increasing demand for energy in the world and the diminishing of fossil energy sources promotes exploitation of other energy sources such as fuel cells, solar energy and other clean energy sources. These energies are usually environmentally friendly [2].

The solar power is almost inexhaustible, cleanest, plentiful than the others renewable energies. It is application area has a spacious range such electric vehicles. There are factors that can affect the performance of solar, these are the conditions like insolation, sunlight tilt, load variations, air mass and cell temperature. MPPT algorithms such as incremental conductance and perturb & observe have been evaluated until now and power converter units should be associated with the PV cells for regulating the transfer of power from cells [3-4].

To share the solar power to the different systems it needs converters capable of providing each systems the suitable power supply. DC-to-DC converters is used in this study. The main utilization of this converters are uninterruptible power supplies, battery devices, clean energy systems and hybrid electric vehicle. [5-10].

In this thesis, the design and implementation of the Single Input Multiple Output DC-DC buck converter is presented. By using the energy of the solar battery, this converter is capable to provide different output voltages. The organization of the thesis is as follows.

The first chapter gives introduction, a literature review, general overview of solar generation, mathematical modeling of solar cells, solar maximum power point tracker, DC-DC converters such as buck converter, boost converter and buck boost converter.

The second chapter gives state space averaging of basic buck converter, different mode of operation of the SIMO converter, steady state analysis, state-space averaging of the presented SIMO converter, Buck Converter Selection of the Parameters, design of inductor, design of snubber circuits and control strategies are explained. SIMO DC-DC buck converter and solar modeling are performed in Matlab/Simulink.

In the third chapter, first an explanation of the main components namely the MOSFET and their drives, logic circuits, snubber circuits, microcontroller and optocoupler are presented. Afterwards, the simulation and experimental results of the SIMO DC-to-DC converter implemented in a solar system are presented.

1.2. Literature Review

The growing demands of energies in the world and the decreasing quantity in fossil energies comes new energy as solar energy, wind energies, and other green energy. These energies are polite with environments and provide a power selection [2].

These green energies have been broadly uses in varied applications, like machines, electric vehicles and hybrid, etc. [11]. The PWM technique based on a DC-to-DC converters become key elements in many industrial areas such as military, communication, computers, automobile industry and also satellites. The adjustment of an independent multiple input or output voltages are required in many electronic devices, like microprocessors, Personal Digital Assistants (PDAs) and digital components etc. [12].

Sometimes in the same system it is required to generate multiple supply voltages. This feeding process can result some problems such as an augmented number of components, the increased Printed Circuit Board (PCB) area and the decreased dependability for the many input used. To overcome this problems DC-to-DC converters is used. these are capable to provide multiple outputs voltage using single input and the opposite[12], [13].

Chiu, et al. [14] have presented a bidirectional DC to DC converters. These converters have transformer in their structures. To overcome the corresponding switching losses, soft switching techniques are used. However, the number of power switches are more than four. Therefore, these structures with isolated transformers results a high conduction losses. Besides, practical implementation of the circuit is complicated and very expensive.

Lee and Chiu [15] have proposed DC-DC converter that can ensure a bidirectional power flow controlling. Unfortunately, this converter have the disadvantages such us current stress and a high switching losses.

Jiang et al. [16] have presented a novel topology for non-isolated bidirectional DC-to-DC converter. This converter has zero voltage-switching capability. To attain the property of soft switching, two extra inductors are required and these inductors should have a good matching characteristic. Additionally a low conversion ratio is obtained.

Ahmadi et al. [18] have presented a non-isolated zero current transition bidirectional converters. This converter has one additional switch. However, to provide soft commutation both in the operation mode of the converter and the values of resonant capacitor three power switches are required. In addition to this, it has a low conversion ratio and the inductor should be precisely designed to make sure that all switches are operating with the property of soft switching.

Hsieh et al.[17] have studied a high-conversion-ratio bidirectional DC-to-DC converter with a coupled inductor. Although this converter add up with two additional switches and capacitors on the secondary side to achieve a high-voltage ratio. In this topologie, five switches are required. The price is unavoidably increase and it is control scheme is complicated.

Patra et al. [19] have presented a multiple-output DC-to-DC converter efficient of providing, boost, buck and inverted outputs at the same time. However, for one output three switches are required. These designs correspond only for low power applications and outputs voltages.

Cho et al. [20] have proposed a high-efficiency and low-cost regulated dual-output LLC resonant converter. However, from this topology two different output voltages is generated. Pulse-Frequency Modulation(PFM) and Pulse widh Modulation (PWM) Controllers could accurately designed to gratify the required output voltage.

Kim et al. [21] have proposed a Zero Voltage Switching (ZVS) post regulation scheme for a multi-output converter. It has synchronous switches under full load conditions. However, for one output two power switches were required. Beside this, because of its complication in the control scheme, the cost of producing is increases.

Nami et al [22] have proposed a multi-output DC–DC boost converter. This shares-out its output voltage for high and low power applications. Two switches were required for one output. Independently this converter can't provide energy for the individual loads and its control scheme was complicated.

Occasionally, in the usual buck converter, an active power switch replace the freewheeling diode [23–27]. Eguchi and Abe[28] have studies on Single Input Dual Output (SIDO) DC-to-DC converters. However, due to it is complicated structure of the converters with more storage components and relatively larger size of the magnetic components, the proposed structures are not suitable in high gain, high-efficiency applications.

Bharath Kumar and Omar[29] have presented SIMO synchronous DC-DC buck converter. This converter has the advantage of a reducing the number of the switches, over three output voltage four switches are required. Unfortunately, this SIMO converter has the disadvantage of requiring a higher current rating for the four switches .

Kwon and Mora [30] have proposed another SIMO DC-DC converters. This converter is capable of providing inverted and boost outputs. Although, in this new configuration, except the negative output, the loads are designed separately.

Dos Santos Jr [31] have presented dual-output DC-DC buck converters with unidirectional and bidirectional property. However, this converter required power switches with high current ratings.

1.3. Purpose of Study

The main purpose of this thesis is to show the design and control of a single-input (48V) dual-output (12V-5V) DC-DC converter feded from the solar energy system. A proportional-integral (PI) controller is used as the control algorithm. In addition, SIMO converter is used for various loads in electric vehicules. Various operation of the SIMO converter are carried out simulation and experimentally and the results are presented. DC distribution system with SIMO converter is shown in Figure 1.

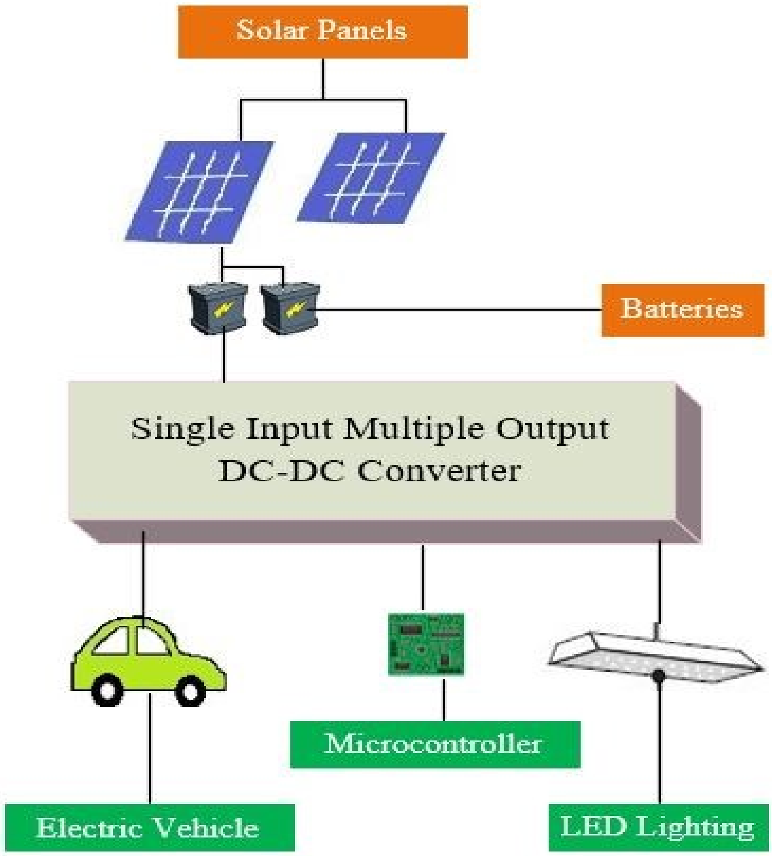

Figure 1. DC distribution system with SIMO converter

1.4. Solar Energy Generation

Solar energy is the electromagnetic energy transmitted by the sun that generated by nuclear fusion. It is responsible for all forms of terrestrial life and represents about 420 kWh. Solar energy is hundred thousand times greater than all the cumulative energies used by the whole world.

Humans have been used the luminous radiation and heat of the sun since antiquity, which resulted in a series of technologies that have continued to develop. Solar radiation, as well as secondary solar energy resources such as biomass, wind tidal power and hydroelectric power account for most of the green energy available on Earth. Nowadays small fraction of the available solar energy is used. The production of solar-powered electricity is based on the photovoltaic effect and on thermal engines. The uses of solar energy have limits only those of human engineering. A few of its applications are: heating and cooling of premises through a solar architecture, the creation of drinking water via distillation, disinfection, the domestication of daylight, solar cooking and solar hot water [32]. Solar panels are used to collect solar energy.

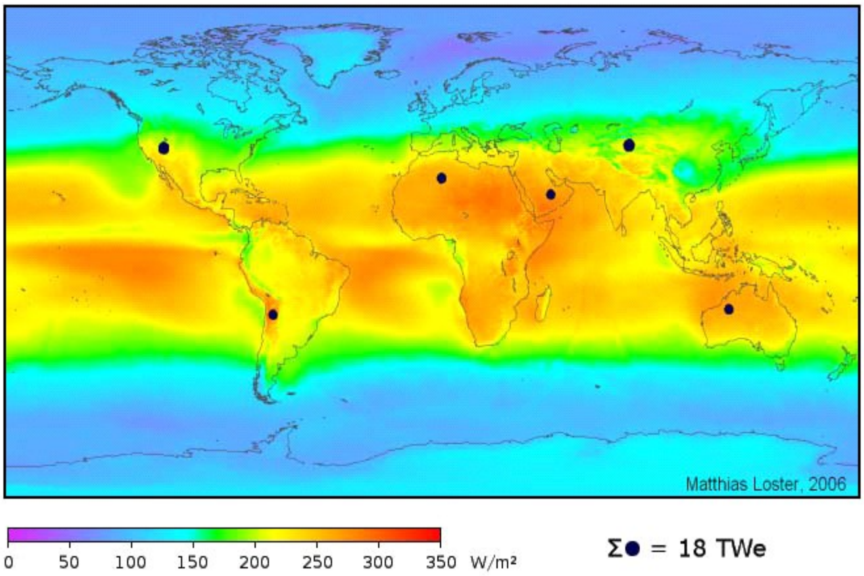

Figure 2. The solar irradiance maps of the world

The colors indicate the solar radiation on average taking into account the nights and the cloud cover over three years. The black spots in the figure above shows that the solar radiation in these regions could supply the world with energy. Even if solar cells with a conversion efficiency of only 8% is installed in these areas marked by the six points on the world map, this solar station would produce an average 18TW of electrical energy[33]. It is more than the total energy currently used including oil, coal, hydraulic, gas and nuclear in the world. [34].

1.4.1. Application of Solar Energy

Edmond Becquerel is the first French Physicist that observed the photoelectric effect, in 1839. He discovered that some materials could provide small amounts of electric current when they are exposed in to light[34].

In the beginning of twentieth century, Albert Einstein obtained a Nobel Prize in Physics by describing the photoelectric effect and the nature of light on which PV technologies are built. In 1954, Bell laboratories construct the first PV module. This was not presented as a solar cell, but a battery because they thought that it was so expensive for it use. In the 1960s the need of electricity on board spacecraft and the insufficiency of the batteries in space push to the space industry to thought of the solar technologies [34].

Thanks to space programs, the solar technologies is progressed and started to decrease in terms of costs. During the energy crisis of the seventies, the PV technologies start to become not only a source of energies in space, but also a source of electricity in earthly.

1.4.2. Mathematical Modeling of Solar Cells

The configuration of a solar system is presented as a combination of numbers of PV cells. This PV cells form a PV modules as shown in igure 3. Cells connects in series or in parallels are used to increase output voltage and current respectively. Many connected PV cells form a photovoltaic array [35].

The equation below describes the I-V characteristic of the ideal PV array cell[36].

$$I = I_{Pv,cell} - I_{O,cell}\left[exp\left(\frac{qV}{\alpha kT}\right) - 1\right] \qquad (1)$$

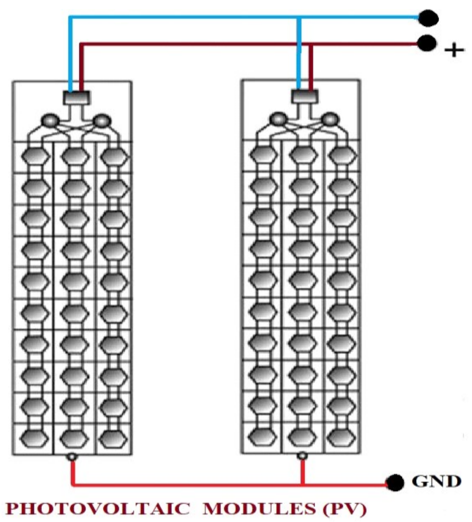

Figure 3. Photovoltaic array

The photovoltaic system requires the implication of additional parameters to the equation above:

$$I = I_{pv} - I_O\left[exp\left(\frac{V+R_SI}{V_t\alpha}\right) - 1\right] - \frac{V+R_SI}{R_p} \tag{2}$$

Where;

R_S = number of series resistance;

R_P= number of parallels resistances

I_O = saturation current

I_D = represents the voltage-dependent current lost to recombination,

$$I_D = I_O\left[exp\left(\frac{V+R_SI}{V_t\alpha}\right) - 1\right] \tag{3}$$

I_{sh} is the current lost caused by the shunt resistances as shown in equation 4.

$$I_{sh} = \frac{V+R_SI}{R_{sh}} \tag{4}$$

The value of the saturation current is calculated using this equation:

$$I_0 = \frac{I_{SC,n}+K_I\Delta_T}{\exp\left(\frac{V_{OC,n}+K_V\Delta_T}{\alpha V_t}\right)-1} \tag{5}$$

From the datasheet of all PV array the values of the nominal short-circuit current ($I_{SC,n}$), nominal short-circuit voltage ($V_{OC,n}$), the current at the MPP (I_{mp}), the voltage at the MPP (Vmp), the short-circuit current/temperature coefficient (K_I) and the short-circuit voltage /temperature coefficient (K_v) are written. The value of I_O is highly dependent on the temperature and has a linear variation effect of the (K_v).

The value I_{PV} found using this equation:

$$I_{pv} = \left(I_{pv,n} + K_I(T_O - T_{ref}\right) * \frac{G}{G_n} \tag{6}$$

Where;

G_n= Nominal irradiance

$I_{pv,n}$ = Nominal light-generated current

T_O=Operating temperature

G = Normal irradiance

T_{ref} =Cell's reference temperature.

The nominal light-generated current is:

$$I_{pv,n} = \frac{R_P+R_S}{R_P} * I_{SC,n} \tag{7}$$

The value R_P is calculated using the equation below and in the beginning it maybe zero.

$$R_{P,min} = \frac{V_{mp}}{I_{SC,n}-I_{mp}} - \frac{V_{OC,n}-V_{mp}}{I_{mp}} \tag{8}$$

Where $R_{P,min}$ is the minimum value of the R_P.

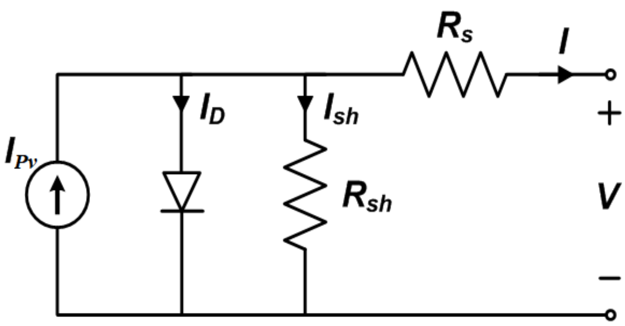

Figure 4. Basic circuit for a single solar cell

1.5. Solar Maximum Powerpoint Tracker

The conversion of sun energy to electric is optimized when the PV device is operating at the MPP. The operating point varies along the I-V plane of the solar cell due to changes in temperature and radiation levels as shown in Figure 5. These factors determine the MPP. Generally, the temperature and solar irradiance affects the output voltage and current respectively [37].

A power electronic circuit that optimizes the energy transfer between the solar panel (photovoltaic panels) the battery bank or the public electricity grid is necessary. These circuits are known as MPPTs (Maximum Power Point Trackers) [38].

In 1970s, companies or research centers such as NASA or Honeywell Inc. used the first methods of maximum power point in the aerospace applications. [39–44]. Since that, many MPPT methods used in the aerospace have been proposed and reported in litterature, particularly MPPT algorithms [45]. The commonly used methods are the conductance incremental (C.I.) and perturbation and observation (P&O).

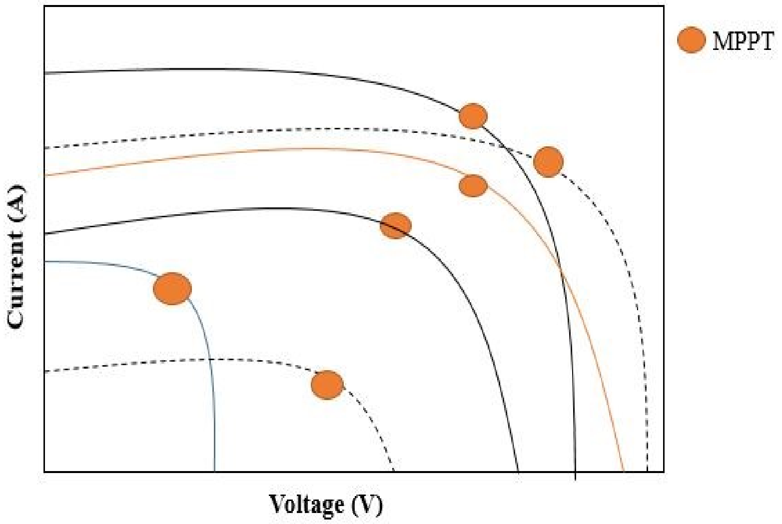

Figure 5. MPPT on the I-V curve with changing solar radiation and temperature levels

1.5.1. Solar MPP Tracking System Combinig with DC-DC Converter

When the PV is directly connected to the load, some problem may occur such us PV panels are always forcing to operate at the battery voltage. The battery voltage is all the time below the maximum peak power point. However some of the output power generated is lost.

To eliminate this unwanted effect on the output power of the PV and draw its maximum power, a DC-DC converter is introduced between the PV generator and the batteries. These converters are called MPP tracker and they can control the searching of the MPP [46].

PV generator block form the input of the DC–DC converter and the load form the output block as shown in Figure 6. The role of the MPPT block is to extract the maximum available power and do not forgetting to assure the operation of the PV at the MPP. In this study, a buck-boost DC-DC converter is used to implement the MPPT.

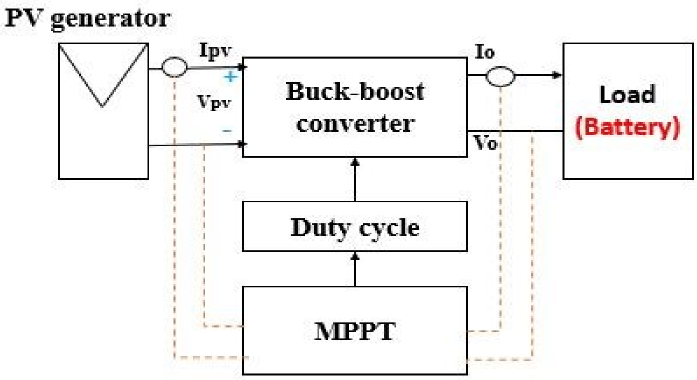

Figure 6. Block diagram of PV system with MPPT

1.5.2. Perturbed and Observe Tracking Algorithm

Perturb and Observe (P&O) method is one of the mostly used tracking MPPT algorithms. It is known by its independence from the environment conditions, simplicity and good accuracy of tracking. This method, current and voltage sensors are needed to be calculated [47]. The following figure shows PV system with resistive load.

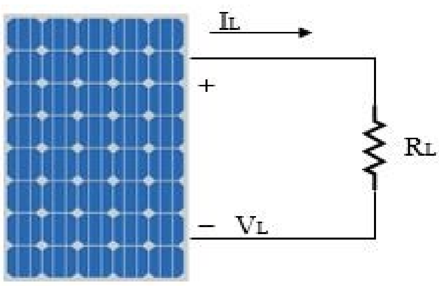

Figure 7. PV system with resistive load

In any photovoltaic panel, PV power and voltage attain the MPPT with the changing irradiance and temperature. This has generated the needs of some tracking method that can efficiently track the maximum power across the hold operation. During this operation, irradiance has a semi-circle curve such sunrise/sunset and the temperature curve varies with the increasing irradiance. This changing irradiance level will dynamically change the PV curve. However, P&O is one such method where it can compute the maximum power at any irradiance conduction. The working principle of this method is as follow[48-50].

Flowchart diagram is used in P&O algorithm method. In this diagram, the value of the duty cycle is measure at the start. The current and the voltage between two points is measured as shown in Figure 7, then the instantaneous power P(k) by multiplying V(k) and I(k). In the first cycle, we have $P(k)_{new}$ then we perturbed the operating point by $+\Delta D$. The perturbation value is a step size that how much change D is desired before the change is observed in the power. Next thing is usually a decision block where a condition is presented. This condition is if the $P(k)_{new}$ is greater than the $P(k\text{-}1)_{old}$. The following figure show the flowchart diagram of this perturb and observe method. The basic principle of this method is to calculate the output power of the PV and perturb by increasing or decreasing the duty cycle. After every perturbation, the output power is recalculating. If it is increased, the perturbation is repeating in the same direction otherwise direction of the perturbation reversed.

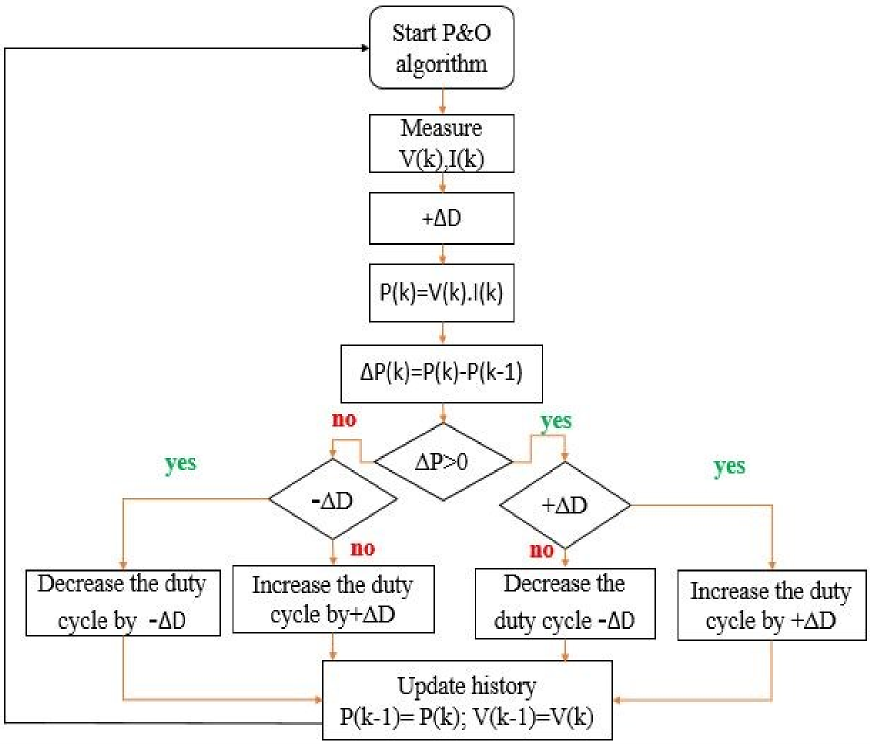

Figure 8. Flowchart diagram of the Perturbe and Observe

1.6. DC-DC Converters

Electronic devices such as DC-DC converters receives a DC input voltage from a power source and provide a DC output voltage to the load. Characteristically the output voltage generated is either less or more than input voltage. Adding that the DC-DC converters are used to provide noise isolation. Some of the well-known DC-DC converter topologies are presented in following sections.

1.6.1. Buck Converter

Buck converter is a step-down DC-DC converter, where the output voltage is lower than the input voltage [51]. The basic buck converter circuit is presented in Figure 9.

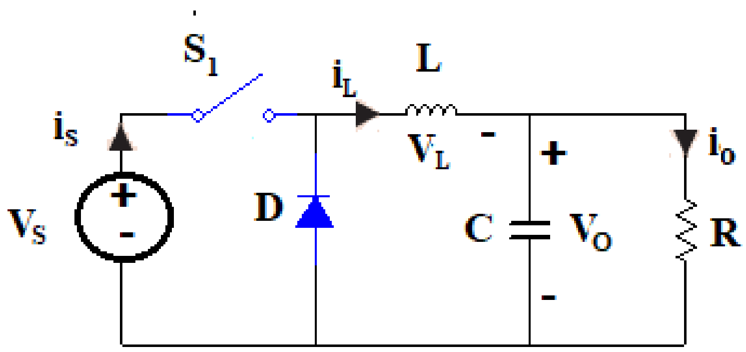

Figure 9. Basic buck converter circuit

For the converter shown above, the current flows through the inductor in to the load when the switch (S_1) is closed. This current charges the inductor (L) by boosting both its magnetic field and voltage output. After a while, the output voltage (Vout) will attain the desired value; then the switch (S_1) is turned off and the current flows through the recovery diode (D). At this state, inductor (L) is discharged and current continues to flow through it. Before the inductor is fully discharged, the S_1 is turned on, D is turned off and the cycle repeats. One can settle the ratio between the input and output voltage by modifying the duty cycle of the switch (S_1).

1.6.2. Boost Converter

Boost converter is a step-up DC-to-DC converter where the output voltage is higher than the input volatge. The basic boost converter circuit is given in Figure 10.

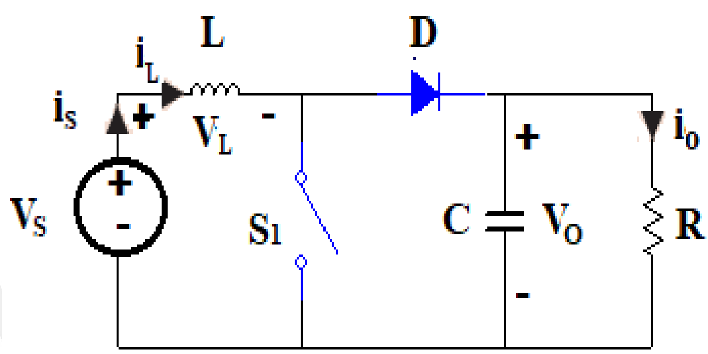

Figure 10. Basic boost converter

For the boost converter shown above, the switching transistor is a MOSFET or Bipolar transistor can be used as a switch. The voltage, current and switching speed are determining the choice of the semiconductor device. All the other components used is same as the component of the buck converter just their positions have been rearranged. In the input circuit the inductor (L) resists a sudden variation of current. Thus when the switch (S_1) is closed, this current charges the inductor (L) by boosting both its magnetic field and stores energy in the form of magnetic energy. Afterwards when the switch S_1 is OFF the inductor is discharge.

1.6.3. Buck-Boost Converter

Buck-boost converter is a both step down and step-up DC-DC converter where the output voltage is higher or lower than the input the volatge. The basic buck-boost converter circuit is given in Figure 11.

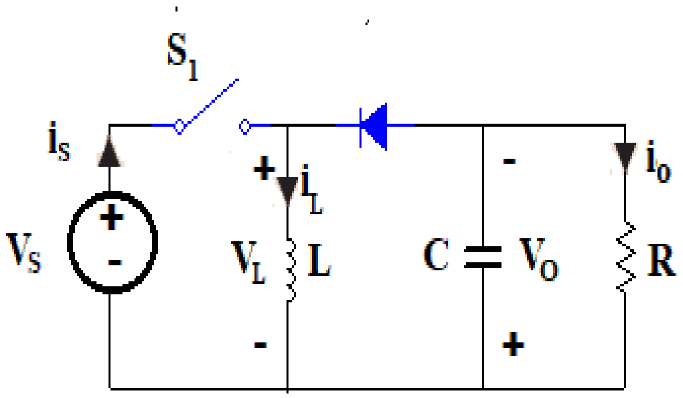

Figure 11. Basic buck-boost converter circuit.

Buck-boost converter is obtain by cascade connection of the two converters. These are the step down and the step up converters. First the diode D is reversed biased when the switch S_1 is closed and the current flows through switch S_1 and charges the inductor (L) .Then, the switch S_1 is turned off. The current, would flow across inductor, capacitor, diode and load. The energy stored in the inductor (L) is transferred to the load. The inductor current (L) will falls until the switch S_1 is turned on again in the next cycle.

2. CASE STUDY AND METHODOLOGY

The scope of this study is to design a single input multiple output DC-DC buck converter. In this chapter, the system transfer function is found and the control method used is presented. The used SIMO DC-DC buck converter is performed in Matlab/Simunlink.

2.1. State Space Averaging of the Buck Converter

In the design of feedback control systems for switched networks, the average state space method is used. In this method the state equations of the system for each position of the switch are subtracted and the resulting sets of equations are rearranged to give the average response by using the durations of the key positions as the weight function. The two states of the switchs are shown in Figure 12 [52].

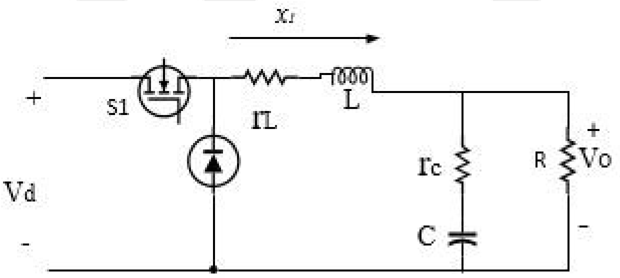

1. Case when 0 < t < dTon

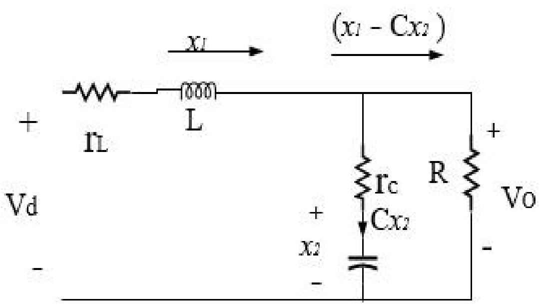

2. Case when dTON < t < T

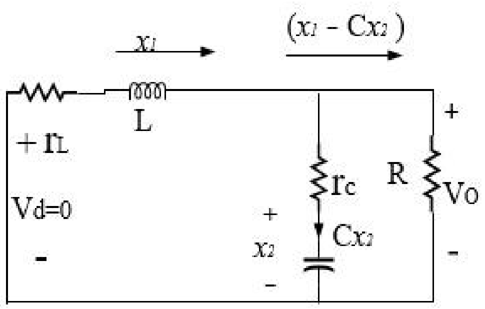

Figure 12. Structure of ON and OFF positions of the switch

There are two state variables in the circuit because there are two energy-storing elements. These state variables are denoted by x_1 and x_2. Their corresponding values are the inductor current and the capacitor voltage.

$$x_1 = i_L \tag{9}$$

$$x_2 = V_C \tag{10}$$

$$i_O = i_L - i_C = i_L - \frac{Cd_{Vc}}{dt} = x_1 - x_2 \tag{11}$$

The circuit in the range 0 < t < d_{TON} (ON position of the switch) is defined by the following Equations.

$$V_d = r_L x_1 + L\dot{x}_1 + x_2 + r_C C\dot{x}_2 \tag{12}$$

and

$$0 = -x_2 - r_C C\dot{x}_2 + R(x_1 - C\dot{x}_2) \tag{13}$$

where $\dot{x}_1 = \frac{d_{i_L}}{dt}$ and $\dot{x}_2 = \frac{Cd_{Vc}}{dt}$; (14)

The first step in resolving the transfer functions of the systems is to find the value of $\dot{x}_2$. Using Equation (13), this value is found;

$$0 = -x_2 - r_C.C\dot{x}_2 + R(x_1 - C\dot{x}_2) \tag{15}$$

$$-R(x_1 - C\dot{x}_2) + r_C.C\dot{x}_2 = -x_2 \tag{16}$$

$$-Rx_1 + RC\dot{x}_2 + r_C.C\dot{x}_2 = -x_2 \tag{17}$$

$$RC\dot{x}_2 + r_C.C\dot{x}_2 = -x_2 + Rx_1 \tag{18}$$

$$\dot{x}_2(RC + r_C.C) = -x_2 + Rx_1 \tag{19}$$

$$\dot{x}_2 = \frac{-x_2+Rx_1}{(RC+r_C.C)} = -\left(\frac{1}{RC+r_C.C}\right)x_2 + (\frac{R}{RC+r_C.C})x_1 \tag{20}$$

After having obtained the value $\dot{x}_2$ change $\dot{x}_2$ by its value in Equation (12) to find the value of $\dot{x}_1$:

$$V_d = r_L x_1 + L\dot{x}_1 + x_2 + Cr_C(\frac{-x_2+Rx_1}{(RC+r_C.C)}) \tag{21}$$

$$V_d = r_L x_1 + L\dot{x}_1 + x_2 + -Cr_C\left(\frac{1}{RC+r_C.C}\right)x_2 + Cr_C(\frac{R}{RC+r_C.C})x_1 \tag{22}$$

$$V_d = (\,r_L + \frac{RCr_C}{RC+r_C.C})x_1 + L\dot{x}_1 + (1 - \frac{Cr_C}{RC+r_C.C})x_2 \tag{23}$$

$$V_d = (\frac{r_L.(RC+r_C.C)+RCr_C}{RC+r_C.C})x_1 + L\dot{x}_1 + (\frac{RC+Cr_C-Cr_C}{RC+Crc})x_2 \tag{24}$$

$$V_d = \left(\frac{\mathrm{C\,(R}r_L+r_Lr_C+\mathrm{Rrc)}}{\mathrm{C(RC}+r_C)}\right)x_1 + L\dot{x}_1 + (\frac{C(R+r_C-r_C)}{C(R+r_C)})x_2 \tag{25}$$

$$V_d = \left(\frac{(\mathrm{R}r_L+r_Lr_C+\mathrm{Rrc})}{(\mathrm{RC}+r_C)}\right)x_1 + L\dot{x}_1 + (\frac{R}{R+r_C})x_2 \tag{26}$$

$$\dot{x}_1 = \frac{V_d}{L} - \left(\frac{(\,\mathrm{R}r_L+r_Lr_C+\mathrm{Rrc})}{(\mathrm{RC}+r_C)}\right)x_1 - \frac{1}{L}\left(\frac{R}{R+r_C}\right)x_2 \tag{28}$$

These equations 20 and 28 can be inserted into the standard state Equation form by performing intermediate operations. In matrix form these Equations can be written as:

$$\begin{bmatrix}\dot{x}_1\\ \dot{x}_2\end{bmatrix} = \begin{bmatrix} -\left(\frac{\mathrm{R}\,r_L+r_Lr_C+\mathrm{Rrc}}{(\mathrm{RC}+r_C)}\right) & -\frac{1}{L}\left(\frac{R}{R+r_C}\right) \\ -(\frac{R}{RC+Cr_C}) & (\frac{1}{RC+Cr_C}) \end{bmatrix} * \begin{bmatrix}x_1\\ x_2\end{bmatrix} + \begin{bmatrix}\frac{1}{L}\\ 0\end{bmatrix} * V_d \tag{29}$$

In general this Equation can be written in this form:

$$\dot{x} = A\,x + B\,u \tag{30}$$

Where $\dot{x}_1$ and $\dot{x}_2$ are defined as the matrices A_1 and B_1.

$$X = \begin{bmatrix} \dot{x}_1 \\ \dot{x}_2 \end{bmatrix} \; ; \; A_1 = \begin{bmatrix} -\left(\frac{\mathrm{R}\, r_L + r_L r_C + \mathrm{Rrc}}{\mathrm{L}(\mathrm{RC} + r_C)}\right) & -\frac{1}{L}\left(\frac{R}{R + r_C}\right) \\ -\left(\frac{R}{RC + Cr_C}\right) & \left(\frac{1}{RC + Cr_C}\right) \end{bmatrix} \begin{bmatrix} x_1 \\ x_2 \end{bmatrix} \; ; \; B_1 = \begin{bmatrix} \frac{1}{L} \\ 0 \end{bmatrix} \tag{31}$$

Identifies the switch in the d_{TON} <t <T when the switch is off position. These are given in the following equations :

$$\dot{x}_1 = 0 - \left(\frac{(\ \mathrm{R}r_L + r_L r_C + \mathrm{Rrc})}{(\mathrm{RC} + r_C)}\right) x_1 - \frac{1}{L}\left(\frac{R}{R + r_C}\right) x_2 \tag{32}$$

$$\dot{x}_2 = \frac{-x_2 + Rx_1}{(RC + r_C.C)} = -\left(\frac{1}{RC + r_C.C}\right) x_2 + \left(\frac{R}{RC + r_C.C}\right) x_2 \tag{33}$$

So finally, the matrix when the switch is off ;

$$\mathrm{X} = \begin{bmatrix} \dot{x}_1 \\ \dot{x}_2 \end{bmatrix} \; ; \; A_2 = \begin{bmatrix} -\left(\frac{\mathrm{R}\, r_L + r_L r_C + \mathrm{Rrc}}{\mathrm{L}(\mathrm{RC} + r_C)}\right) & -\frac{1}{L}\left(\frac{R}{R + r_C}\right) \\ -\left(\frac{R}{RC + Cr_C}\right) & \left(\frac{1}{RC + Cr_C}\right) \end{bmatrix} \begin{bmatrix} x_1 \\ x_2 \end{bmatrix} \; ; \; B_2 = \begin{bmatrix} 0 \\ 0 \end{bmatrix} \tag{34}$$

With these Equations, it can deduce that the only difference between (31) and (34) is the vector B_2 that is zero in (34). During a switching period, to provide an average description of the circuit. The Equation corresponding to the two previous states are averaged by using the average state space Equation 35.

$$x = dA_1X + (1 - d)A_2X + dB_1u + (1 - d)B_2u \tag{35}$$

The matrix of coefficients A_1 is defined in Equation (29) and Equation (30) the matrix A_2 defined for the second interval. Instead of defining two separate matrices such as A_1 and A_2, it can use a single matrix A. The B_2 vector is also zero. Moreover, this way is again arrangeable:

$$x = AX + Bu \tag{36}$$

Here;

$$B = dB1 \tag{37}$$

Considering that, the resistance of R is much larger than the resistances of r_C and r_L, the matrix A can be simplified as follows. R ⋙ r_L and R ⋙ r_C.

$$A = \begin{bmatrix} -\left(\frac{\mathrm{R}\, r_L + r_L r_C + \mathrm{Rrc}}{\mathrm{L(RC}+r_C)}\right) & -\frac{1}{L}\left(\frac{R}{R+r_C}\right) \\ -\left(\frac{R}{RC+Cr_C}\right) & \left(\frac{1}{RC+Cr_C}\right) \end{bmatrix} \tag{38}$$

$$A = \begin{bmatrix} -\left(\frac{(R(r_L+r_C)+r_L r_C)}{L(R+rc)}\right) & -\frac{1}{L}\left(\frac{R}{R+r_C}\right) \\ +1/C(\frac{R}{R+r_C}) & -(\frac{1}{RC+Cr_C}) \end{bmatrix} \tag{39}$$

$$A = \begin{bmatrix} -\left(\frac{r_L+r_C}{L}\right) & -\frac{1}{L} \\ +(\frac{1}{C}) & (-\frac{1}{RC}) \end{bmatrix} \tag{40}$$

Since the magnitude observed in the circuit is the output voltage, it should be expressed in terms of its variables:

$$Vo = R(x_1 - C\dot{x}_2) \tag{41}$$

$$Vo = R(x_1 - C\left(\frac{Rx_1 - x_2}{RC+Cr_C}\right) \tag{42}$$

$$Vo = (Rx1 - \left(\frac{CR^2x1 - RCx2}{RC+Cr_C}\right) \tag{43}$$

$$Vo = \left(R - \frac{CR^2}{RC+Cr_C}\right)x_1 - \left(\frac{-RC}{RC+Cr_C}\right)x_2 \tag{44}$$

$$Vo = \left(\frac{CR^2 + RCr_C - CR^2}{RC+Cr_C}\right)x_1 + \left(\frac{RC}{RC+Cr_C}\right)x_2 \tag{45}$$

$$Vo = \left(\frac{C}{C}\frac{(R^2+Rr_C-R^2)}{(R+r_C)}\right)x_1 + \frac{C}{C}\left(\frac{R}{R+r_C}\right)x_2 \quad (46)$$

$$Vo = \left(\frac{Rr_C}{R+r_C}\right)x_1 + \left(\frac{R}{R+r_C}\right)x_2 \quad (47)$$

In this case, the second equation of the state Equations set is written as:

$$Y = Cx = \begin{bmatrix}\frac{\mathrm{R}r_C}{\mathrm{R}+r_C} & \frac{\mathrm{R}}{\mathrm{R}+r_C}\end{bmatrix}\begin{bmatrix}x_1\\x_2\end{bmatrix} \quad (48)$$

If the internal resistance of the capacitor is neglected along with the load resistance, the new state of C vector become:

$$\mathrm{C} = [r_C \quad 1] \quad (49)$$

Relationship between input and output voltage is writted in the form of;

$$\mathrm{y} = \mathrm{Cx} = CA^{-1}\mathrm{Bu} \quad (50)$$

Here u = V_d is the voltages defined, after the interim, the transfer function.

Dynamic variation of the system with Laplace transform in s domain can be calculated in Equation (51). This result gives the average relation between input and ouput. However, dynamic change is not seen in this relation:

$$Tp(s) = \frac{\overline{V_O(s)}}{d(s)} = C.[SI-A]^{-1}\big[[A_1-A_2].x + (B_1-B_2).Vd\big] + (C_1-C_2).x \quad (51)$$

In this expression, since $A_1 = A_2$, $B_2 = 0$ *and* $C_1 = C_2$ we can end up that Tp like:

$$Tp(s) = C.[SI-A]^{-1}B_1.Vd \quad (52)$$

$$[SI - A]^{-1} = \frac{\overline{[SI - A]}}{[|SI - A|]} \tag{53}$$

$$\overline{[SI - A]} = s\begin{bmatrix}1 & 0\\0 & 1\end{bmatrix} - A \tag{54}$$

$$\overline{[SI - A]} = s\begin{bmatrix}s & 0\\0 & s\end{bmatrix} - A = \begin{bmatrix}s & 0\\0 & s\end{bmatrix} - \begin{bmatrix}-\left(\frac{rl+rc}{L}\right) & -\frac{1}{L}\\ +(\frac{1}{C}) & (-\frac{1}{RC})\end{bmatrix} \tag{55}$$

$$\overline{[\mathrm{SI} - \mathrm{A}]} = \begin{bmatrix}\mathrm{s} - (-\frac{\mathrm{rl+rc}}{\mathrm{L}}) & -\frac{1}{\mathrm{L}}\\ +\frac{1}{\mathrm{c}} & \mathrm{s} - (-\frac{1}{\mathrm{RC}})\end{bmatrix} \tag{56}$$

$$\overline{[\mathrm{SI} - \mathrm{A}]} = \begin{bmatrix}\mathrm{s} + \frac{\mathrm{rl+rc}}{\mathrm{L}} & -\frac{1}{\mathrm{L}}\\ +\frac{1}{\mathrm{c}} & \mathrm{s} + \frac{1}{\mathrm{RC}}\end{bmatrix} \tag{57}$$

Finally, the values of $\overline{[\mathrm{SI} - \mathrm{A}]}$ is found.

$$\overline{[\mathrm{SI} - \mathrm{A}]} = \begin{bmatrix}\mathrm{s} + \frac{1}{\mathrm{RC}} & +\frac{1}{\mathrm{L}}\\ -\frac{1}{\mathrm{c}} & \mathrm{s} + \frac{\mathrm{rl+rc}}{\mathrm{L}}\end{bmatrix} \tag{58}$$

The next step is to find the determinant $|\mathrm{SI} - \mathrm{A}|$:

$$det|\mathrm{SI} - \mathrm{A}| = \begin{bmatrix}\mathrm{s} & 0\\0 & \mathrm{s}\end{bmatrix} - \begin{bmatrix}-\left(\frac{\mathrm{rl+rc}}{\mathrm{L}}\right) & -\frac{1}{\mathrm{L}}\\ +\left(\frac{1}{\mathrm{C}}\right) & \left(-\frac{1}{\mathrm{RC}}\right)\end{bmatrix} = \begin{bmatrix}\mathrm{s} + \frac{\mathrm{rl+rc}}{\mathrm{L}} & -\frac{1}{\mathrm{L}}\\ +\frac{1}{\mathrm{c}} & \mathrm{s} + \frac{1}{\mathrm{RC}}\end{bmatrix} \tag{59}$$

$$|\mathrm{SI} - \mathrm{A}| = \left(\mathrm{s} + \frac{\mathrm{rl+rc}}{\mathrm{L}}\right)\left(\mathrm{s} + \frac{1}{\mathrm{RC}}\right) - (-\frac{1}{\mathrm{L}})(\frac{1}{\mathrm{C}}) \tag{60}$$

$$|\mathrm{SI}-\mathrm{A}| = \mathrm{s}^2 + \frac{\mathrm{S}}{\mathrm{RC}} + \frac{\mathrm{Src}+\mathrm{Srl}}{\mathrm{L}} + \frac{\mathrm{rc}+\mathrm{rl}}{\mathrm{RLC}} + \frac{1}{\mathrm{LC}}$$

(61)

$$|\mathrm{SI}-\mathrm{A}| = \mathrm{s}^2 + \left(\frac{1}{\mathrm{RC}} + \frac{\mathrm{rc}+\mathrm{rl}}{\mathrm{L}}\right)\mathrm{S} + \frac{\mathrm{rc}+\mathrm{rl}}{\mathrm{RLC}} + \frac{1}{\mathrm{LC}} \quad (61)$$

$$|\mathrm{SI}-\mathrm{A}| = \mathrm{s}^2 + \left(\frac{1}{\mathrm{RC}} + \frac{\mathrm{rc}+\mathrm{rl}}{\mathrm{L}}\right)\mathrm{S} + \frac{1}{\mathrm{LC}}\left(1 + \frac{\mathrm{rc}+\mathrm{rl}}{\mathrm{r}}\right) \quad (62)$$

Finally;

$$[\mathrm{SI}-\mathrm{A}]^{-1} = \frac{\overline{[\mathrm{SI}-\mathrm{A}]}}{|\mathrm{SI}-\mathrm{A}|]} = \frac{1}{\mathrm{s}^2 + \left(\frac{1}{\mathrm{RC}} + \frac{\mathrm{rc}+\mathrm{rl}}{\mathrm{L}}\right)\mathrm{S} + \frac{1}{\mathrm{LC}}\left(1 + \frac{\mathrm{rc}+\mathrm{rl}}{\mathrm{r}}\right)} \begin{bmatrix} \mathrm{s} + \frac{1}{\mathrm{RC}} & +\frac{1}{\mathrm{L}} \\ -\frac{1}{\mathrm{c}} & \mathrm{s} + \frac{\mathrm{rl}+\mathrm{rc}}{\mathrm{L}} \end{bmatrix} \quad (63)$$

By using the Equations (51.52 and 63) the transfer function of the buck converter is written as in Equation (64). This transfer function is obtained between the duties ratios. By making the required, Laplace transform:

$$Tp = \frac{\overline{V_O}}{\overline{d(s)}} * \frac{V_d}{L.C} \frac{(1 + s.r_c\ .C)}{\{\mathrm{s}^2 + \left(r_c.\frac{r_L}{L} + \frac{1}{RC}\right).\mathrm{s} + LC\}} \quad (64)$$

The term in the curly brackets in the denominator of Equation (64) are in the form of $s^2 + 2\varepsilon\omega_o s + {\omega_o}^2$.

Where,

$$\omega_o = \frac{1}{\sqrt{LC}} \quad (65)$$

and

$$\varepsilon = \frac{\frac{1}{RC} + r_c.\frac{r_L}{L}}{2\omega_o} \quad (66)$$

2.2. The Used SIMO DC-DC buck Converter

The single input multiple output topology used in this study is given in Figure 13. The bidirectional DC-DC converter used in this study has less power loss distribution among the power switches than unidirectional characteristics [53]. The topology consists of three power switches S_1, S_2 and S_3 as well as two low pass filters (L_1-C_1 and L_2- C_2) as illustrated in Figure 13. The state of the switches are represented as *switch x* = OFF (0) and *switch x* = ON. Since there are three switches and two states for each switch, eight ways of operating of the presented converter are obtained [26]. Only three switching states are operational. The other combinations were not included in this study. Table I presents the topological states (TS) of the system designed.

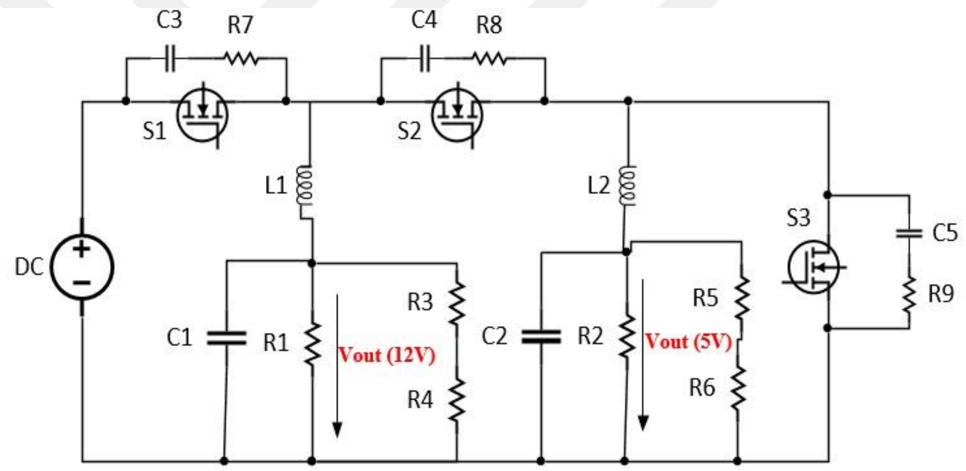

Figure 13. Bidirectional SIMO DC-DC buck converter

The different switching states of SIMO converter are shown in Table 1. It can be observed from the Figure 14 that:

-In state TS-1: Switch 1 = 1, Switch 2 = 1 and Switch 3 = 0. The input voltage (V_s) supplies energy to the loads and to the inductors, in this state both L_1 as well as L_2 is charged.

- *In state TS-2*: Switch 1 = 1, Switch 2 = 0 and Switch 3 =1. The input voltage (V_s) supplies energy to R_1–L_1 and current of the inductor L_2 (i_{L2}) flows through S_2, delivering some of its energy to the load R_2. In this circumstance, inductance L_1 and L_2 will be respectively charged and discharged.

- *In state TS-3*: Switch 1 = 0, Switch 2 = 1 and Switch 3 =1. The current in the inductor L_1 (i_{L1}) flows through S_2 and S_3, while i_{L2} flows only through S_3, delivering its stored energy to both loads R_1 and R_2. In this situation the inductors L_1, and L_2 are discharged.

Table 1. Topological states of the used SIMO converter

Topological states	TS-1	TS-2	TS-3
Switch1	ON	ON	OFF
Switch2	ON	OFF	ON
Switch3	OFF	ON	ON

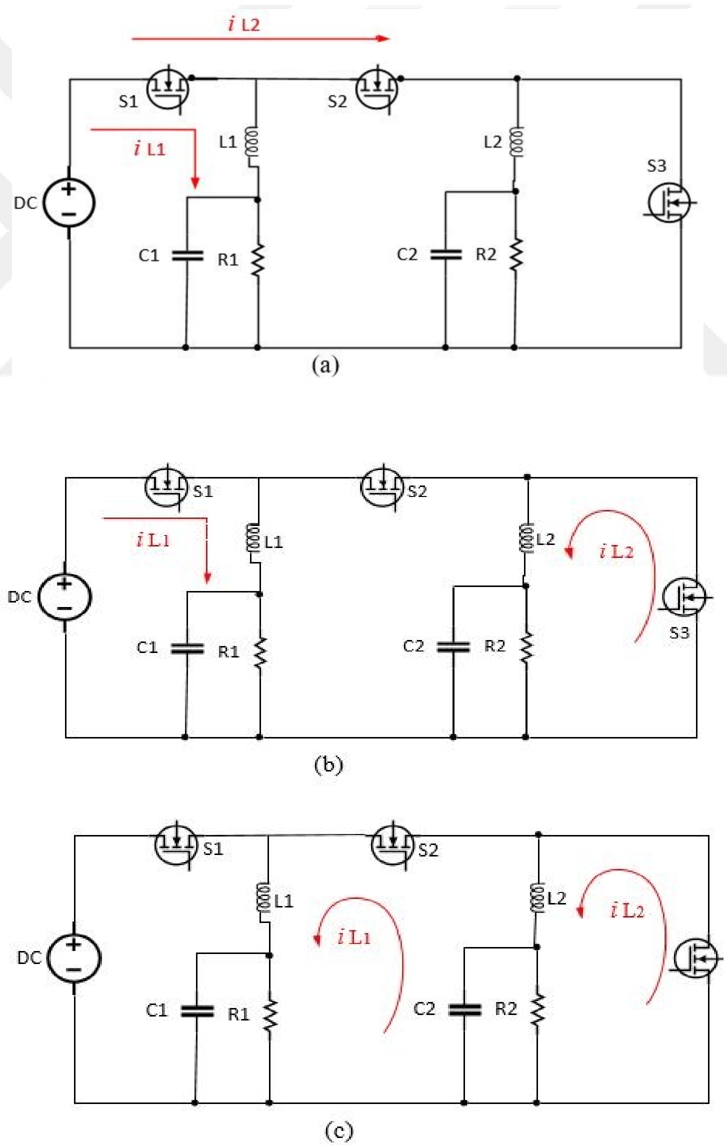

Figure 14. The different switching states of the SIMO converter: (a) TS-1, (b) TS-2, (c) TS-3

2.2.1. Steady State Analysis of SIMO Converter

The presented SIMO converter is conceived to operate in continuous conduction mode (CCM). T_{on1} and T_{on2} are the periods which the PWM generators one and two are generating the logic "1" at their corresponding outputs. The current and voltage waveforms of inductors are presented in Figure 15.

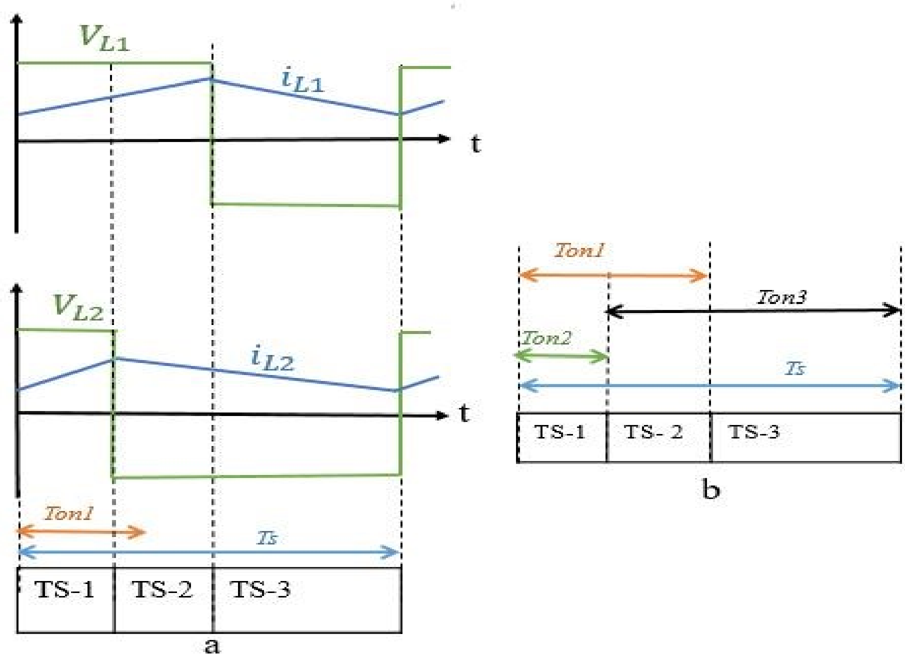

Figure 15. Steady-state analysis of the SIMO converter: (a) Inductors current and voltage related with topological states, (b) Times in which the switches are turned ON

From the topological states and waveforms found in the foregoing section, it can be inferred that the output voltage V_{01} and V_{02} controls voltage V_{R1} and V_{R2} respectively. Noting that the average inductor voltage is zero. The following Equations are written in (67)-(68):

$$(V_S - V_{01}) * T_{ON1} = V_{01} * (T_S - T_{ON1}) \quad (67)$$

$$(V_S - V_{02}) * (T_S - T_{ON3}) = V_{02} * T_{ON3} \quad (68)$$

According to the Equations (67, 68), the different output voltages come out as a function of their input voltage and duty cycles. V_{01} and V_{02} are expressed in the following Equations:

$$V_{01} = (D_1)V_S \tag{69}$$

$$V_{02} = (1 - D_2)V_S \tag{70}$$

Where D_1 and D_2 represent the duty cycles of the system.

2.2.2. Generalized State-Space Average Model

The voltage and the current dynamics are described by the state space average and it is given in (71)-(74):

$$L_1 \frac{di_{L1}}{dt} + Vo_1 = D_1\, Vs \tag{71}$$

$$C_1 \frac{dV_{01}}{dt} = i_{L1} - \frac{V_{01}}{R_1} \tag{72}$$

$$L_2 \frac{di_{l2}}{dt} + Vo_2 \quad = \ D_2 Vs \tag{73}$$

$$C_2 \frac{dV_{02}}{dt} = i_{L2} - \frac{V_{02}}{R_2} \tag{74}$$

State space averaging for the first output is calculated as following:

$$\dot{I}_{L1} = \frac{D_1 V_S}{L_1} - \frac{V_{01}}{L_1} \tag{75}$$

$$\dot{V}_{01} = \frac{i_{L1}}{C_1} - \frac{V_{01}}{R_1\, C_1} \tag{76}$$

Where $\frac{d_{iL}}{dt} = \dot{I}_{L1}$ and $\frac{dV_{01}}{dt} = \dot{V}_{01}$

Now, using state space averaging of the SIMO buck converter the matrices are found

$$A = \begin{bmatrix} 0 & -\frac{1}{L1} \\ \frac{1}{C_1} & -\frac{1}{R_1\, C_1} \end{bmatrix} . \mathrm{B} \begin{bmatrix} \frac{\mathrm{D}1VS}{L1} \\ 0 \end{bmatrix} ;\ \mathrm{C}\,[0 \quad 1] \tag{77}$$

Using these matrices written above and the following formula. The transfer function of the $[SI - A]^{-1}$ is found.

$$[SI - A]^{-1} = \frac{\overline{[SI - A]}}{|SI - A|]} \tag{78}$$

First the $\overline{[\mathrm{SI} - \mathrm{A}]}$ is found;

$$\overline{[\mathrm{SI} - \mathrm{A}]} = \begin{bmatrix} s & 0 \\ 0 & s \end{bmatrix} - \begin{bmatrix} 0 & -\frac{1}{L1} \\ \frac{1}{C_1} & -\frac{1}{R_1\, C_1} \end{bmatrix} = \begin{bmatrix} \mathrm{s} - 0 & -\left(-\frac{1}{L1}\right) \\ 0 - \left(\frac{1}{C_1}\right) & \mathrm{s} - \left(-\frac{1}{R_1\, C_1}\right) \end{bmatrix} = \begin{bmatrix} \mathrm{s} & +\left(\frac{1}{L1}\right) \\ -\frac{1}{C_1} & \mathrm{s} + \left(\frac{1}{R_1\, C_1}\right) \end{bmatrix} \tag{79}$$

The value of $\overline{[\mathrm{SI} - \mathrm{A}]}$ is :

$$\overline{[\mathrm{SI} - \mathrm{A}]} = \begin{bmatrix} \mathrm{s} + \left(\frac{1}{R_1\, C_1}\right) & -\frac{1}{L1} \\ +\frac{1}{C_1} & s \end{bmatrix} \tag{80}$$

Second $|SI - A|$ is found;

$$|SI - A| = \begin{bmatrix} s & 0 \\ 0 & s \end{bmatrix} - \begin{bmatrix} 0 & -\frac{1}{L1} \\ \frac{1}{C_1} & -\frac{1}{R_1\, C_1} \end{bmatrix} = s.\left(s + \frac{1}{R_1\, C_1}\right) - \left(-\frac{1}{C_1} . \frac{1}{L_1}\right) \tag{81}$$

The value of $|SI - A|$ is :

$$|SI - A| = \ +s^2 + \frac{s}{R_1\, C_1} + \frac{1}{L_1 C_1} = \frac{(R_1\, C_1 L_1 s^2 + L_1 s + \ +R_1\,)}{R_1\, C_1 L_1} \tag{82}$$

Using the Equation (81) and (82), the value of $[SI - A]^{-1}$ is given in the Equation (83):

$$[SI - A]^{-1} = \frac{1}{\frac{R_1\,C_1L_1s^2 + L_1s + + R_1}{R_1\,C_1L_1}} * \begin{bmatrix} s + \left(\frac{1}{R_1\,C1}\right) & -\frac{1}{L1} \\ +\frac{1}{C_1} & s \end{bmatrix} \quad (83)$$

$$Tp(s) = C.[SI - A]^{-1}B_1.Vd \quad (84)$$

$$C.[SI - A]^{-1} = [0 \quad 1] = \begin{bmatrix} s + \left(\frac{1}{R_1\,C_1}\right) & -\frac{1}{L1} \\ +\frac{1}{C_1} & s \end{bmatrix} = \left(+\frac{1}{C_1}.s\right) \quad (85)$$

Finally the transfert of the system is:

$$Tp(s) = \frac{+\frac{s}{C_1}.\frac{V_sD_1}{L_1}}{\frac{R_1\,C_1L_1s^2 + L_1s + R_1}{R_1\,C_1L_1}} \quad (86)$$

$$Tp(s) = \frac{V_sD_1\,R_1}{R_1\,C_1L_1s^2 + L_1s\; + R_1} \quad (87)$$

Similarly, using the same instructions, the Equation of the second output is found. Equations (88), (89) and (90) are the main Equations used to find the transfer function.

$$\mathrm{Tp(s) = C.[SI - A]^{-1}}B_1.Vd \quad (88)$$

$$L_2\,\frac{di_{L2}}{dt} + V_{02} \;\; = D_2V_S \quad (89)$$

$$C_2\frac{dV_{02}}{dt} = i_{L2} - \frac{V_{02}}{R_2} \quad (90)$$

The transfer function of the second output (5V) is written as follows.

$$Tp(s) = \frac{V_s D_2\, R_2}{R_2\, C_2 L_2 s^2 + L_2 s\ + R_2} \tag{91}$$

2.3. Buck Converter Selection of the Parameters

In this part of the chapter gives the formulas to calculate the different components of the circuit. The first step is to determine the duty cycle, D. The duty cycle is the ratio of the output voltage into the input voltage [54]. The maximum duty cycle is calculated using this formula.

$$Duty\ ratio = \frac{V\ out}{V\ \ in} \tag{92}$$

The second step is to calculate the inductor ripple current or inductor current. The following Equation is required for inductor:

$$L = \frac{D(1-D).V_{input}}{f * \Delta I_L} \tag{93}$$

ΔI_L= The maximum current ripple permitted through the inductor

Generally using low-ESRcapacitors is good to minimize the ripple on the output voltage. If the dielectric material is like X5R capacitor or better, so ceramic capacitors are a good choice for that [54]. The Equations below are used to adjust the output capacitor values for a required output ripple value:

$$C = \frac{\Delta I_L}{8.f.\Delta Vc} \tag{94}$$

In here;

C = Output capacitance.

f = frequency.

ΔV_C = Output voltage ripple.

ΔI_L = The estimated inductor ripple current.

The ESR of the output capacitor adds some more ripple, given with the Equation 97.

$$\Delta Vc = Kind.\ Voutput \tag{95}$$

2.3.1. Setting the PI Controller Parameters

The formulas written above make it possible to find the values of the SIMO components.

The transfer function of the output (12V) and (5V) are given in Equations (87) and (91) respectively. Similarly, using these formulas and the Routh Hurwitz criterion, the approximate values of the PI parameters can be found.

Firstly, the required output voltage is 12V while the input voltage is 48V. The duty cycle can be calculated as;

$$\text{Duty} = \frac{V\ out}{V\ in} = 12/48 = 0.25. \tag{96}$$

Let say that ΔI_L the maximum ripple current through the inductor is 1V

$$L = \frac{\mathrm{D(1-D).Vinput}}{\mathrm{f*\Delta I_L}} = 0.25*(1-0.25)*48/(50000) = 180\mu H \tag{97}$$

To calculate C let say that for a good estimation of inductor current ripple is 10%, so Kind =0.1;

$$\Delta Vc = 0.1 * 12 = 1.2 \tag{98}$$

$$C = \frac{\Delta I_L}{8.f.\Delta Vc} = 1/\,(8*50000*1.2) = 20\mu F \tag{99}$$

For the first output (12V) the value of the inductor and capacitor are increase in order to have a good response. The resistance is R = 1000Ω; C=2200 μF ; L=8.5mH. The transfer function of the first output is:

$$Tp(s) = \frac{12000}{0.00396s^2 + 0.0018s\ + 1000} \tag{100}$$

The Figure (16) shows the bode diagram of the transfer function for the first output (12V) in Matlab/Simulink.

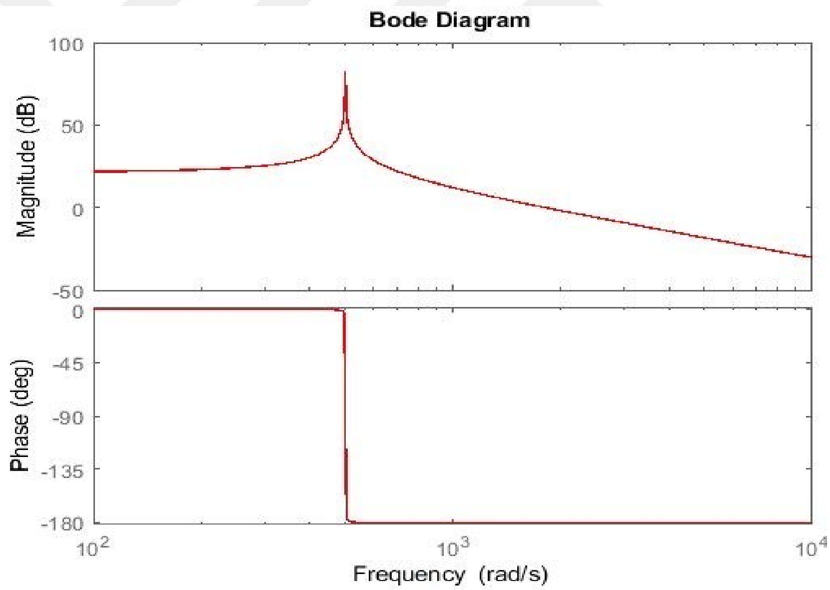

Figure 16. Bode diagram for the first output (12V)

The transfer function of the single input multiple output is found as shown in equation (100). The next step is to calculate the value of the PI controller. The basic transfer function of PI controller with second order system is written in Equation (101). The Figure 17 shows the block diagram of the PI controller.

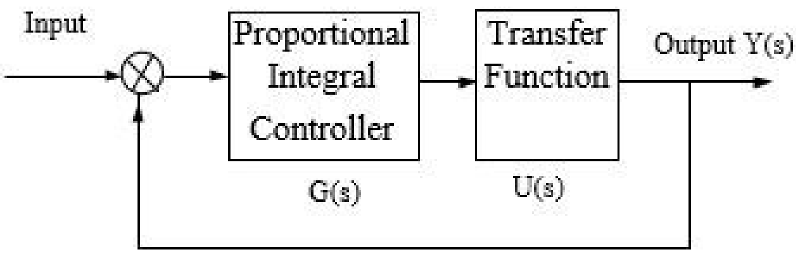

Figure 17. Block Diagram of PI Controller

$$Y(s) = \frac{U(s)G(s)}{1 + U(s)G(s)} \tag{101}$$

Where $\quad G(s) = (K_P + K_I/s)$ (102)

$$Tp(s) = \mathrm{U(s)} = \frac{12000}{(0.00396s^2 + 0.0018s \ + 1000)} \tag{103}$$

Finaly using the Equation (101) the second order transfer function of PI controller is written:

$$\mathrm{Y(s)} = \frac{12000(\mathrm{Kps} + \mathrm{Ki})}{(0.00396\mathrm{s}^3 + 0.0018\mathrm{s}^2 \ + 1000\mathrm{s}) + 12000(\mathrm{Kps} + \mathrm{Ki})} \tag{104}$$

Obtaining the step response;

$$T(s) = Y(s) * R(s) = \frac{12000(Kps+Ki)}{(0.00396s^4+0.0085s^3 +1000s^2)+12000Kps^2+12000Kis} \tag{105}$$

For $R(s)= 1/R_S$ (106)

Obtaining the unite ramp;

$$Y(s) = T(s) * R(s); \tag{107}$$

$$Y(s) = (s) * \frac{1}{s^2} \frac{12000Kps + Ki}{(0.00396s^3 + 0.008.5s^2 \ + 1000s) + 12Kps + Ki} * \frac{1}{s^2} \quad (108)$$

Table 2. Routh hurwitz criterion

s^3	0.00396	1000+12000Kp
s^2	0.0018	12000Ki
s^1	$\frac{0.0018 * (1000 + 12000\text{Kp}) - \ 0.00396 * 12}{0.0018}$	0

Using the Routh hurwitz citerion of stability the value of the K_P is between:

$7.010^{-4} < KP < 8.5$ (109)

And the value of Ki

0 < Ki < 2.

Likewise the input voltage is 48 volt and 5 volt is required in the output of the SIMO converter. Therefore, same like the first output the duty cycle is:

Duty $=\frac{V\ out}{V\ in}$ = 5/48 = 0.104 (110)

Let say that ΔI_L the maximum ripple current through the inductor is 1 Amper.

$L = \frac{\text{D(1−D).Vinput}}{\text{f}*\Delta \text{I}_\text{L}}$ 0.104- (1-0.104) *48/ (1*50000) = 89µH (111)

To calculate C let say that a good estimation of inductor current ripple is 10% so Kind=0.1:

$\Delta Vc = 0.1 * 5 = 0.5$

$$C = \frac{\Delta I_L}{8.f.\Delta Vc} = 1/\ (8*50000*0.5) = 5\mu F \qquad (112)$$

For second output voltage (5V), the value of the inductor and capacitor are multiplied respectively by 4.5 and 660. The resistance is 1000 Ω. So R=1000Ω; C=3300μF; L 400μH. The transfer function of the output one is :

$$Tp(s) = \frac{4992}{0.00132s^2 + 0.000400s\ + 1000)} \qquad (113)$$

The Figure (18) shows the bode diagram of the transfer function for the second output (5V) in Matlab/Simulink.

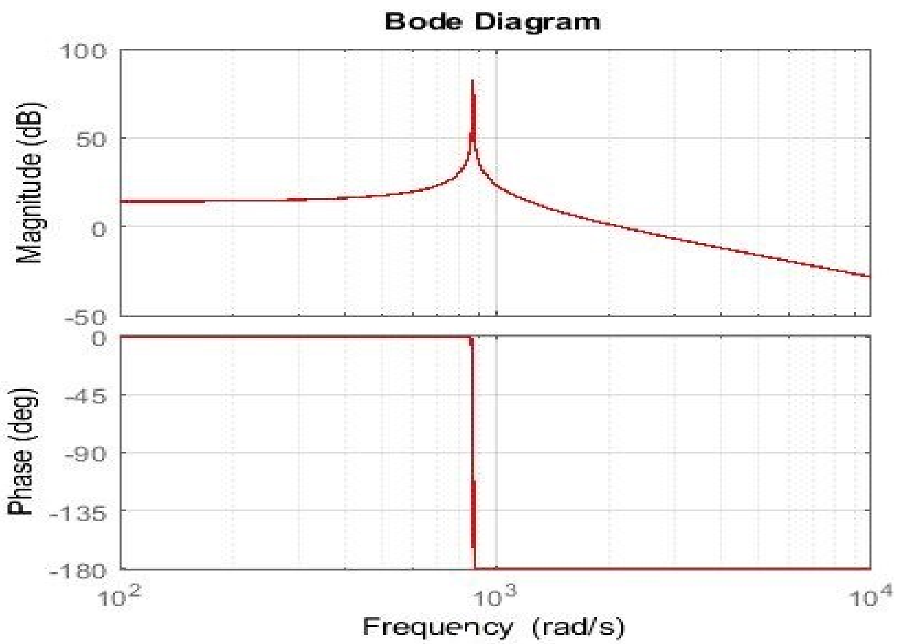

Figure18. Bode diagram of the second output

2.4. SIMO DC-DC Buck Converter in Matlab/Simulink

The SIMO model is exemplified with illustrative calculation of the transfer function and this converter have the parameters listed in the Table 3.

Table3. The parameters of the SIMO converter

Parameters	Values	Parameters	Values
DC input	48V	Duty ratio (D_1& D_2)	0 - 1
Switching frequency(fs)	50kHz	Load resistance (R_1)	1000Ω
Inductor (L_1)	8.5mH	Load resistance (R_2)	1000Ω
Inductor (L_2)	400µH	Output DC voltage (V1)	12 V
Output capacitance (C1)	3300 µF	Output DC voltage (V2)	5V
Output capacitance (C2)	2200 µF		

The simulation diagram of single input multiple output (SIMO) converter represented with transfer function and the results are shown in Figure 19 and 20 respectively.

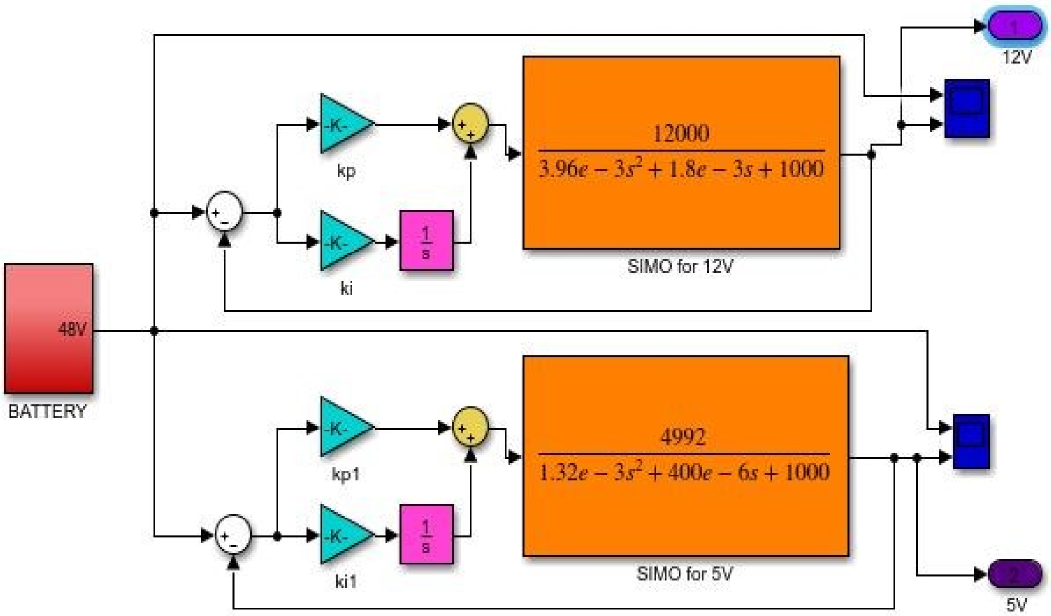

Figure 19. SIMO converter with transfer function diagram

Figure 20 shows the simulation results of the transfer function of DC-DC converter. It can be deduced that all outputs reach their values in short time.

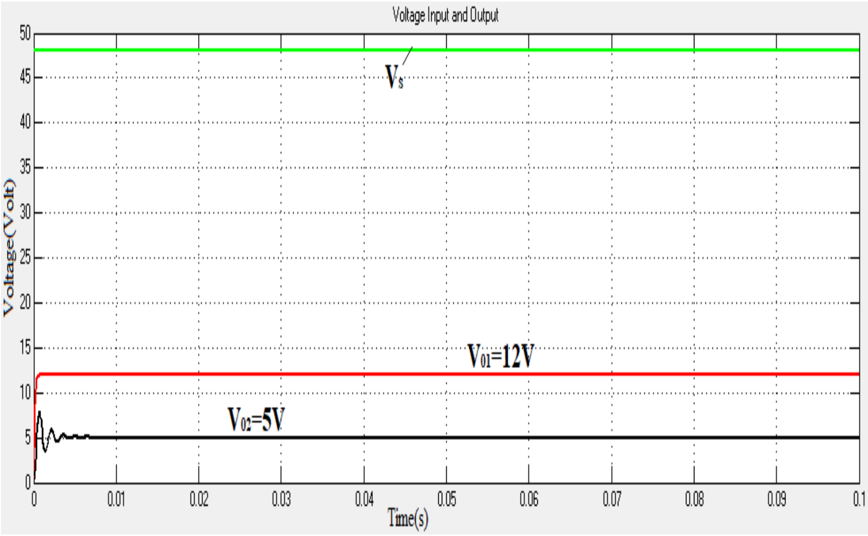

Figure 20. The SIMO DC-DC converter with transfert function

2.5. Simulink Model of SIMO Converter Without Transfert Function

The simulation model of the whole system is shown in Figure 21. The system is composed of two PWM block, one logic block and the SIMO converter. The input voltage of the converter is 48 V and the outputs are composed of 5 and 12 Volts.

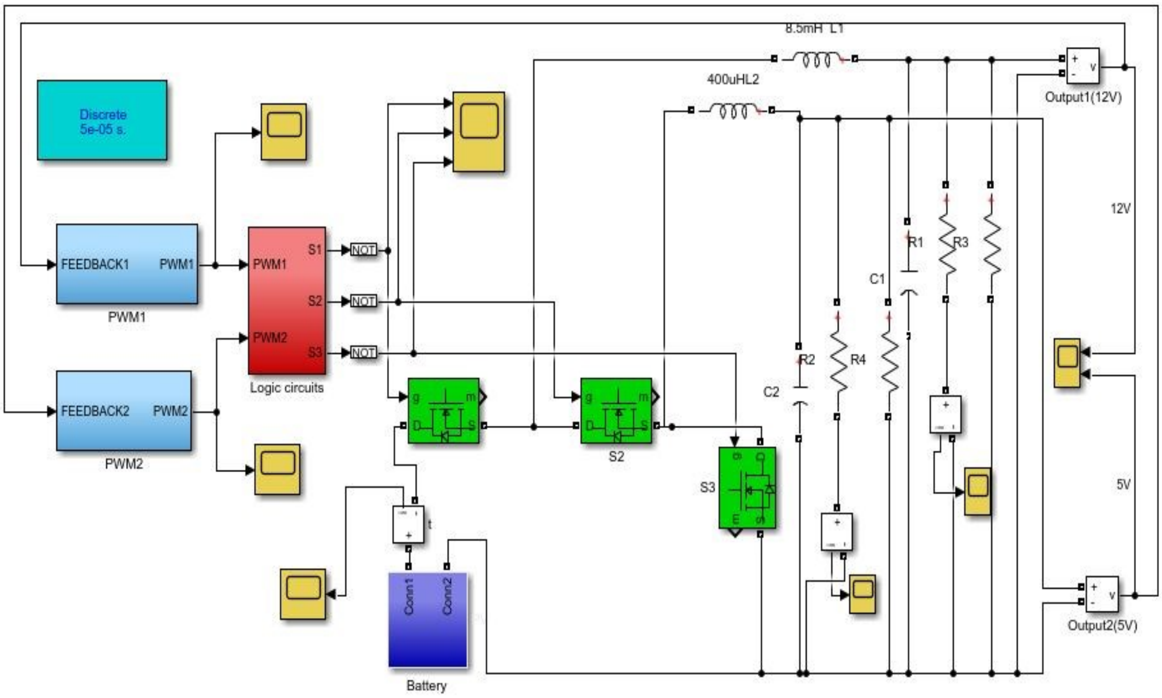

Figure 21. Simulink diagram of the SIMO DC-DC buck converter

2.5.1. PWM Generator Implementation and PI Controller

All three switches in the converter are derived using PWM. PWM block includes PI controller. The Simulink model is given in Figure 22. DC- DC converters use switches to change the DC from one level to another [64]. The system operates at 50 kHz with an output value between 0 and 1. The PWM1 and PWM2 generators produce an error signal and inserted into the PI block. The output of the PI block is compared to the sawtooth. Thus, logic 1 and 0 values are produced. The PI controller is a proportional-integral controller. PI controller is used to control the output voltage coming from the SIMO DC-DC buck converter output voltage sensor [65]. The values of the gains K_P, and K_I, are chosen carefully using Routh–Hurwitz stability criterion analysis. The output would reach the reference value with a very short settling time and without an overshoot.

$$G(s) = K_p + \frac{K_I}{s} \tag{114}$$

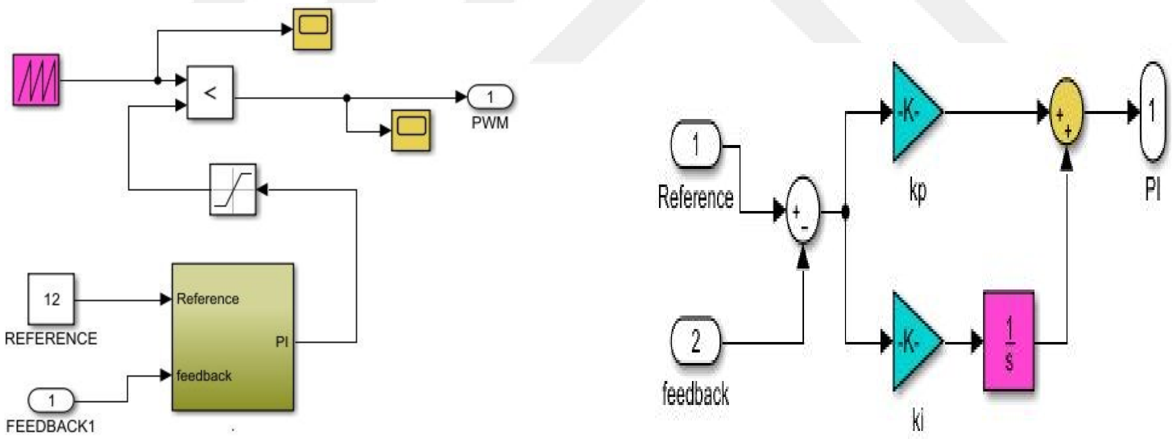

(a) (b)

Figure 22. Simulink model of: (a) PWM; (b) PI controller

The PI controller continuously detect an error signal as the difference between feedback loop and the reference voltage. During the first zone, the feedback signal (black line) is less than the reference value (green line) as seen in Figure 23, so error is negative. The PI controller produces signal (red color line) to eliminate the difference between feedback and reference and the switch S_1 is ON. During this period, the PWM is generated pulses. In the second section, when the feedback is higher than reference value of 12 V, so error is positive.When the PI is not generating a signal the switch S_1 is OFF. The following figure shows working principle of PI controller designed with Matlab/Simulink.

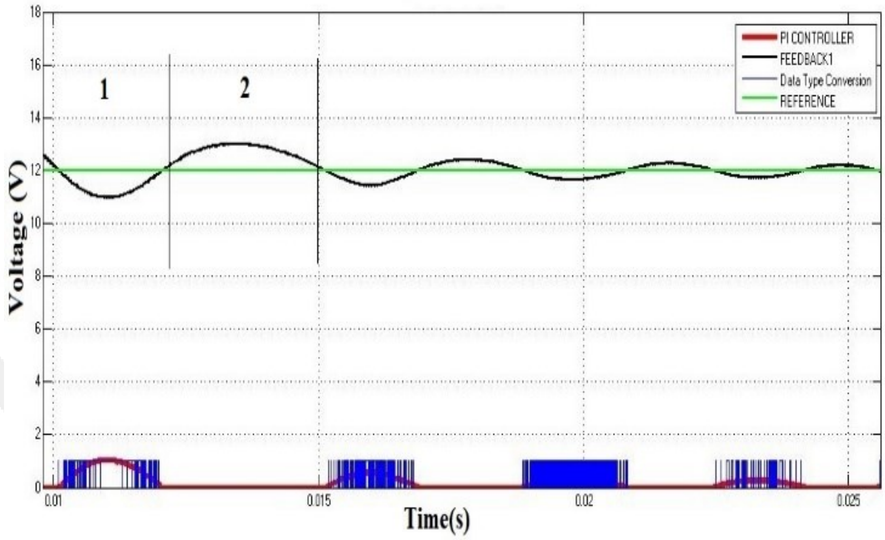

Figure 23. PI controller designed with Matlab/Simulink

2.5.2. Modelling the Logic Circuits

The outputs of the PWM1 and PWM2 generators, which are illustrated in Figure 21 go through a logic circuit block as given in Figure 22. This logic circuit block command the state of the switches S_1, S_2 and S_3. From the topological states point of view (shown in Table 1), it can be deduced that the charging of the inductor L_1 is fully reliant to switch 1 (S_1), consequently to control V_{O1} the PWM1 is directly connected to S_1. In contrary, either charging or discharging of L_2 is not reliant on the state of S_2 since when the L_2 is discharging in the TS-3 the switch S_2 is ON. The second PWM generator defines an interval that the switch S_2 should begin to operate. In addition, switch S_2 should be controlled in such a way that prohibited states are avoided. These requirements are achieved by using a two input “OR” gate and a “NOT” gate shown. Lastly, the other two switches specify the switch S_3. This deduces that the only work for the switch S_3 to avoid the prohibited states. This is achieved using NAND gate. The logic block is shown in Figure 24(a) and the gate signals of S_1, S_2 and S_3 are shown in Figure 24(b).

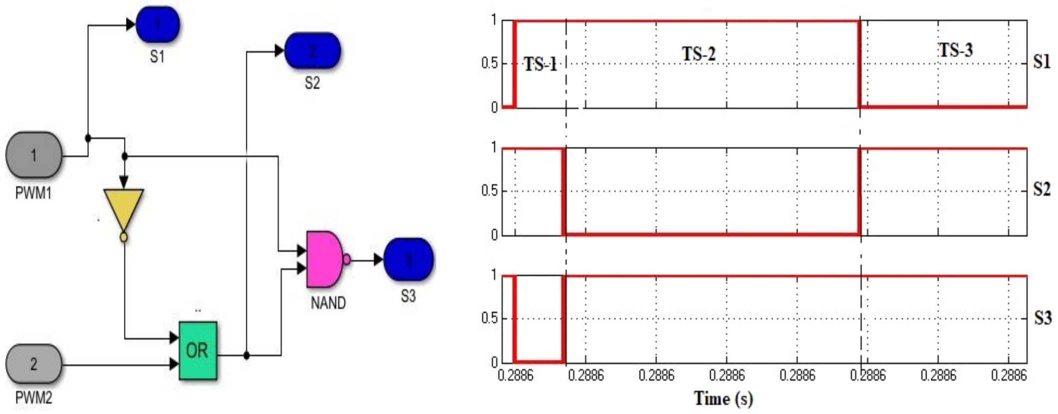

(a) (b)

Figure 24. Gate signals of the switches: (a) Logic block; (b) Output signals of the Block.

2.6. Simulation of the Solar System

The simulink model of the solar system is presented. The solar system is composed of a PV Panel, buck-boost converter and a battery. Inside the buck boost simulink block, MPPT controller and buck-boost circuit are presented. Figure 25 shows the simulink diagram of the whole solar system.

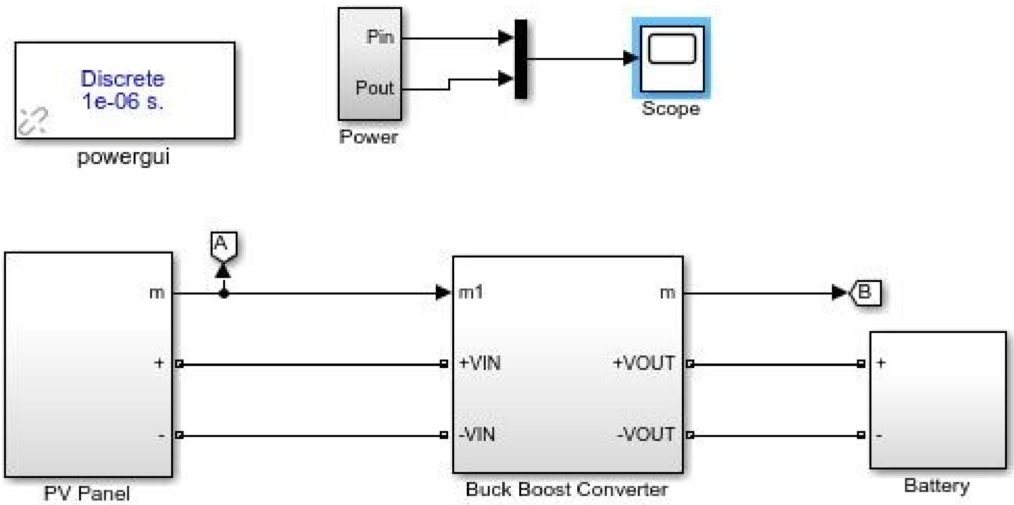

Figure 25. Solar system with mppt controller.

Table 4. Parametres of the solar cells.

Number of serial connected cells	10	Parallel resistance	200Ω
Open circuit voltage	64.2V	Numberof module in series	1
Series resistance	0.18Ω	Number of module in parallel	10

The results of the simulik model of the solar system shown in Figure 25, are presented in Figure 26. The output power of the PV panel and the output power coming from the output of the buck-boost converter shown in Figure 26 .

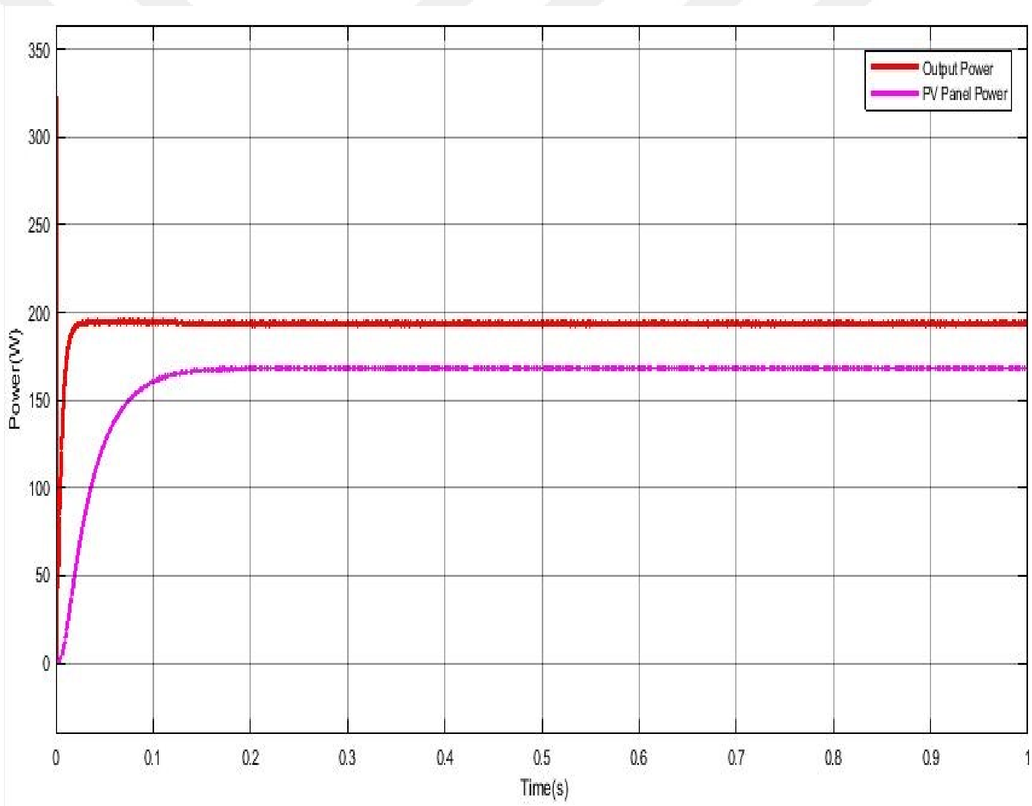

Figure 26. PV Panel power and output power of the converter.

3. IMPLEMENTATION

3.1. SIMO Converter Circuits

First section of this chapter include the design of some circuits on the single input multiple output DC-DC buck converter and the calculations of the inductor turns and the MOSFET coolers. These circuits and component helps the system to work properly. These circuits are snubber circuits, voltage divider.

3.1.1. Design of the Inductors

Two inductors were designed in the laboratory in order to save time and money. The common purpose of the inductor in a circuit is to store energy. The inductance occurs because of the magnetic filed that forms on every side of a current-conductor. The magnetic field is stored as long as the current flow. Thus, the inductance is noted depending on the flow or the changing in current [55]. The type of conductor, the number of windings or turns, material wrapped around the inductance and the size of each turns are the parameter that define the inductance of each inductor. The inductors is manufactured in different sizes and shapes like Ferromagnetic cored toroids, a circular wire loop and air-cored solenoid. In this study ferromanetic cored are used [56].

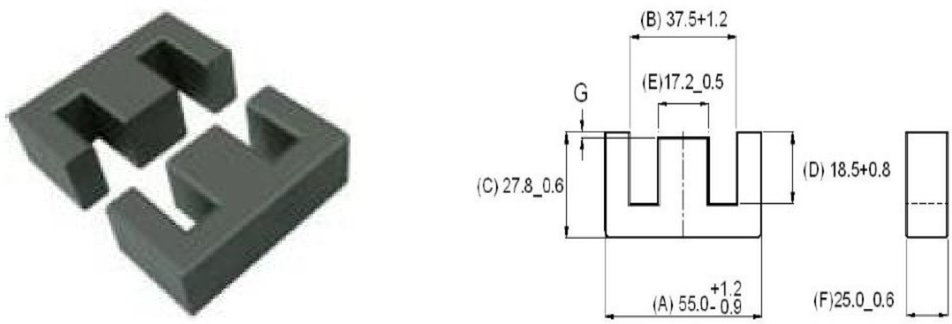

(a) (b)

Figure 27. Ferrite E-Round AI-7900- ungapped

The factor on which the resistance of a conductor R depend are:

$$R=\rho \frac{L}{A} \tag{115}$$

Where ρ is resistivity of a material in Ohm meter, A is the cross section area and L is length of the wire. The electrical resistance is greater for a longer wire (L) and less for a wire of large cross sectional area. However at high frequencies, the current in the conductor tends to flow near the surface because of the Foucault currents produced in the material. Therefore, less current flow through the conductor near the center of the wire while an important curent tends to flow at annulus or in a layer near the surface. This phenomene is called skin effect [57]. In order to prevent this skin effect, a Litz wire is used. It is composed of many thin wire strands, individually insulated and woven or twisted together. This is designed to reduce the skin effect. The following figure shows the litz wire turned with a ferrite inductor.

Figure 28. Ferrite inductor of the second output (5volt)

From the previous section the value of the inductance is first calculed. For the first output of the SIMO converter (12V) the inductance value is about 1.8mH. The maximum current through the inductor is around 10 A. In this part the number of turns without gap is calculated and the maximum energy that can be stored on the inductor is:

$$LI^2 = (1.8*10^{-3})*(10)^2 = 180*10^{-3}\ J \quad (116)$$

From Table 4, the value of the coefficient of inductance without gap as well as the initial permeability are: A_L = 7900 nH μ_i = 2100 are given. From the formulas in [58] the value of the effective permeability is found:

$$\mu e = \frac{A_L * l_e}{4\pi * A_e} = 715.4 \quad (117)$$

Where Effective Length and Effective Area are given in the datasheet of the materiel. Using the following relation the number of turns for inductor are obtained.

$$\mathrm{N} = 10^3 \sqrt{\frac{L}{A_L}} = 28 \text{ turns} \quad (118)$$

Table 5. Coefficient of inductance and effective permeability without gap (CF1)

Material Grade	Initial Permeability (µiac)	AL Value (nH)	PV (W/set)	Ordering code
CF196	2000 ±20%	7600 +30%/-20%	≤6.98(200mT,16kHz,100^{0}C)	CF196EE5525OL
CF139	2100 ±20%	7900 +30%/-20%	≤5.06(100mT,100kHz,100^{0}C)	CF139EE5525OL
CF297	2300 ±20%	8500 +30%/-20%	≤4.56(100mT,100kHz,100^{0}C)	CF297EE5525OL

Table 6. Dimensioning inductance CF139

Symbol	Name	value	unit
	materials	CF139	
	Base Material	MnZn	
L	Inductor	1.8	mH
N	Number of spire		
A_L	Inductance Factor	7900	nH
I_e	Effective Length	120.0	mm
μe	Effective Permeability	715.4	
Ae	Effective Area	422.0	mm^2

Using the same instruction that for the first input, the second output (5V) of single input multiple output DC-DC converter has a number of the turns egual to N= 15 turns.

3.1.2. Design of the Snubber Circuits

Snubber circuits are an important part of power electronic circuits. The purpose of this is to absorb energy from the reactive elements in the circuit [59]. It results higher switching frequency, higher efficiency, smaller size and lower weight. Snubber circuits are placed on the MOSFETS or IGBTs to improve the performance of system and gives protection. There are many variety of snubber circuits, but the RC damping network is used here. Using the following Equations the value of R_S (Snubber Resistor) and C_S (Snubber Capacitor) are found [60-63].

$$R = \frac{V_{in}}{I} \quad \text{or} \quad R_S = \frac{2}{t_{on} .minC_s}; \tag{119}$$

and

$$C_S = \frac{1}{f_s {V_{in}}^2} \tag{120}$$

The following Figure (29) shows where the snubber circuits are placed.

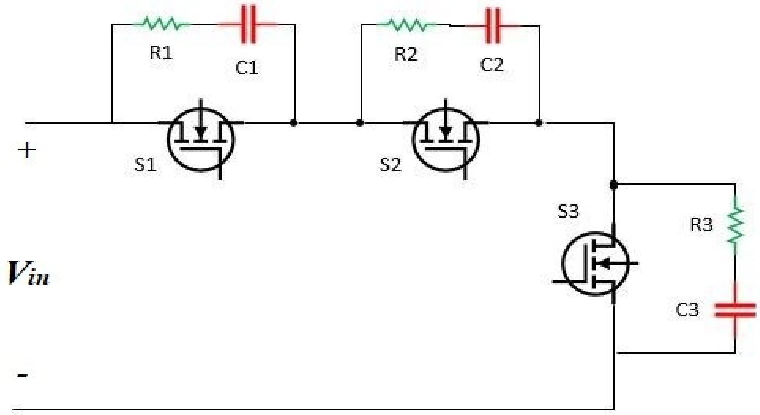

Figure 29. Snubber circuits on SIMO MOSFET's

The resistors (R_1, R_2 and R_3) and capacitor (C_1, C_2 and C_3) are the RC snubber circuits of the three switches composed by the SIMO converter. The values these components are R=10Ω and C=33nF.

3.1.3. Design of the Voltage Divider

A voltage divider bridge is formed of two resistors. This part of the study presents in a simple and clear way the principle and the calculations for a divider bridge. The purpose of the divider bridge is to provide a smaller voltage from a larger voltage. For example, one may wish to create a voltage that is half or one tenth of the original voltage.

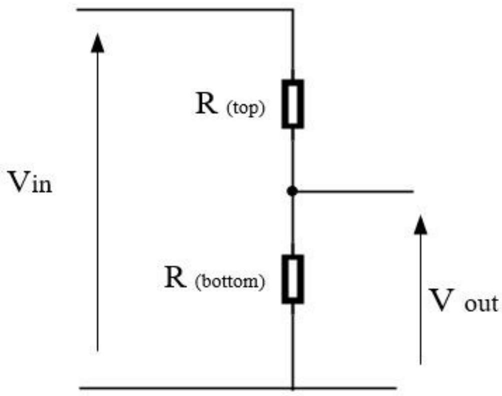

Figure 30. Voltage divider

Vin = input voltage, Vout= output voltage. The voltage divider works properly if no resistor or other dipole is connected to its output. No current therefore leaves the terminal "output voltage". The following equation allows to calculate the output voltage (V_{out}).

$$V_{out} = V_{in} * \left(\frac{R_b}{R_b + R_t}\right) \tag{113}$$

Where R_b and R_t is the resistance bottom and resistance on the top respectivelly. The voltage divider is a fundamental part for the feedback circuits. Microcontrollers such as ARDUINO or DSP can accept analog inputs vary between 3.3 and 5V and on the other side the output voltages of the SIMO converter are about 5 volts and 12 volts. The voltage divider permit to decrease the output voltages in order to make these readable in the analogue pins of the microcontrollers. The voltage divider for the first output (12V) has R_b = 4Ω and R_t =1kΩ and for the second output (5 volt) it has R_b=1kΩ and R_t= 2kΩ.

3.1.4. Mosfet-Coolers

It is necessary to design a cooler to prevent the warming caused by the power losses in the MOSFET elements. Special silicones are used to ensure the maximum thermal conductivity between the connections made by the coolers. For the selection of the cooler the size and thickness are important. Since there is no insulating material and sheath between MOSFETs and the coolers, the resistance can be calculated using these following Equations:

$$R_{\theta,cond} = \frac{\Delta T}{Pcond} = \frac{d}{\lambda A} \tag{114}$$

$$T_j = P_d * R_{\theta C} + T_a \tag{115}$$

ΔT: Temperature difference (Tj-Ta), λ: Thermal permeability of refrigerant, A: Area, d: Thickness. The temperature difference in the designed system was 20^0C and Aluminum was selected as material. Thermal conductivity of aluminum 220W/m^{-1} ^{0}C^{-1}. Thickness of material d = 0.5 cm. If selected, for 200W power.

$$P = \frac{\lambda A(T_2 - T_1)}{d} = 200W \qquad (116)$$

A = 113 cm^2 and the volume is volume = Ax = 56 cm^3. The catalog a cooler with a thermal resistance of Rθ sa (° C/W) = 3.2 would suffice for this study.

3.2. Mosfet Driver Circuits and Logic Circuits

3.2.1. Design of the Implemented Logic Circuits

The logic circuit allows the operation of the state of the switches, from logic gates such as OR NOT and NAND, the operational mode of the different states of three switches are designed. The figure 31 shows the logic circuits diagram performed in Eagle Software.

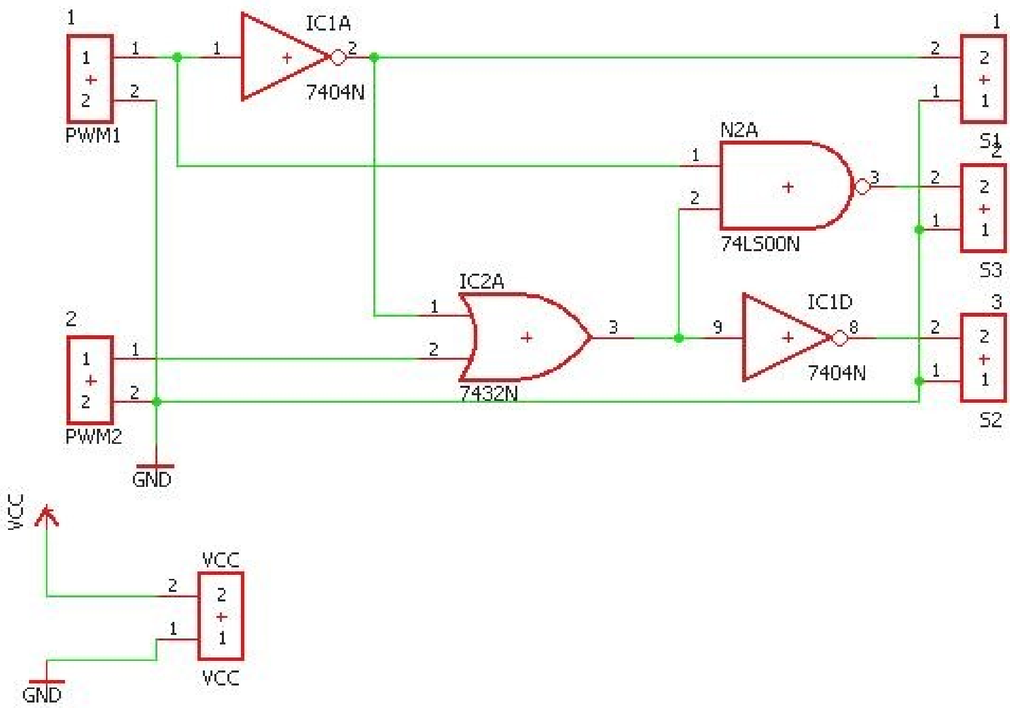

Figure 31. Connection diagram of the proposed logic circuits

In figure 32 , the oscillocope screen shows the different signals of the switches S_1, S_2 and S_3. These signals are suitable with the theory and simulation results.

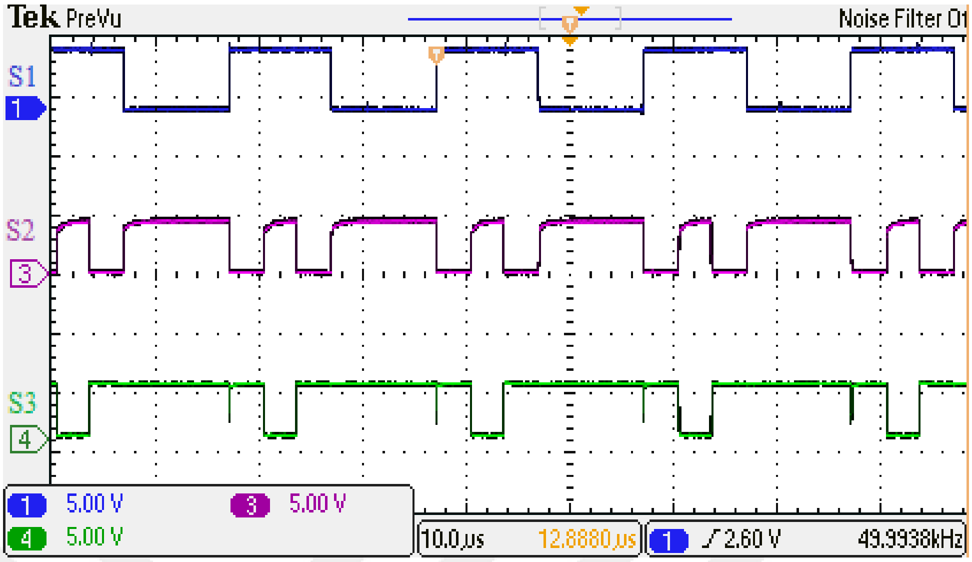

Figure 32. Produced control signals for the switches (S1, S2 and S3)

3.2.2. Dead Time Circuit Modeling

Since the switching event is made at high frequency, the switching elements of the circuit should not turn off at the same time. In other words, the switching element must take a certain time to pass, so the second switch must not pass through before the first switch is turned off. Otherwise, the voltage at the input of the converter will short-circuit for a short time at this transition time. To avoid this situation, there is a short delay time called dead time during these transition times. Thus, after waiting for the delay time when the first switch has been cut off, the signal of the second switch is applied to make the transmission pass. The dead time circuits is composed of two element such resistor (R) and capacitor (C)[65]. The required dead time value are determined by the values of R and C connected to output of the MOSFET driver circuits as shown in Figure 33. It define a quantity called characteristic time of charging of the capacitor (or time constant of the circuit R-C). τ is the time required for the capacitor to accumulate 63% of its maximum charge. In other words, it is the time necessary for the voltage across the capacitor to be equal to 63% of the maximum voltage at its terminals. After a time equal to 5τ it is considered that the capacitor is fully charged (or discharged) since the voltage at its terminals exceeds 99% (or is less than 1%). The values of R and C, which determine the dead time is calculated by the equation given in the equation (117). Accordingly, if R = 150 Ω and C = 4 nF, a dead time of approximately 0.6 μs will be obtained.

$$5\tau = RC \tag{117}$$

In Figure 33, the oscilloscope screen shows the signals obtained by inserting a switching signal from MOSFET driver. The amplified signal coming from the MOSFET drivers (CH3) is conducted into the dead time circuits. On the oscilloscope (CH1) shows the outputs with dead time circuits as seen in Figure 33.

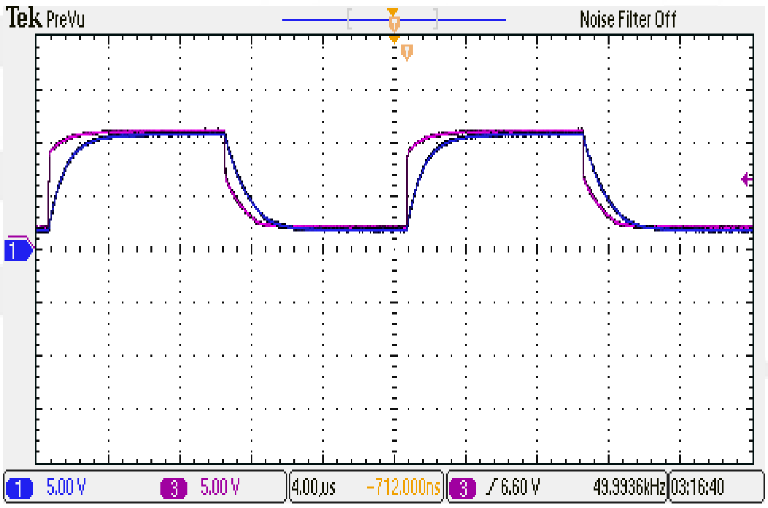

Figure 33. Dead time circuit effect on the switching signal

3.2.3. Design and Implemented of MOSFET Driver Circuit

FET (Field Effect Transistor) technology was invented in the 1930s. This technology is older than that of the bipolar transistor [66]. MOSFET (Metal Oxide Semiconductor Field Effect Transistor) is a special type of FET and it is the main element of high efficiency, high frequency application in the modern electronics industry. MOSFETs has three terminals: a gain, a drain and a source.

IRFP064 type MOSFET is one of the third generation power MOSFETs manufactured by Vishay Trade Company. It is a voltage controller and has a lot of advantage such us low on-resistance$R_{DC(on)}$, fast switching and cost-effectiveness [67]. The datasheet of this

MOSFET is given in appendix. The current flows across the source and the drain terminals. The gate voltage controls this current. In order to turn on this MOSFET some voltage source is required between gate and source. This gate-to-source voltage is called threshold voltage $V_{GS\ (th)}$ and it is given in datasheets of MOSFETs. $V_{GS\ (th)}$ should be less than maximum gate-to-source voltage V_{GS} defined in the datasheets. The following Figure 34 shows the IRFP064 MOSFET that is used in the system.

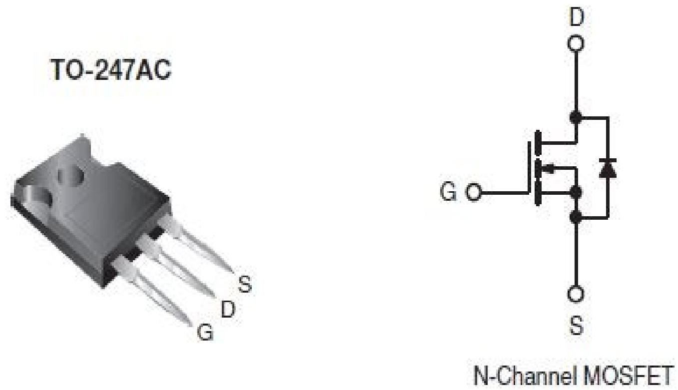

Figure 34. IRFP064 MOSFET circuit

A capacitor is formed in the isolated gate-electrode of the MOSFET. This capacitor (gate capacitor) is charged and discharged each time that the IRFP064 is turned on and off respectively. In order to turn on the switch a gate voltage is required then the gate capacitor is charged. When the MOSFET is turned off, the gate capacitor is discharged. Therefore, this charge must be dissipated. For that, a gate driver is required, mostly for high frequencies.

The integrated circuit of the drivers translate a complementary metal-oxide semiconductor (CMOS) or Transistor-to-Transistor Logic (TTL) signals into a higher current and voltage. The microcontrollers such us Arduino or DSP have maximum output voltage pulses around 3.3 to 5V so this can be driven only MOSFETs that have a small-signal logic level. The signals delivered by a microcontroller is not enough to drive large MOSFETs. This kind of MOSFETs usually needs around 8 to 12V to be turned on because they have higher gate capacitance.

The aim of MOSFET drivers are rapidly and fully switching the gate of the MOSFET and they are designed to handle back current because during the switching of MOSFET a back current coming from the gate of the MOSFET goes to the drivers. In this study, three switches (S1, S2, and S3) require MOSFET drivers. For S_1 and S_2 high side drivers and S3 low side drivers. The following figure shows the schematic diagram of the high-side driver IR2117 that is used for MOSFETs S_1 and S_2.

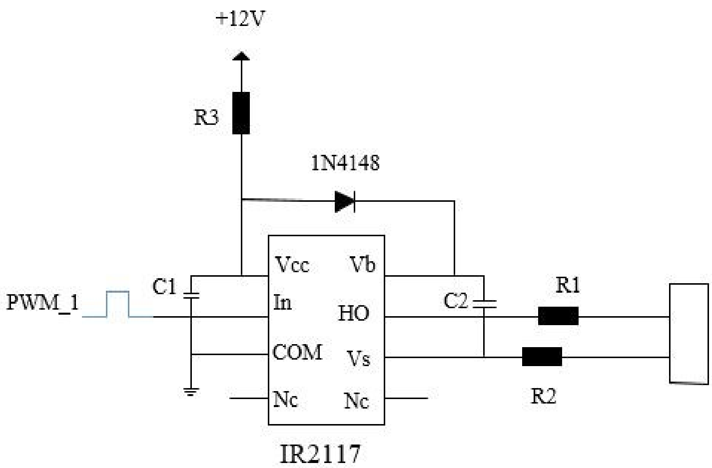

Figure 35. Hight side MOSFET driver circuit with IR2117

The Figure 36 shows the screen of the oscilloscope for the input signal coming on the microcontroller (CH3) and the amplified signal of the MOSFET drivers (CH1). The MOSFET driver IR2117 permit to increase the voltage in order to trigger the MOSFETs.

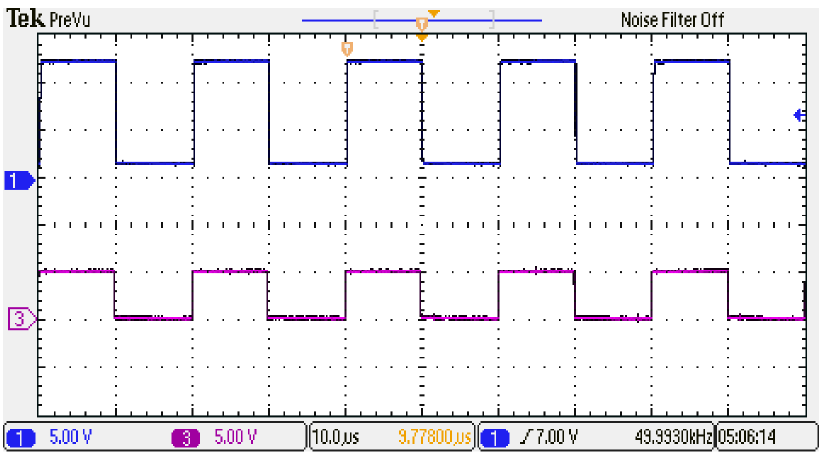

Figure 36. Produced control signals (CH3) and amplified state for switch 1 (CH1)

The output of the MOSFET driver is added with a RC dead time circuits . The Figure 37 shows the the input signal (CH3) and the amplified signal with dead time (CH1).

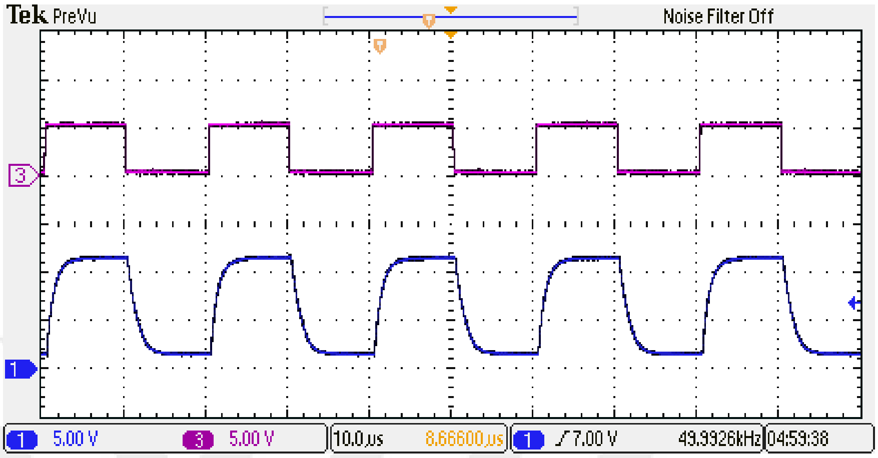

Figure 37. Produced control signals (CH3) and amplified state for switch 1(CH1) with dead time

The MOSFET driver IR2117 is used for switch 1 (S1) and the switch 2 (S2). Therefore for the second switch the input pulse coming from the logic circuit specially from the OR gate and the amplified signal of the mosfet drivers are shown in Figure 38.

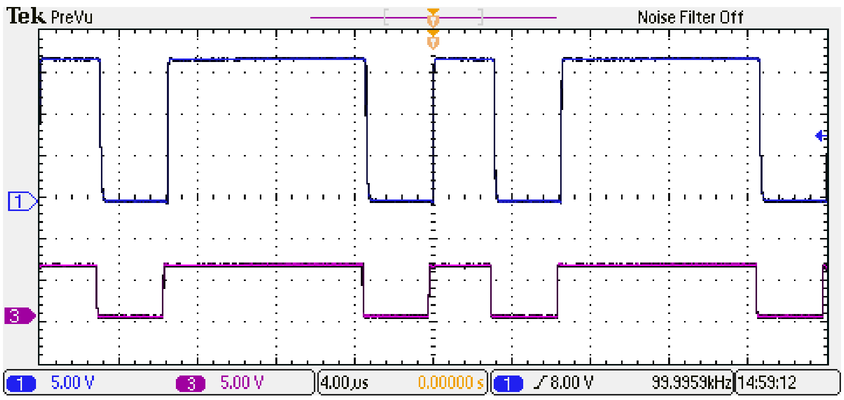

Figure 38. Produced control signals (CH3) and amplified state for switch 2 (CH1)

The Figure 39 shows the output of the MOSFET driver for the switch 2 (S2) with dead time circuit.

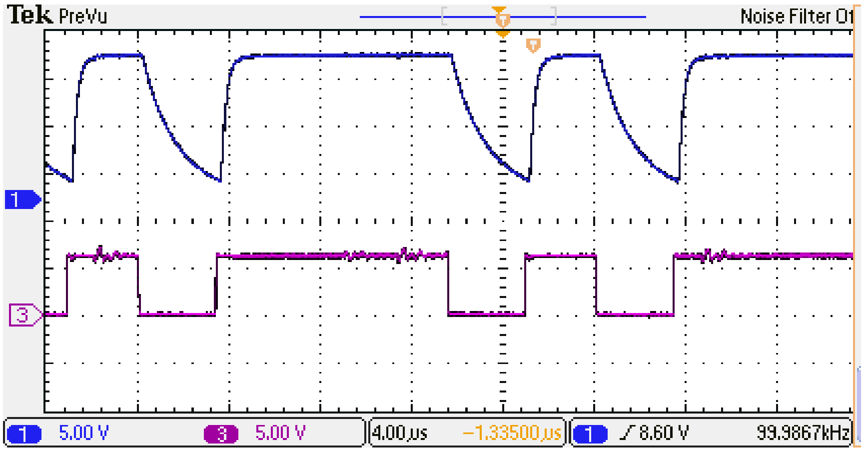

Figure 39. Produced control signal (CH3) and amplified state
for switch 2 (CH1) with dead time

In this study, three switching MOSFET’s (IRFP064) are used. First and second switches are driven by IR2117 MOSFETdriver. When the MOSFET (that you're using as a switch) flows current, it is a low-side switch. For that the load will be between the drain and +Vin supply. The source will be connected to ground. Gate will be driven with respect to ground. The switch 3 (S3) is driven by a low side driver. İn this study instead of using an integrated MOSFET drivers such as IR2110 or others, by using BC337 amplifier transistors a low side driver is built. The following figure shows the circuits diagram of low side MOSFET driver circuit with BC337 amplifier transistors.

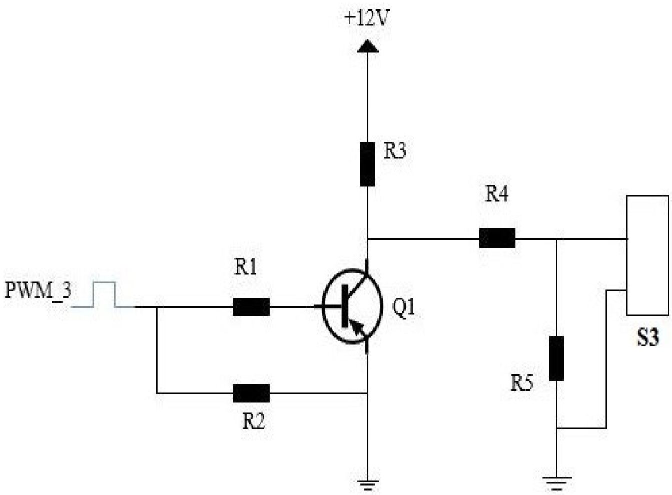

Figure 40. Low side MOSFET driver circuit
with BC337 amplifier transistors

The Figure 41 shows the screen of the oscilloscope for the switch 3 (S3). These are the signals produced and amplified using the MOSFET driver.

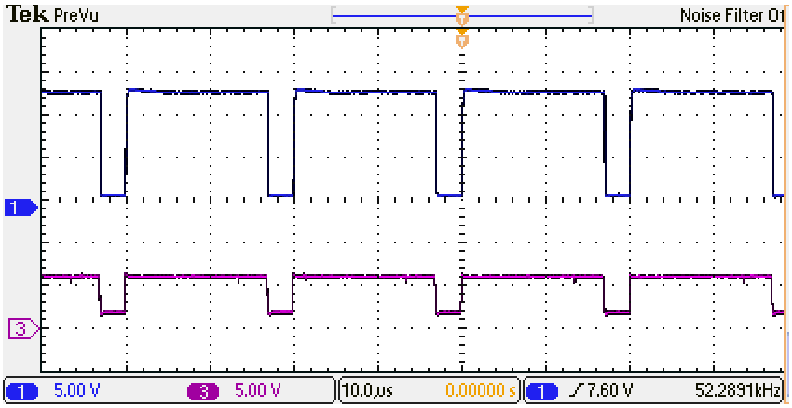

Figure 41. Produced control signals (CH3) and amplified state for switch 3 (CH1)

3.2.4. Selection of the Optocoupler

High speed optocoupler such as 6N137 is a component that enables the transfer an electrical signal between circuits while keeping them electrically isolated from each other. The goal of an optocoupler is to provide isolation meaning the protection between the input voltage and the output voltage. It has a high speed of 10 MBit/s and +5 V CMOS compatibility. This component gives the output voltage pulses that goes through the drivers. This output must be higher than the input pulses coming from the microcontroller because some drivers accept high pulses. Figure 42(a) is the typical connection of the optocoupler as given in the datasheet [68] and the Figure 42(b) is the picture of the optocoupler.

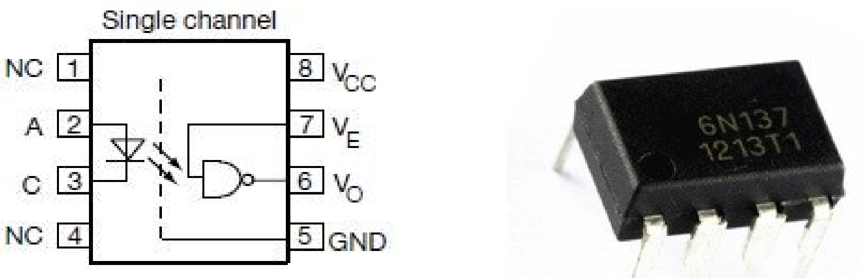

(a) (b)

Figure 42. 6N137 hight speed optocoupler: (a) single channel circuit, (b)6N137 optcoupler picture

The Figure 43 shows the 6N137 high speed optocoupler circuit diagram.

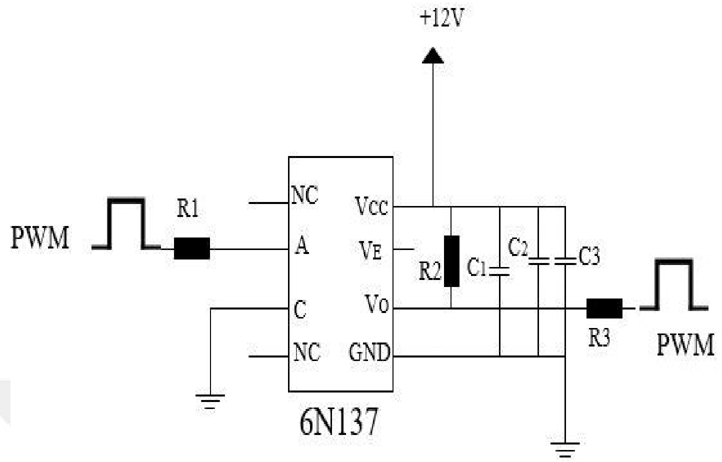

Figure 43. Optocoupler (6N137) application circuit diagram.

3.3. The Designed SIMO Converter and Driver Circuits

The design and implemention of the converter is the most important part of this study. The designed SIMO DC-DC buck converter circuit diagram is given in Figure 43. In this circuit, damping RC type (snubber) circuits are added. These circuits help to make the output signal smoother while reducing high switching losses. Fuses have been added to protect the system from excessive and short circuit currents. Both parallel arms are designed independently of each other and parallel connections will be made through the input and output connectors. Gate 1, 2 and 3 are the gates of the MOSFET drivers. DSP 1 and DSP2 are feedback outputs used in microcontroller.

The completed circuit is shown in Figure 44. The MOSFETs elements in the circuit are connected to coolers. MOSFETs with a very small R_{DS} value and 100V-50A nominal value have been chosen .

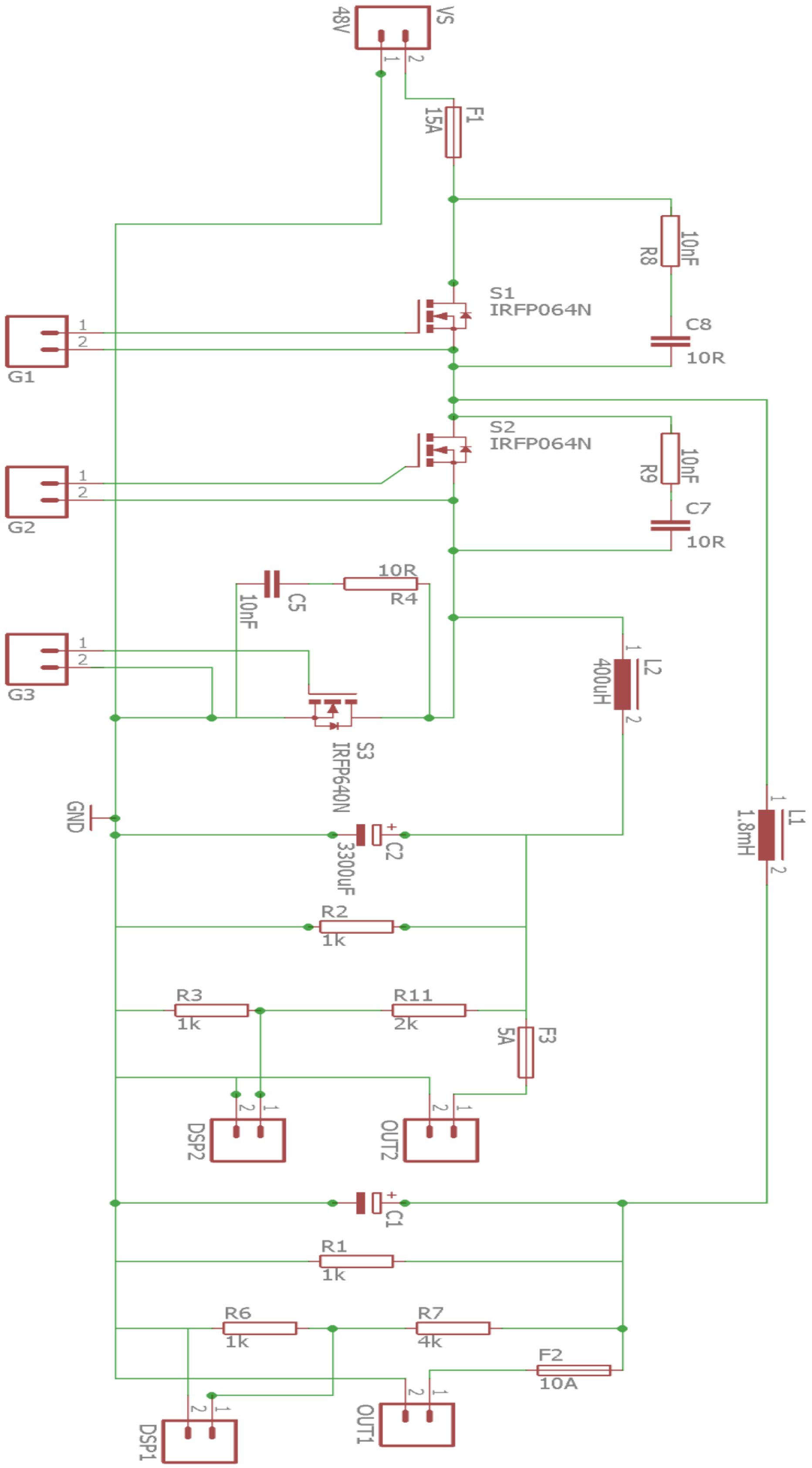

Figure 44. Simulink diagram of the designed SIMO converter circuit diagram

Two types of inductors surrounded by a special Litz wire previously designed and adjusted to 8.5mH and 400µH are placed in the center of the ferromagnetic core type E and mounted on the circuit. These inductors have been put at the farthest point to try to avoid electormagnetic interaction or interference. The circuit diagram of the designed and realized SIMO DC-DC buck converter circuit is shown in Figure 45 and the printed circuit board (PCB) of the converter are shown in Appendix 3.

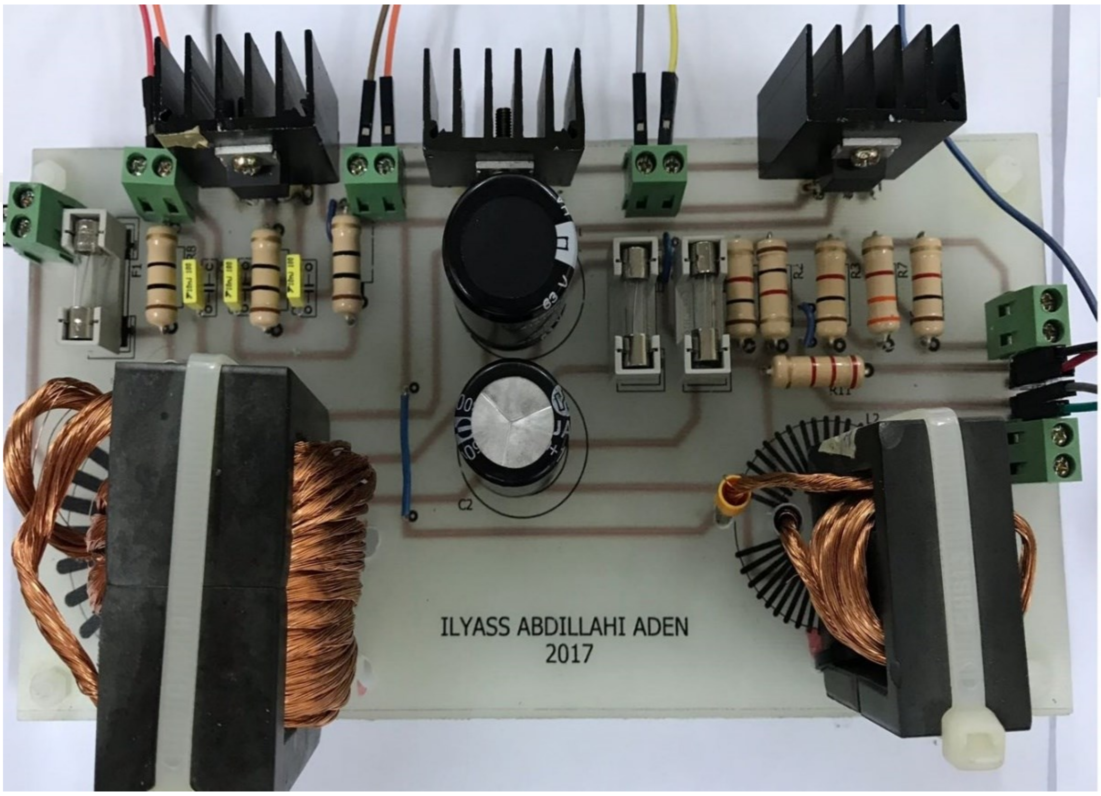

Figure 45. Designed and realized SIMO DC-DC buck converter circuit

3.4. Design and Implementation of MOSFET Drivers

The design and the implemenation of the driver circuits are very important since the SIMO converter have three MOSFETs. Logic circuits are directly connected to the microcontroller. The output of the logic circuits dictates the state of the switches as presented in the section 3.2.1. However, the pulses coming from the logic circuits are around 2.7 to 5 volt and they are not enought to trigger the MOSFET drivers. Beside this to protect the microcontroller from the other circuits whose are working at high voltage a high-speed opotocouplers are used. As explained previously optocoupler feed the MOSFET drivers at their required voltage and protect the microcontroller. The opotocoupler are connected to MOSFET drivers. In the end, dead time circuits composed of R and C are implemented in order to prevent the short circuit. MOSFET drivers circuit for three switches is shown in Figure 46. and print board of the MOSFET drivers in Appendix 4.

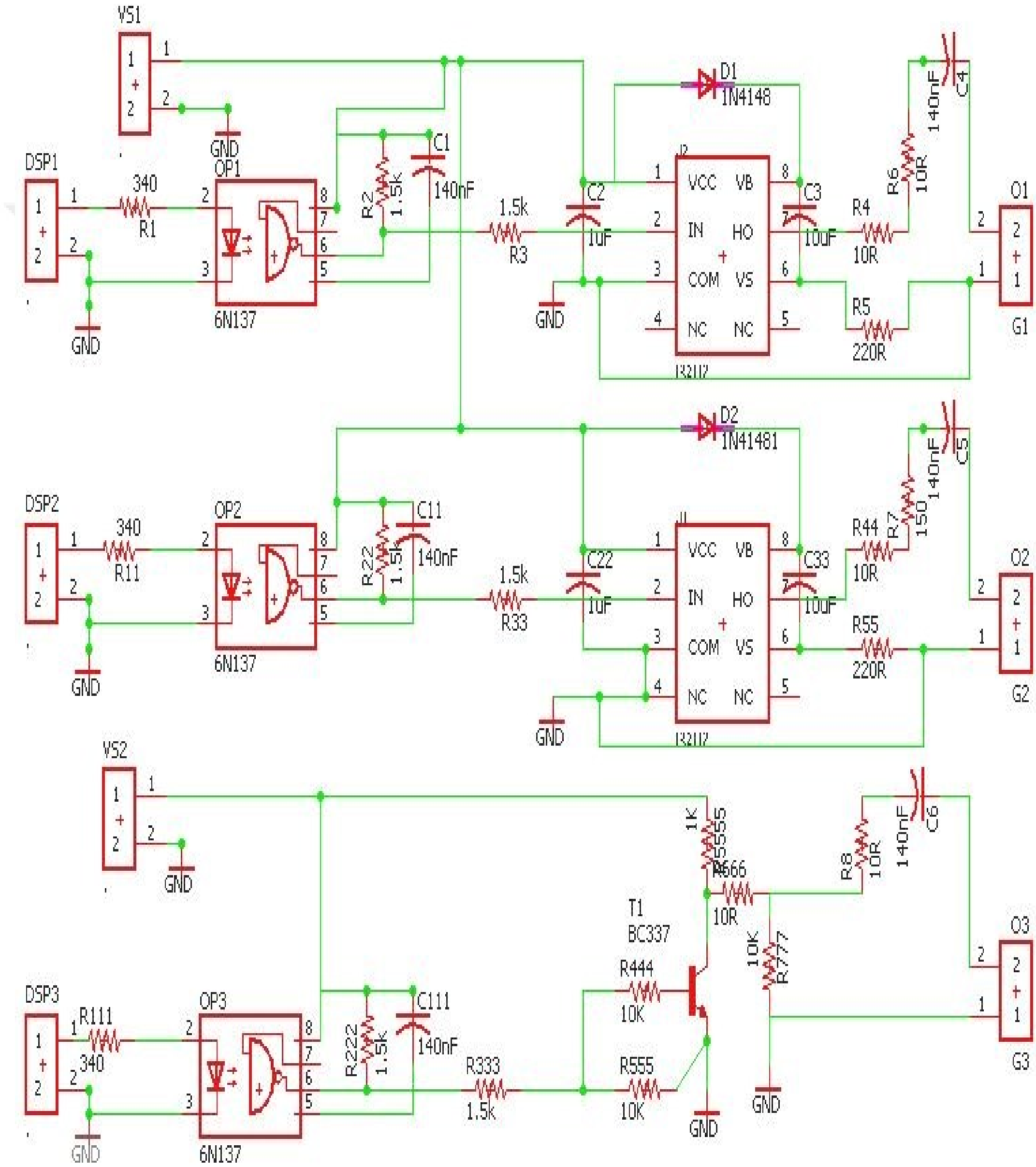

Figure 46. MOSFET drivers circuit for three switches

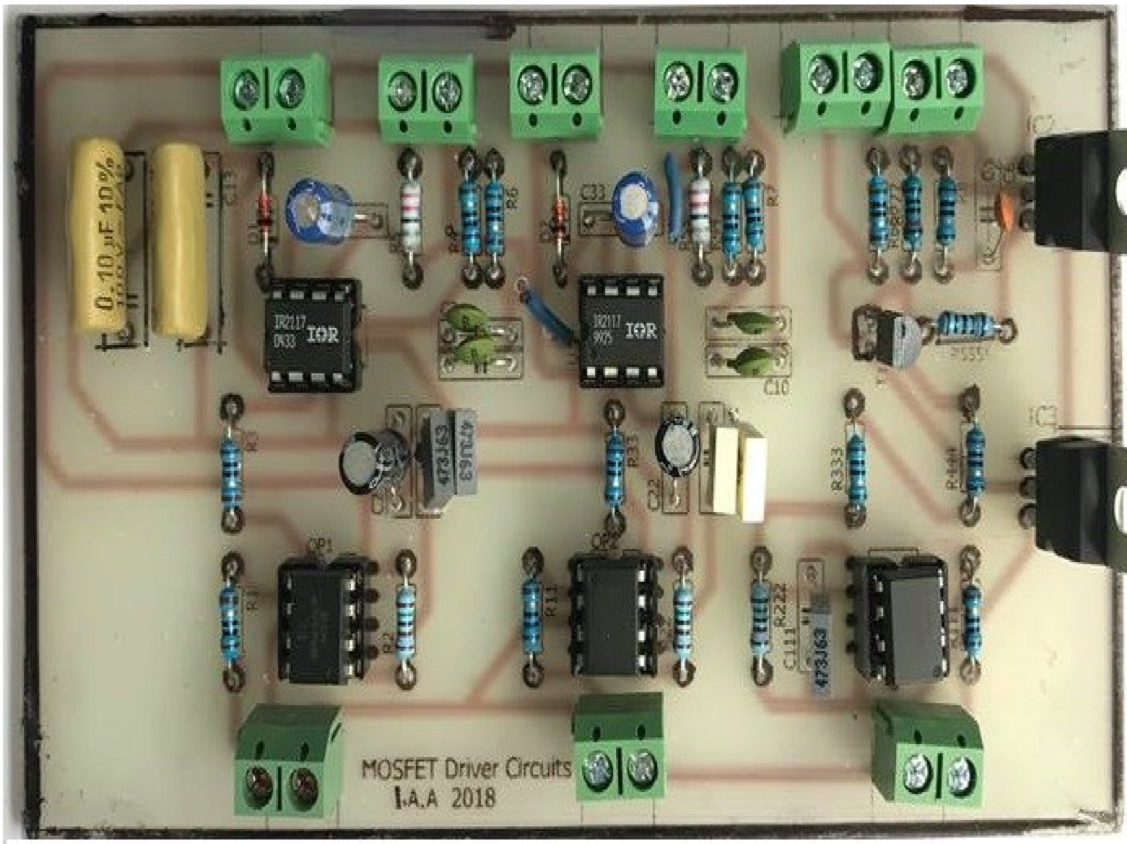

Figure 47. Designed and realized Mosfet driver circuits

3.5. Isolation Circuits

The switching of the MOSFETs are guaranteed by the MOSFET drivers. However, each drivers provide two outputs signals. First one is high side driver signal and the other is negative signal coming from the V_S. However, these negative signal coming from the IR2117 drivers are ground signal and can generate some short circuits problems. Because of difference ground between the mosfet drivers and the single input and multiple output buck converter the system exposed to a short circuit . To overcome this ground problem, isolation circuits are designed as shown in Figure 48. The print board of isolation circuit is shown in appendix 1.

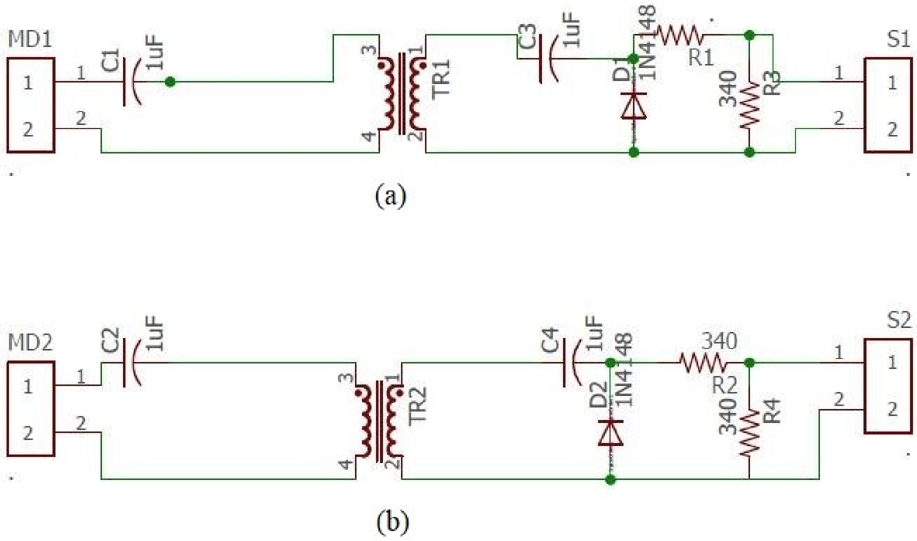

Figure 48. Isolation circuits for S1 and S2

For the isolation circuit toroid cores are used. The turns are calculated and turned around a core and tested.

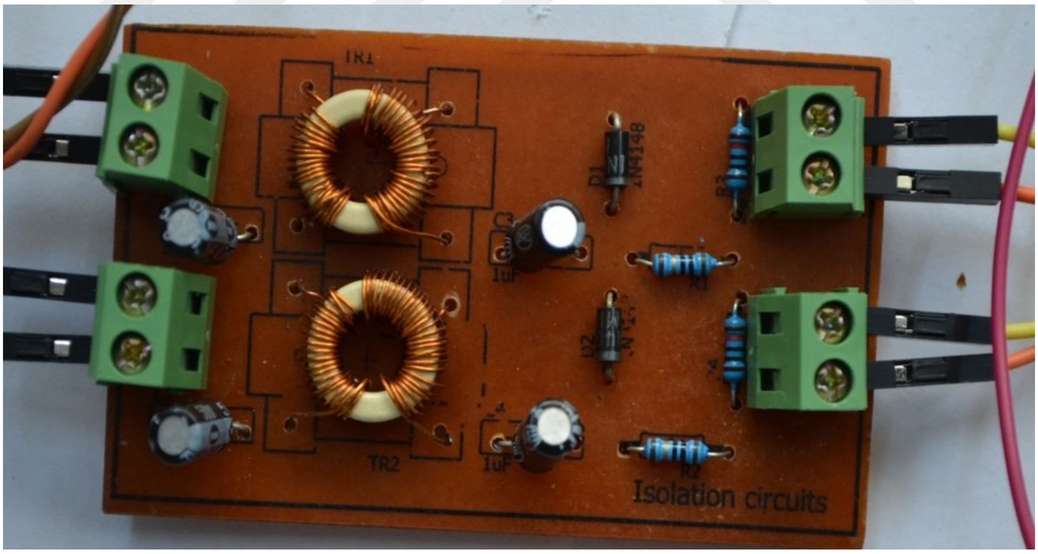

Figure 49. Designed and realized Isolation circuits for S1 and S2

Figure 50. Designed and realized logic circuits

3.6. Control System Implementation on Microcontroller

The microcontroller used in this thesis is Arduino Uno. The operating principle of the Arduino is as follows: first, the output voltage coming from the volatge divider goes into the analog input. However, from the analog inputs a small voltage are read. Therefore, in order to find the output voltage of the single input multiple output DC-DC step-down converters, an analog-to-digital converter (ADC) is used as seen in Figure 51. This allows giving the normal output voltages. Two-pulse width modulation (PWM) signals are coded in Arduino. These have frequency of 50 kHz. In addition to the Arduino coding program, an integral proportional (PI) controller is encoded. This controls the systems and makes them stable in their required outputs.

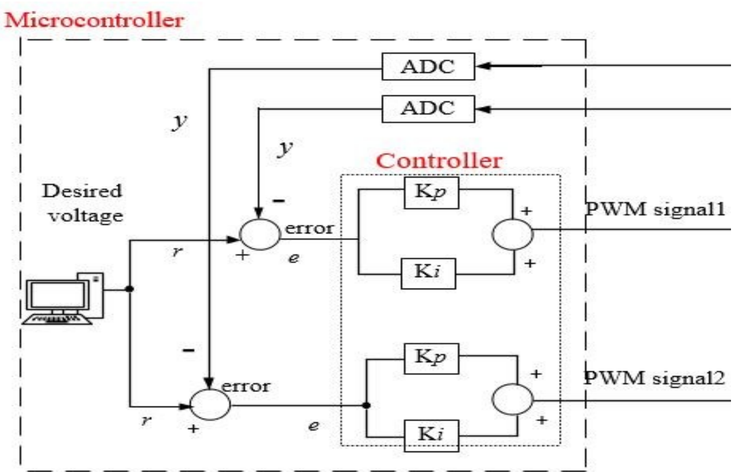

Figure 51. Control system diagram in the microcontroller

3.7. General Structure of the SIMO Converter System and Results

In the previous section, SIMO DC-DC buck converter, the logic circuits, the MOSFET drivers and arduino were explained in details. In order to give a summary, a block diagram which includes the whole system (SIMO, driver circuits, Microcontroller..ect) is designed as in Figure 52.

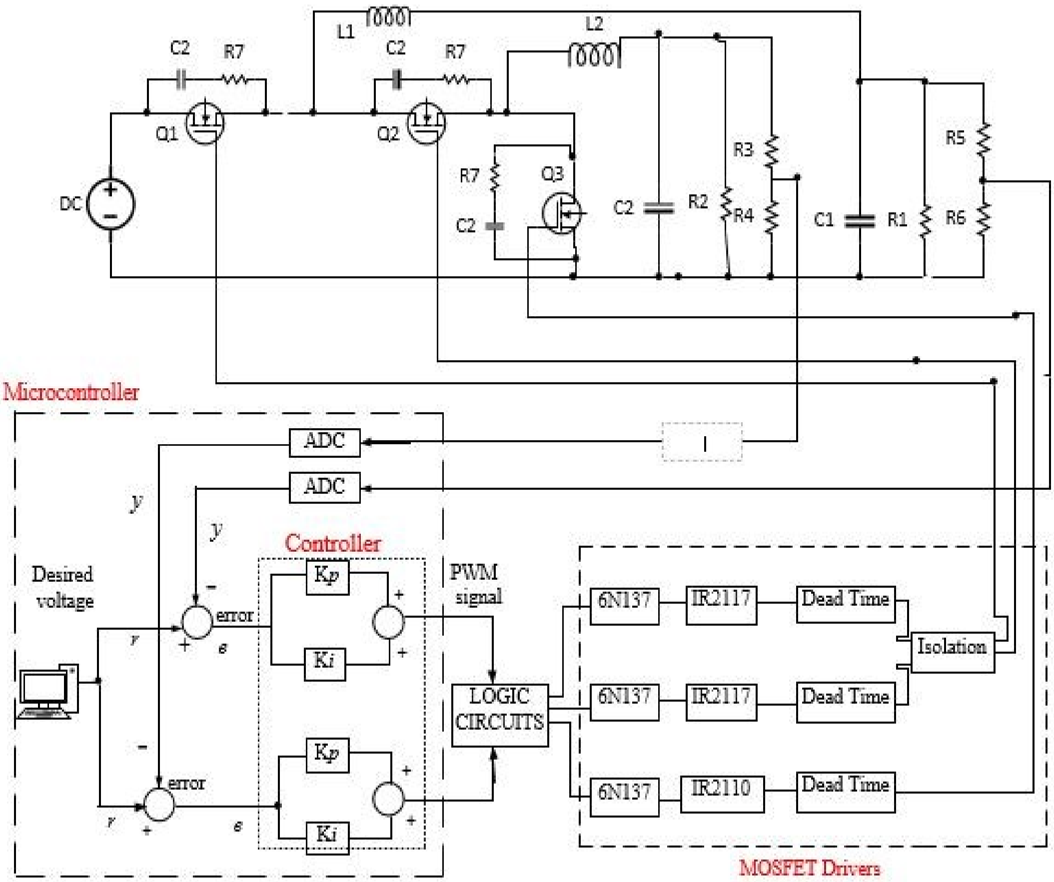

Figure 52. General structure of the SIMO converter

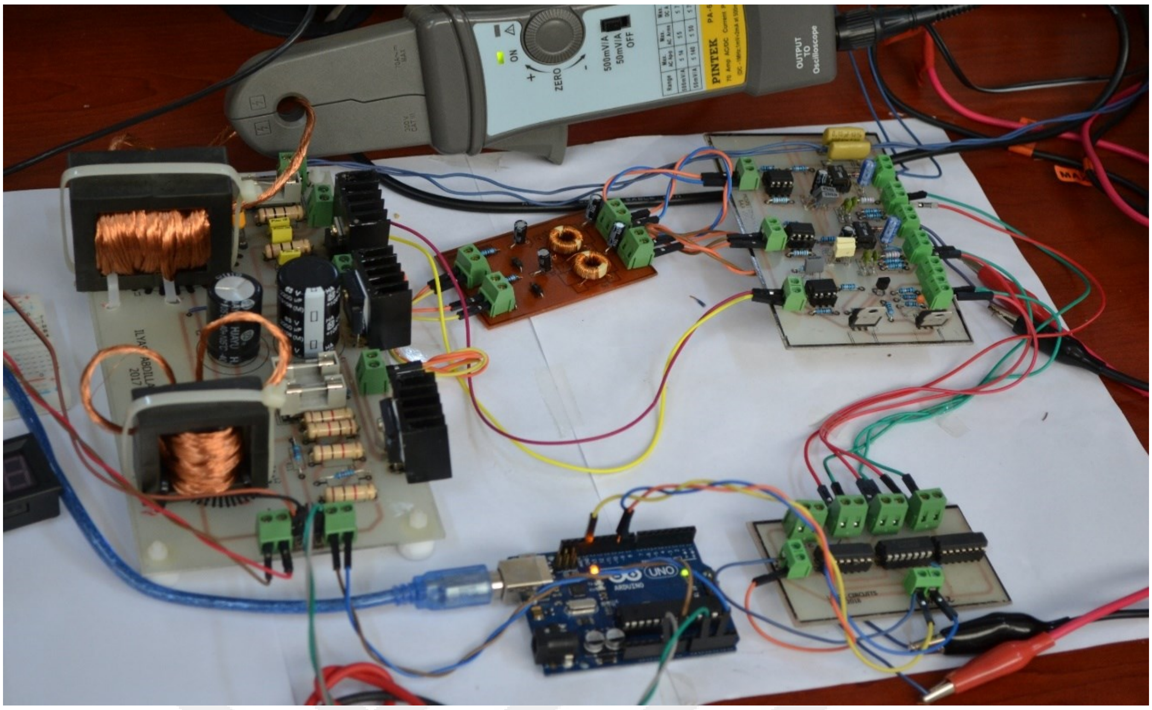

(a)

(b)
Figure 53. Experimental Setup (a) SIMO converter close-up view ; (b) far out view of the system

4. RESULTS AND DISCUSSIONS

Current R_1 and R_2 load is shown in Figure 54 (a, b) respectively when both loads are equal to 1Ω. When load is increased to R_1= R_2 =1.5 Ω, it can observe that the output current decrease as shown in Figure 55 (a, b). This implies that the output currents depend on the load. When the load is increased, the current decreases. Similarly when the load decreases, the current increases.

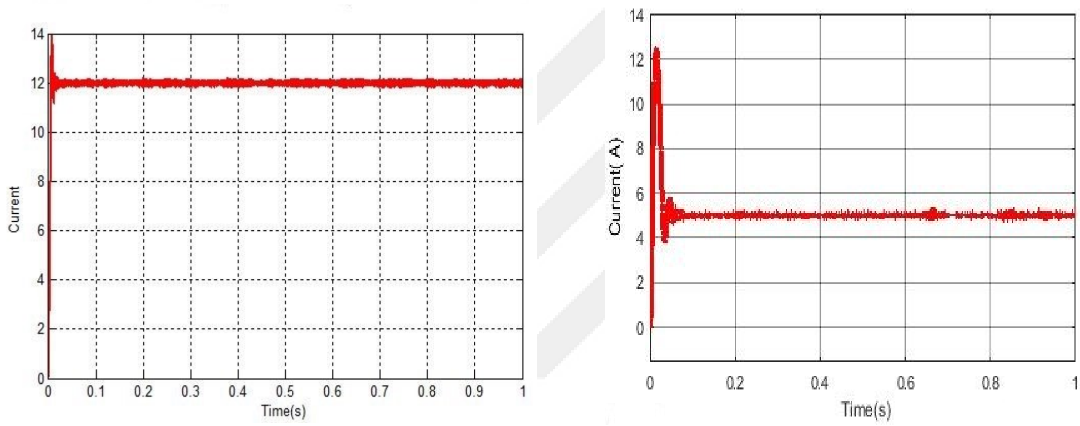

(a) (b)

Figure 54. The current as a function of loads: (a) Load R1=1 Ω (b), Load R2=1 Ω

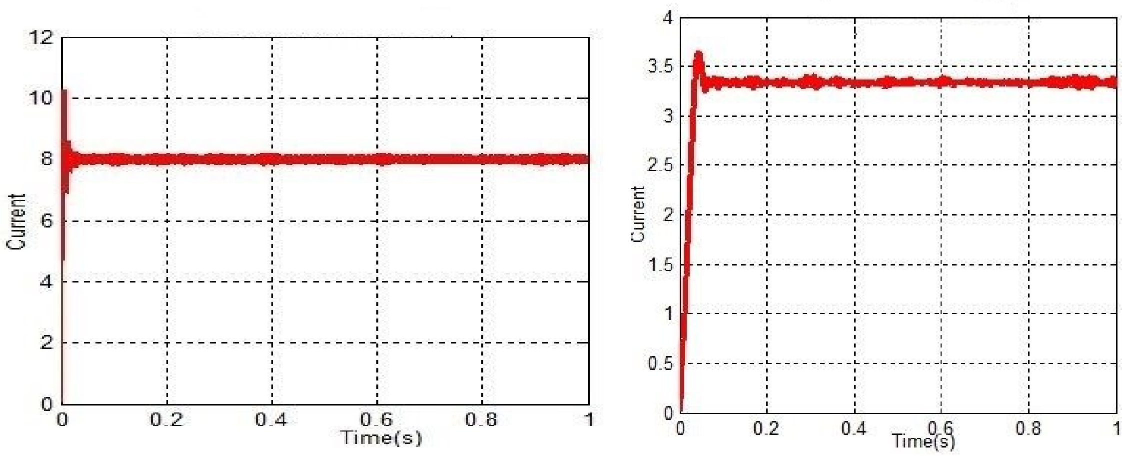

(a) (b)

Figure 55. The current as a function of loads: (a) Load R1=1.5 Ω (b), Load R2=1.5

The Figure (56) show the current and the voltages of the inductances L_1 at different level of voltages. The signals in (CH4) and (CH1) in Figure 56(a, b) are respectvely the currents and the voltages of inductance. The frequency of the system is 50kHz. The results presented in the following figures are taken under the load. The difference between this two oscilloscope results are the input voltages. The Figure 56(a) and 56(b) have respectivelly 48 and 30 V.

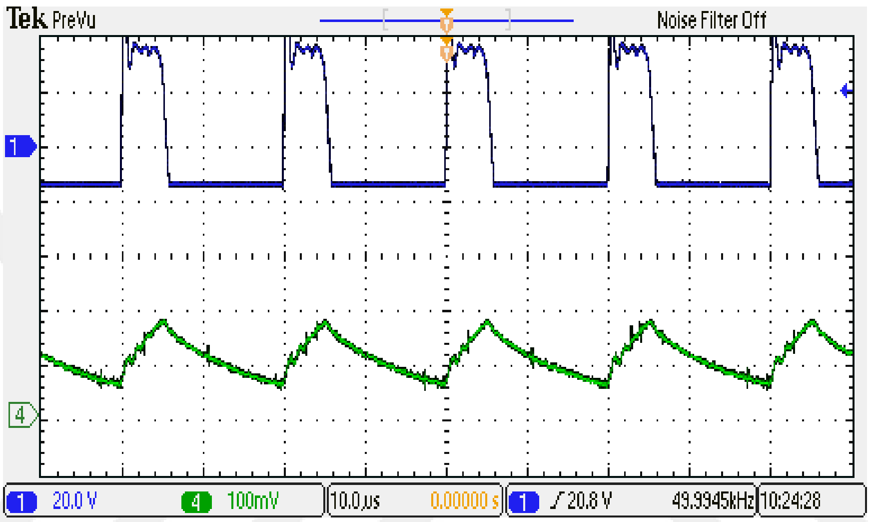

(a)

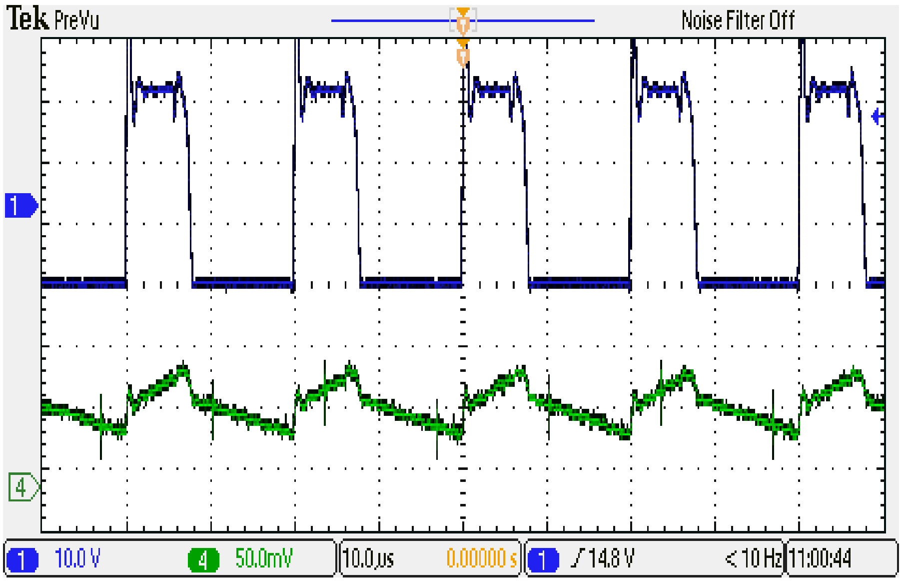

(b)

Figure 56. Current and volatge in Inductance L_1: current (CH4); volatge (CH1)

Same as in the Figure (56), the screen of the oscilloscope shows the currents and the voltages of the inductances L_2 at different level of voltages. The signals in (CH4) and (CH1) in the Figure 57(a, b) are respectvely the currents and the voltages of inductance.
The frequency of the system is 50kHz. The results presented in the following figures are taken under the load. The difference between this two oscilloscope results are the input voltages. The Figure 57(a) and 57 (b) have respectivelly 48V and 30 volts.

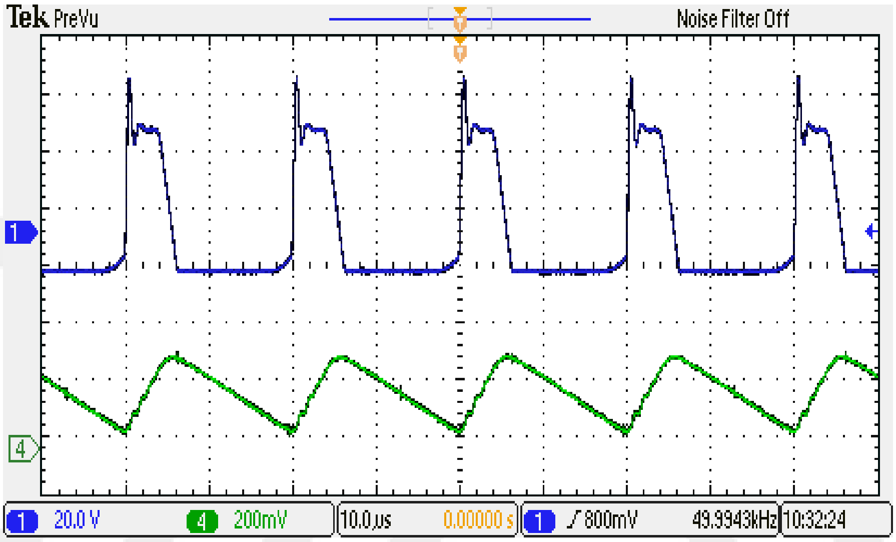

(a)

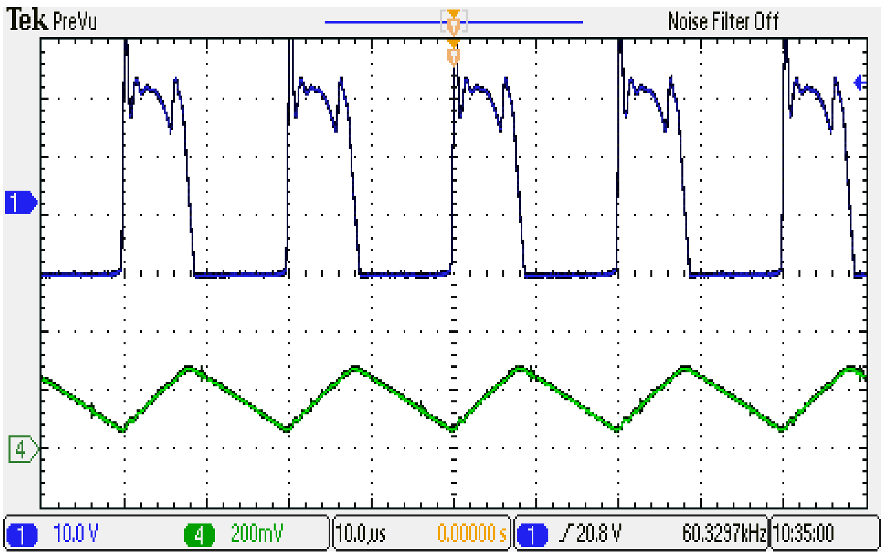

(b)

Figure 57. Current and volatge in Inductance L_2: current (CH4); volatge (CH1)

Figure 58 (a, b) shows the result of simulating and experimenting of the system with an input voltage of 48V. The Figure 58(a) is the simulation results of the SIMO converter performed in Matlab. The input voltage is drawn in blue color, the outputs are drawn in red (12V) and pink (5V). The experimental results is shown in figure 58(b). Input voltage is shown on (CH1) and outputs voltages in (CH3) (12V) and (CH4) (5V).

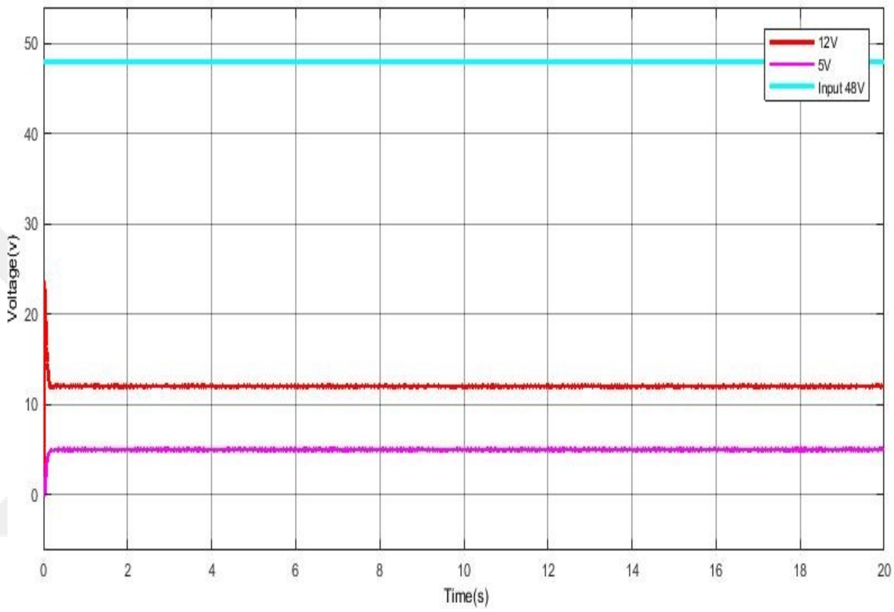

(a)

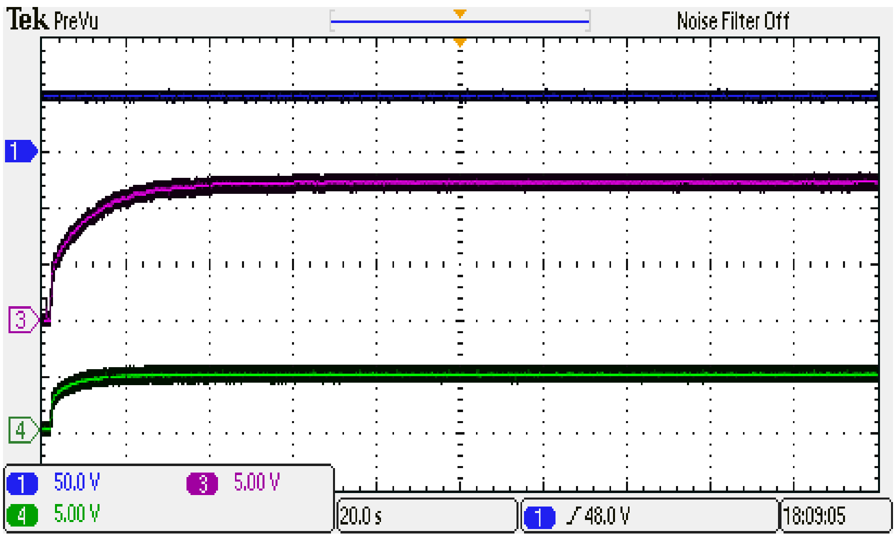

(b)

Figure 58. Comparison of output voltages : (a) Simulation results, (b). Experimental results

Figure 59 (a, b) shows the result of simulating and experimenting of the system with an input voltage of 30 V. The Figure 59(a) is the simulation results of the SIMO converter performed in Matlab. The input voltage is drawn in blue color, the outputs are drawn in red (12V) and pink (5V). The experimental results is shown in figure 59(b). Input voltage is shown on (CH1) and outputs voltages in (CH4) (12V) and (CH3) (5V).

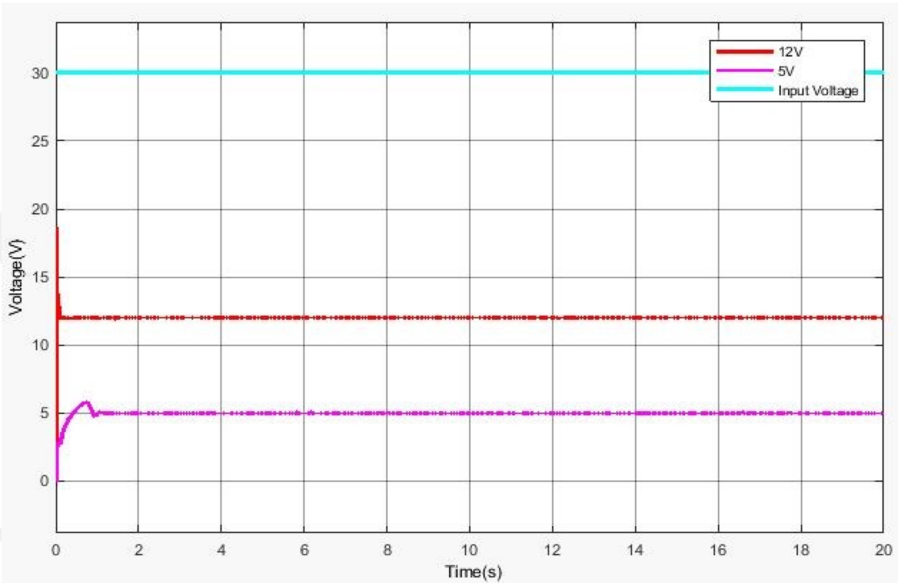

(a)

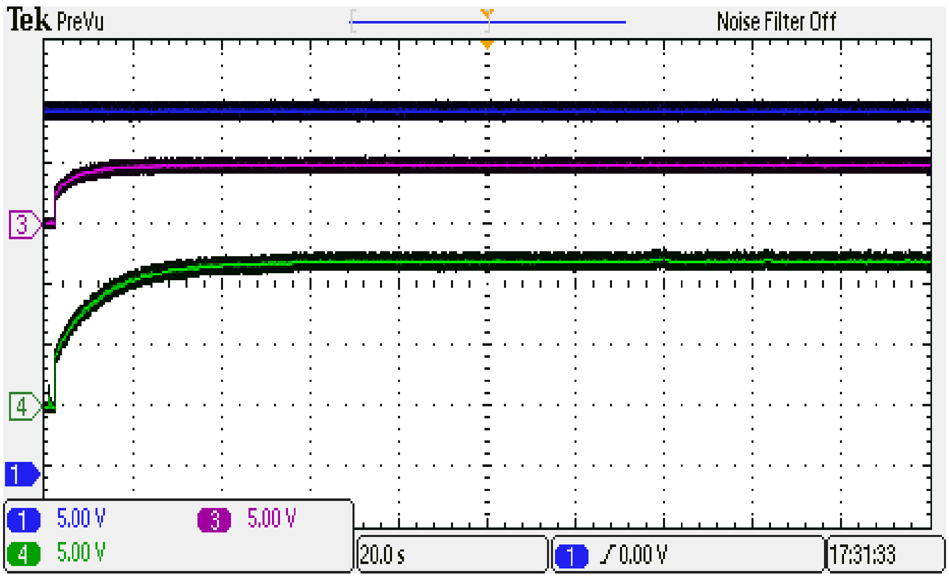

(b)

Figure 59. Comparison of output voltages : (a) Simulation results, (b) Experimental results

The results obtained through the experiments are the same as those obtained in simulation for the different inputs. We have seen that in simulation, the output voltages reached their required values with a very short settling time. However, in experimentation, the output voltages reach their values around 1 to 2 seconds. The control method used to adjust the output voltages is a Proportional Integral controller. It can be revised using another controller such as fuzzy logic to obtain a very short settling time.

5. CONCLUSION

This study introduces theoretical concepts and presents overall discussions to the field of Single Input Multiple Output (SIMO) DC-DC buck converters. First, the converter topology, operational modes and modulation techniques were presented. Similar analysis, which was carried out in the section 2.1, is performed on the topology presented in the same chapter for determining the transfer function of the system.

The simulation of the system were performed using Matlab/Simulink software. However, simulation does not always match implementation. The first issue that caused problems was the MOSFETs drivers that we had chosen. These drivers had all the ideal functions and would were perfect for the implementation. However, the logic supply voltage for each drivers were 10V and from the ouput of the logic circuit, we had 2.7 to 3V. Therefore, in order to supply these drivers and to protect the microcontroller from the other circuits whose are working at high voltage an optocoupler were used. Although there were, many problems involved with the implementation process of this Single input multiple output DC-DC buck converter like ground problems between the MOSFET drivers and SIMO converter. Several MOSFETs were rendered useless when the circuit was in operation because of the ground problems, which caused shortcircuits. For that, Isolation circuits were designed in ordor to separate the grounds of the driver circuits and the SIMO buck converter used in this study. The values of the inductances, dead time circuits, snubber circuits and the SIMO DC-DC buck converter were calculated using different process. There are some other problems that we encountered like shipping delays, faulty components and difficulty when translating the designed schematics to the physical board. Simulation and experimental results were presented in this study. At the end, by comparing the simulation and experimental results, following observations are made: Results obtained through the experiments carried out in the laboratory are identical to those of simulation results. The presented SIMO converter has a disadvantage of having power switches with higher current ratings. Furthermore, the advantages of this configuration include reduction of the number of driver circuits, and better power loss distribution among the switches. The experience was enlightening and challenging at the same time.

6. Future Work

Realization of the presented Single input Multiple Output DC-DC buck converter in software and hardware are considered in this thesis. MATLAB simulations have validated the theoretical of the non- isolated SIMO converters, but it is always interesting to study whether their practical implementation would be effective for a specific application such as the DC distribution system of a smart home with several DC sources and loads at different voltage levels. During this study, solar energy was presented as the main energy used in the system. However, we used the energy stored in the solar battery, not directly the solar energy. It would be advantageous to connect the SIMO converter to the solar energy system, and then look the difference when you connect the converter to the battery and when you are connected directly to the solar system.

In the future, it would be beneficial to eliminate the noise associated with the circuit. There was no significant work in minimizing the noise in the circuit while attempting to implement a working circuit both quickly, and efficiently. There are very few downsides with taking the time and effort to design filters to decrease the inherent noise found in a switching circuit.

There were several problems encountered throughout the implementation of the single input multiple output DC-DC buck converter that we would like to prevent in the future. Firstly, the amount of the time spended for the design and implementation was not sufficient. It would have been beneficial to spend more time testing rather than taking the time to make sure that each part was the ideal one for the circuit. Secondly, better time management will be a key success that should definitely be worked out for future reference.

PI controller is employed with the SIMO converter. In order to improve the control of the systeme some other controllers like fuzzy logic can be used. Since the converter configuration posses several advantages and has an innumerable applications, introducing this product into the market would be a game changer. To make the implementation of these circuits as a product some additional analysis has to be done in this area such us developing new control strategies, Thermal analysis, testing the operating limits and tests to evaluate the life expectancy of the equipement.

7. REFERENCE

1. Aldabas, E., Ortega, J. Rosero, J. and Romeral, L., Moving towards a more electric aircraft, IEEE Aerospace and Electronic Systems Magazine, 22, 13, March 2007, 3-9.

2. Urtasun, A., Sanchis, P. and Marroyo, L., Adaptive voltage control of the DC/DC boost stage in PV converters with small input capacitor, IEEE Trans. Power Electron, 28,11, (2013), 5038–5048.

3. Kempton, W. and Tomi, J., Vehicle to-grid power implementation: From stabilizing the grid to supporting large-scale renewable energy, Journal of Power Sources 144 (2005) University of Delaware, Newark, DE 19716, USA, 280–294.

4. Femia, N., Petrone, G., Spagnuolo, G. and Vitellio, M., Optimization of Perturb and Observe Maximum Power Point Tracking Method, IEEE Trans. Power Electronics, 20, 4 (2005) 963–973.

5. Ghodke, D., Chatterjee, K. and Fernandes, B., Modified soft-switched three-phase three-level dc–dc converter for high-power applications having extended duty cycle range, IEEE Trans. Ind. Electron,59, 9, (2012), 3362–3372.

6. Tan., Abe, N.M.L.T. and Akagi, H., Design and performance of a bidirectional isolated dc–dc converter for a battery energy storage system, IEEE Trans. Power Electron, 27, 2, (2012), 1237–1248.

7. Ouyang, Z., Zhang, Z., Thomsen, O.C., Andersen, M.A.E., Planar-integrated magnetics (PIM) module in hybrid bidirectional DC–DC converter for fuel cell application, IEEE Trans. Power Electron, 26, 11, (2011), 3254–3264.

8. Ouyang, Z., Zhang, Z., Thomsen, O.C., Andersen, M.A.E., Analysis and design of a bidirectional isolated dc–dc converter for fuel cells and super capacitors hybrid system, IEEE Trans. Power Electron, 27, 2, (2012), 848–859.

9. Yang, K., Jin, K., M, Xu. and Ruan., Power management for fuel-cell power system cold start, IEEE Trans. Power Electron, 24, 10, (2009), 2391–2395.

10. Wang, L., Wang, Z. and Li, H., Asymmetrical duty cycle control and decoupled power flow design of a three-port bidirectional DC–DC converter for fuel cell vehicle application, IEEE Trans. Power Electron, 27, 2, (2012), 891–904.

11. Rathore, A. K. and Prasanna, U. R., A novel single-reference six-pulse modulation (SRSPM) technique-based interleaved high-frequency three-phase inverter for fuel cell vehicles, IEEE Trans on power electronics, 28, 12, (2013), 5547-5556.

12. Kursun, V., Narenda, S.G., De, V.K. and Friedman, E.G., Analysis of buck converters for on-chip integration with a dual supply voltage microprocessor, IEEE Trans on Very Large Scale Integration (VLSI) Systems, 11, (2003), 514 – 522.

13. Arbetter, B., Erickson, R. and Maksimovic, D., DC-DC converter design for battery-operated systems, IEEE Power Electronics Specialist Conference, 1, (1995), 103 – 109.

14. Chiu, H. J. and Lin, L. W., A bidirectional dc-dc converter for fuel cell electric vehicle driving system, IEEE Trans. Power Electron, 21,4, (2006), 950–958.

15. Lee, Y. S. and Chiu, Y. Y., Zero-current-switched-capacitor bidirectional dc-dcconverter, IEE Proc. Electr. Power Appl,152,3, (2005), 1525–1530.

16. Jiang, L., Zhang, X., Yin, C. L., Mi, C., Li, S. and Zhang, M. Y., A novel soft-switching bidirectional dc-dc converter with coupled inductors, in Proc. IEEE Appl. Power Electron. Conf, (2013),3040–3044.

17. Ahmadi, M., Mohammadi, M. R., Adib, E. and Farzanehfard, H., Family of non-isolated zero current transition bi-directional converters with one auxiliary switch, IET Power Electron, 5, 2, (2012), 158–165.

18. Hsieh, Y. P., Chen, J. F., Yang, L. S., Wu, C. Y. and Liu, W. S., High conversion ratio bidirectional dc-dc converter with coupled inductor, IEEE Trans. Power Electron, 61, 1, (2014), 201–222.

19. Patra, P., Patra, A. and Misra, N., A single inductor multiple output switcher with simultaneous buck, boost, and inverted outputs, IEEE Trans. Power Electron, 27, 4, (2012), 1936–1951.

20. Cho, S. H., Kim, C. S. and Han, S. K., High-efficiency and low-cost tightly regulated dual-output LLC resonant converter, IEEE Trans. Ind. Electron,59, 7, (2012), 2982–2991.

21. Kim, J. K., Choi, S.W. and Moon, G.W., Zero-voltage switching post regulation scheme for multi-output forward converter with synchronous switches, IEEE Trans. Ind. Electron, 58, 6, , (2011), 2378–2386.

22. Nami, A., Zare, F., Ghosh, A. and Blaabjerg, F., Multiple-output DC–DC converters based on diode-clamped converters configuration: Topology and control strategy, IET Power Electron, 3, 2, (2010), 197–208.

23. Babazadeh, V. A., Yousefzadeh., Ramachandran, B., Pao, L., Maksimovic, D. and Alarcon, E., Proximate time optimal digital control for synchronous buck dc-dc converters, IEEE Transaction on Power Electronics, 23, 4, (2008), 2018–2026.

24. Lee, F., Yao, K., Xu, M. and Ye, M., Tapped-inductor buck converter for high-step-down dc-dc conversion, IEEE Transaction on Power Electronics, 20, (2005).

25. Maksimovic, D. and Zhang, X., Multimode digital controller for synchronous buck converters operating Over wide ranges of input voltages and load currents, IEEE Transaction on Power Electronics, 25, 8, (2010), 1958–965.

26. Yao, K., Qiu, Y., Xu, M. and Lee, F., A novel winding coupled buck converter for high-frequency, high-stepdown DC-DC conversion, IEEE Transaction on Power Electronics, 20, (2005), 1017–1024.

27. Mai, Y. Y. and Mok, P., A constant frequency output ripple-voltage-based buck converter without using large esr capacitor, IEEE Trans. Circuits and Systems II, 55, (2008), 748–752.

28. Eguchi, K., Abe, K ., Terada, S., Oota, I., A Single-Input Dual-Output Step-Up/Step-Down DC-DC Converter Designed by Switched Capacitor Techniques, Proceedings of the 3rd International Conference on Industrial Application Engineering , (2015), 201-208.

29. Sabbarapu, B K., Nezamuddin, O., McGinnis, A., Single-Input Multiple-Output (SIMO) Synchronous DC-DC buck converter, IEEE Transaction on Power Electronics, 978, 1, (2016), 5090-0737.

30. D. Kwon, Graduate Student Member, IEEE, and G. A. R. Mora, Senior Member, IEEE,―Single-Inductor–Multiple-Output Switching DC–DC Converters, IEEE transactions on circuits and systems, 56, 8, (2009).

31. dos Santos Jr. E. C., Dual-output DC-DC Buck converters with bidirectional and unidirectional Characteristics, IET Transaction on Power electronics, 6, 5, (2013), 999–1009.

32. Converting Sunlight into Electricity, Kyocera Corporation, retrieved from Kyocera website: http://global.kyocera.com/solarexpo/solar_power/mechanism.html, (2016) .

33. Energy and the Environmenth, The Pennsylvania State University,PEENSTATE website https://www.e-education.psu.edu/earth104/node/950, (2017).

34. Raza, M.Q,. Nadarajah, M. and Ekanayake, C., On recent advances in PV output power forecast, Solar Energy, 136, (2016), 125–144.

35. "Photovoltaics Report". Fraunhofer ISE. 28 July 2014. Archived from the original (PDF) on 31 August (2014).

36. Sumathi, S. et al., Chapter 2 Springer Solar PV and Wind Energy Conversion Systems, Green Energy and Technology, International Publishing Switzerland DOI 10.1007/978-3-319-14941-7_2, (2015).

37. Science 2.0 join the revolution , retrieved from Science 2.0 website: http://www.science20.com/cool_science/blog/albert_einstein_and_solar_panels 156134, (2012).

38. Natarajan, S. P., Basanth, A. J. and Sivakumaran, T. S., Simulation and DSP based implementation of conventional controller for double output elementary LUO converter, in Proceedings, IEEE Power Electronics Systems and Applications, Hong Kong, May 2, 1, (2009), 2599-2606.

39. Pandey, A., Dasgupta, N. and Mukerjee, A., Design Issues in Implementing MPPT for Improved Tracking and Dynamic Performance, IEEE Conference on Industrial Electronics, (2007), Paris 4387-4391.

40. Onat, N., Recent Developments in Maximum Power Point Tracking Technologies for Photovoltaic Systems, International Journal of Photoenergy, 2010, (2010) 1-11.

41. Islam MA., and et al., Maximum power point tracking of photovoltaic arrays in matlab using fuzzy logic controller, Presented at the India conference (INDICON), (2010).

42. Paine, T.O., Maximum Power Point Tracker, National Aeronautics and Space Administration, NASA, Patent US3, 566, 143, (1969).

43. Togneri, M. and Elliott, H., DC to AC and AC to DC converter systems, Patent, US3, (1974), 825-816.

44. Hans, G.M., Solar cell and test circuit, Patent US3, 1967, 350-635.

45. Hartman, J.D., Power-conditioning system, Patent US3, 384, 806, (1968).

46. Louis, A.U., System for detecting and utilizing the maximum available power from solar cells, Patent US3, 696,286, (1972).

47. Wilkerson, A., Power maximization circuit, Patent US4, 200,833, (1980).

48. Baker, R.H., Method of and apparatus for enabling output power of solar panel to be maximized, US, Patent 4,375,662, (1983).

49. Olias, E., Salas, V., Lazaro, A. And Barrado, A., Review of the maximum power point tracking algorithms for stand-alone photovoltaic systems, Solar Energy Materials and Solar Cells, 90, 11, (2006).

50. Tan, C. W., Green, T. C., and Hernandez-Aramburo, C. A., Analysis of Perturb and Observe Maximum Power Point Tracker Algorithm for Photovoltaic Applications, IEEE 2nd International Power and Energy Conference, Johor Bahru, (2008), 237-242.

51. El-Sharkawi, M. A., Fundamentals of Electric Drives, CI-Engineering, 2.Edition, 68-73, (2000).

52. N. Mohan, Power electronics, John Wiley and sons Inc., (2. Edition), 10-5, (1989), 299-354.

53. Mai, Y. Y. and Mok, P., A constant frequency output ripple-voltage-based buck converter without using large ESR capacitor, IEEE Trans. Circuits and Systems II, 55, (2008),748–752.

54. Hauke, B., Basic Calculation of a Buck Converter's Power Stage, TEXAS INSTRUMENTS, (2011)–Revised (2015).

55. Sahin, M.E., Okumuş H.I., Small Signal Analyses and Hardware Implementation of a Buck-Boost Converter, International Conference on Renewable Energy Research and Applications, Madrid, Spain, (2013), 330-335.

56. Product Specification DATASHEET Cosmo Ferrites Ltd, Corre EE 5525; http://www.cosmoferrites.com/Downloads/Downloads/bcb70e7c-ae33-40ec-a881-0d5120db57b6_GTC.pdf, (2016).

57. Butay, D.F., Miller, M.T., Maximum Peak Power Tracker: A Solar Application, A Major Qualifying Project Report, (2008).

58. MAGNETICS ., Design Guides., Inductor Design with Magnetics Ferrite Cores https://www.mag-inc.com/Design/Design-Guides, (2017).

59. McMurray, W., Optimum Snubbers for Power Semiconductors, IEEE Transactions on Industry Applications, (1972), 593- 600.

60. Chen, Y-M., RC Snubber Design using Root-Loci Approach for Synchronous Buck SMPS, A thesis presented to the University of Waterloo in fulfillment of the thesis requirement for the degree of Master of Applied Science in Electrical & Computer Engineering.. Waterloo, Ontario, Canada, (2005).

61. Todd., Snubber Circuits: Theory, Design and Application, Snubber Circuits, Unit Rode Corporation 2-,Texas Instrument (1993).

62. Şahin, M.E. and Okumus, I.H, Small Signal Analyses and Hardware Implementation of a Buck-Boost Converter for Renewable Energy Applications, International Conference on Renewable Energy Research and Applications, Madrid, Spain, October (2013), 20-23.

63. Mohan, N., Converters, Applications, and Design, John Wiley and sons Inc., 2. Edition, (1995), 161-200.

64. Şahin, M.E., Design and Control of Parallel Connected Buck-Boost Converter for Hybrid Energy System, Karadeniz Technical University,Phd thesis, The Graduate school of Natural and Applied Science, Trabzon, (2014).

65. Şahin, M.E., Design an Electrolyses system with DC-DC buck Converter, , Master thesis, GAZI UniversityInstitude of Science and Technology, Ankara, (2006).

66. Leu, Q., Jung, W., Do, T. D., Kim, E. K., Choi, H. H., Adaptive PID Speed Control Design for Permanent Magnet Synchronous Motor Drives, IEEE Transaction on Power Electronics, 30, 2, (2015), 900-908.

67. Balogh, L., Design And Application Guide For High Speed MOSFET Gate Drive Circuits, IET Transaction son Power electronics, 6, 5, (2013), 999–1009.

68. Kalaff, L., How to Implement a MOSFET with a Gate Driver , ECE 480 Team 8, (2014).

69. 6N137 datasheet VISHAY INTERTECHNOLOGY, INC, 2017.

8. APPENDIX

Appendix 1., Isolation print circuit board

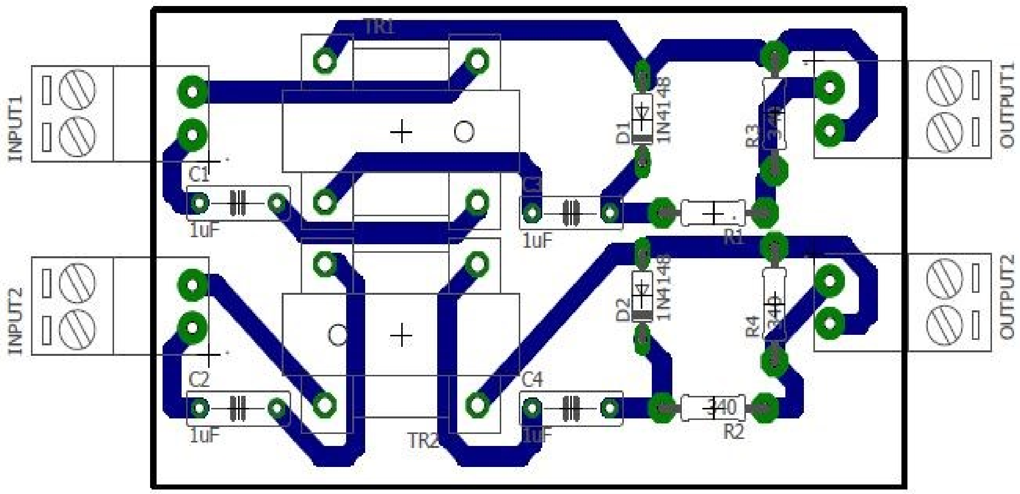

Appendix 2., Logic print circuit board

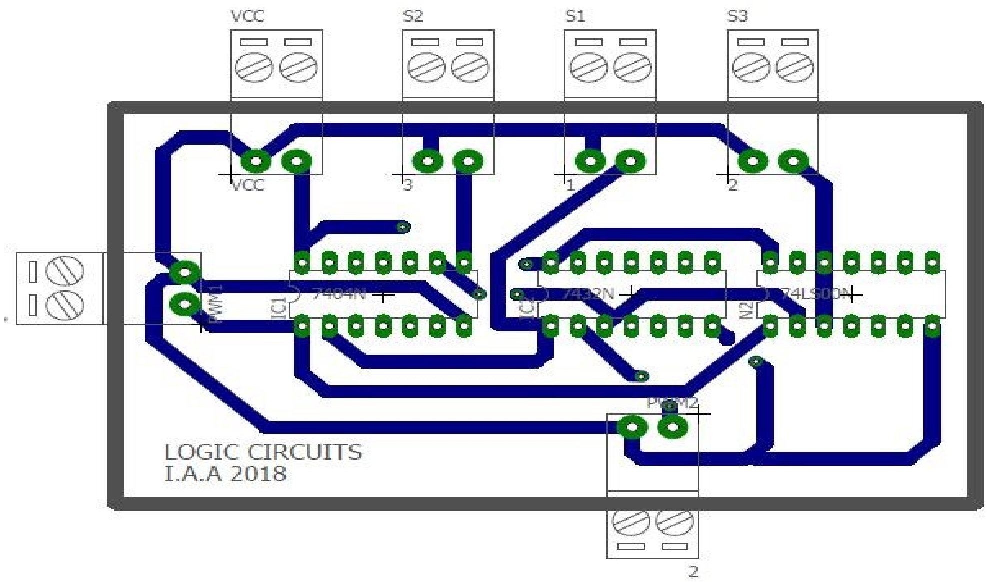

Appendix 3., SIMO converter print circuit board

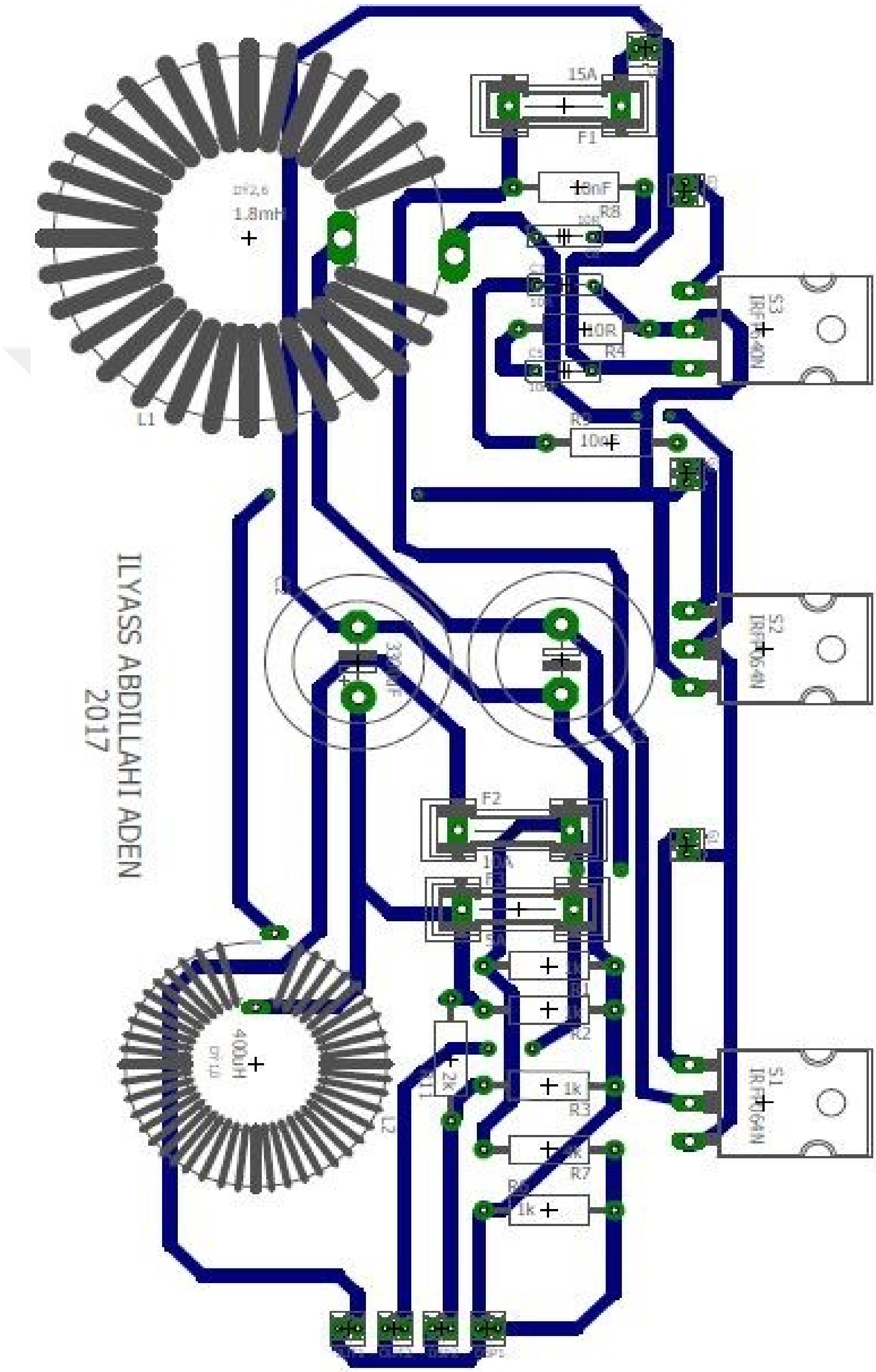

Appendix 4., the MOSFETs drivers print circuit board

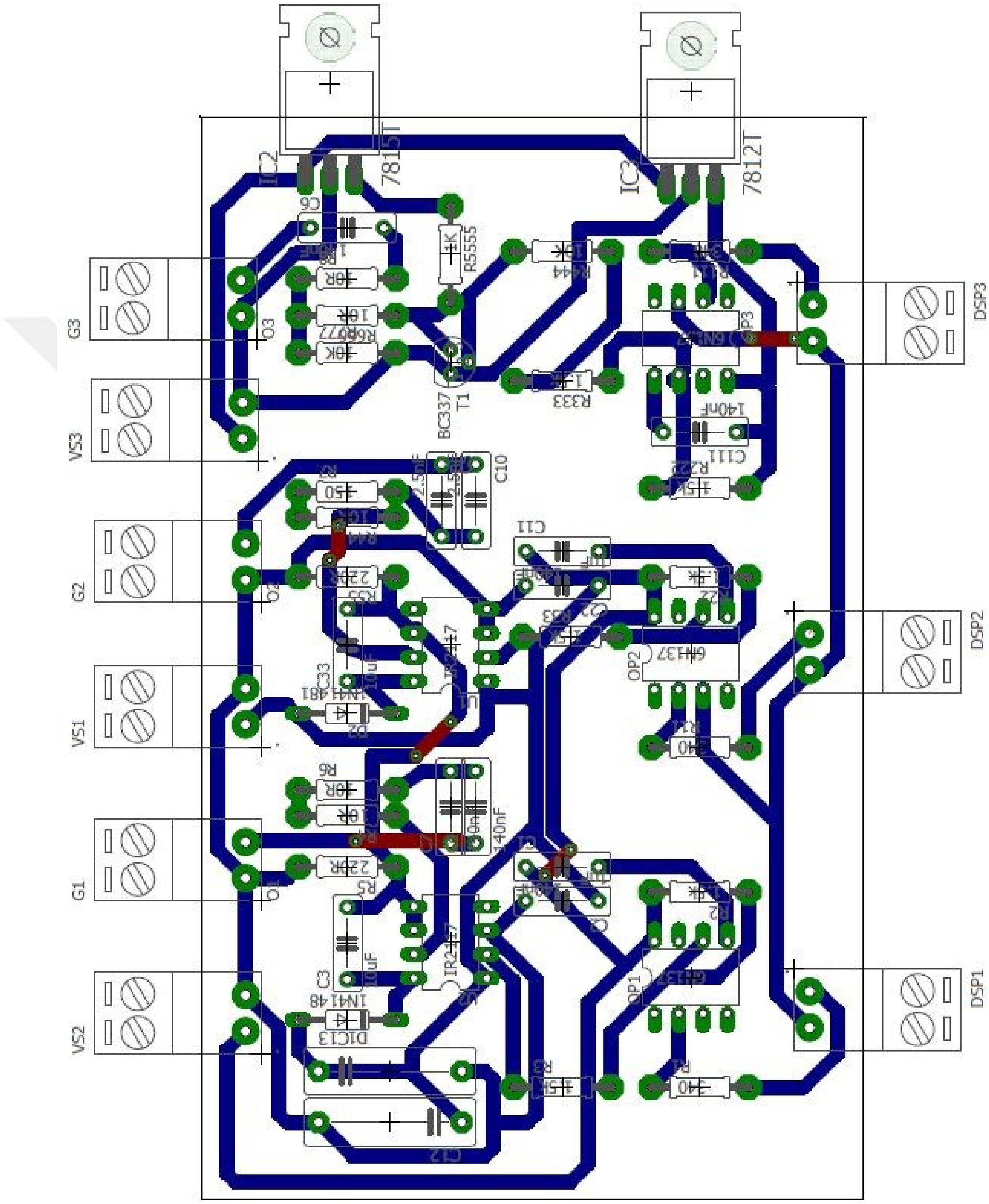

Appendix 5., IR2117 datasheet catalog

International
IOR Rectifier

Data Sheet No. PD60146 Rev O

IR2117(S)/IR2118(S) & (PbF)

SINGLE CHANNEL DRIVER

Features

- Floating channel designed for bootstrap operation
  Fully operational to +600V
  Tolerant to negative transient voltage
  dV/dt immune
- Gate drive supply range from 10 to 20V
- Undervoltage lockout
- CMOS Schmitt-triggered inputs with pull-down
- Output in phase with input (IR2117) or out of phase with input (IR2118)
- Also available LEAD-FREE

Description

The IR2117/IR2118(S) is a high voltage, high speed power MOSFET and IGBT driver. Proprietary HVIC and latch immune CMOS technologies enable ruggedized monolithic construction. The logic input is compatible with standard CMOS outputs. The output driver features a high pulse current buffer stage designed for minimum cross-conduction. The floating channel can be used to drive an N-channel power MOSFET or IGBT in the high or low side configuration which operates up to 600 volts.

Product Summary

V_{OFFSET}	600V max.
I_O+/-	200 mA / 420 mA
V_{OUT}	10 - 20V
$t_{on/off}$ (typ.)	125 & 105 ns

Packages

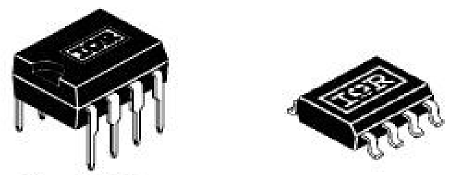

8-Lead PDIP
IR2117/IR2118

8-Lead SOIC
IR2117S/IR2118S

Typical Connection

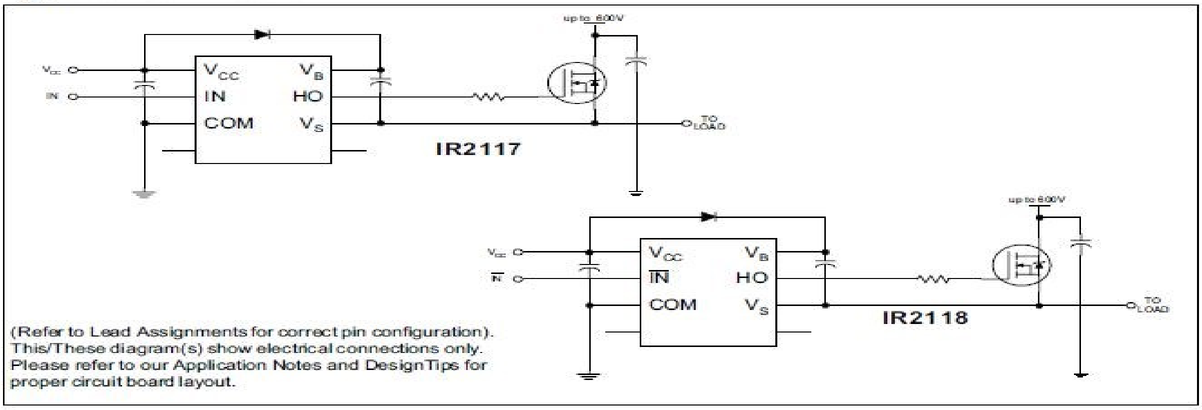

Absolute Maximum Ratings

Absolute maximum ratings indicate sustained limits beyond which damage to the device may occur. All voltage parameters are absolute voltages referenced to COM. The thermal resistance and power dissipation ratings are measured under board mounted and still air conditions. Additional information is shown in Figures 5 through 8.

Symbol	Definition		Min.	Max.	Units
V_B	High side floating supply voltage		-0.3	625	V
V_S	High side floating supply offset voltage		V_B - 25	V_B + 0.3	
V_{HO}	High side floating output voltage		V_S - 0.3	V_B + 0.3	
V_{CC}	Logic supply voltage		-0.3	25	
V_{IN}	Logic input voltage		-0.3	V_{CC} + 0.3	
dV_S/dt	Allowable offset supply voltage transient (figure 2)		—	50	V/ns
P_D	Package power dissipation @ $T_A \leq +25°C$	(8 lead PDIP)	—	1.0	W
		(8 lead SOIC)	—	0.625	
Rth_{JA}	Thermal resistance, junction to ambient	(8 lead PDIP)	—	125	°C/W
		(8 lead SOIC)	—	200	
T_J	Junction temperature		—	150	°C
T_S	Storage temperature		-55	150	
T_L	Lead temperature (soldering, 10 seconds)		—	300	

Recommended Operating Conditions

The input/output logic timing diagram is shown in figure 1. For proper operation the device should be used within the recommended conditions. The V_S offset rating is tested with all supplies biased at 15V differential.

Symbol	Definition	Min.	Max.	Units
V_B	High side floating supply absolute voltage	V_S + 10	V_S + 20	V
V_S	High side floating supply offset voltage	Note 1	600	
V_{HO}	High side floating output voltage	V_S	V_B	
V_{CC}	Logic supply voltage	10	20	
V_{IN}	Logic input voltage	0	V_{CC}	
T_A	Ambient temperature	-40	125	°C

Note 1: Logic operational for V_S of -5 to +600V. Logic state held for V_S of -5V to $-V_{BS}$. (Please refer to the Design Tip DT97-3 for more details).

Dynamic Electrical Characteristics

V_{BIAS} (V_{CC}, V_{BS}) = 15V, C_L = 1000 pF and T_A = 25°C unless otherwise specified. The dynamic electrical characteristics are measured using the test circuit shown in Figure 3.

Symbol	Definition	Min.	Typ.	Max.	Units	Test Conditions
t_{on}	Turn-on propagation delay	—	125	200	ns	V_S = 0V
t_{off}	Turn-off propagation delay	—	105	180		V_S = 600V
t_r	Turn-on rise time	—	80	130		
t_f	Turn-off fall time	—	40	65		

Static Electrical Characteristics

V_{BIAS} (V_{CC}, V_{BS}) = 15V and T_A = 25°C unless otherwise specified. The V_{IN}, V_{TH} and I_{IN} parameters are referenced to COM. The V_O and I_O parameters are referenced to COM and are applicable to the respective output leads: HO or LO.

Symbol	Definition	Min.	Typ.	Max.	Units	Test Conditions
V_{IH}	input voltage - logic "1" (IR2117) logic "0" (IR2118)	9.5	—	—	V	
V_{IL}	Input voltage - logic "0" (IR2117) logic "1" (IR2118)	—	—	6.0		
V_{OH}	High level output voltage, V_{BIAS} - V_O	—	—	100	mV	I_O = 0A
V_{OL}	Low level output voltage, V_O	—	—	100		I_O = 0A
I_{LK}	Offset supply leakage current	—	—	50	µA	V_B = V_S = 600V
I_{QBS}	Quiescent V_{BS} supply current	—	50	240		V_{IN} = 0V or V_{CC}
I_{QCC}	Quiescent V_{CC} Supply Current	—	70	340		V_{IN} = 0V or V_{CC}
I_{IN+}	Logic "1" input bias current (IR2117)	—	20	40		V_{IN} = V_{CC}
	(IR2118)					V_{IN} = 0V
I_{IN-}	Logic "0" input bias current (IR2117)	—	—	1.0		V_{IN} = 0V
	(IR2118)					V_{IN} = V_{CC}
V_{BSUV+}	V_{BS} supply undervoltage positive going threshold	7.6	8.6	9.6	V	
V_{BSUV-}	V_{BS} supply undervoltage negative going threshold	7.2	8.2	9.2		
V_{CCUV+}	V_{CC} supply undervoltage positive going threshold	7.6	8.6	9.6		
V_{CCUV-}	V_{CC} supply undervoltage negative going threshold	7.2	8.2	9.2		
I_{O+}	Output high short circuit pulsed current	200	250	—	mA	V_O = 0V, V_{IN} = Logic "1", PW ≤ 10 µs
I_{O-}	Output low short circuit pulsed current	420	500	—		V_O = 15V, V_{IN} = Logic "0", PW ≤ 10 µs

Functional Block Diagram (IR2117)

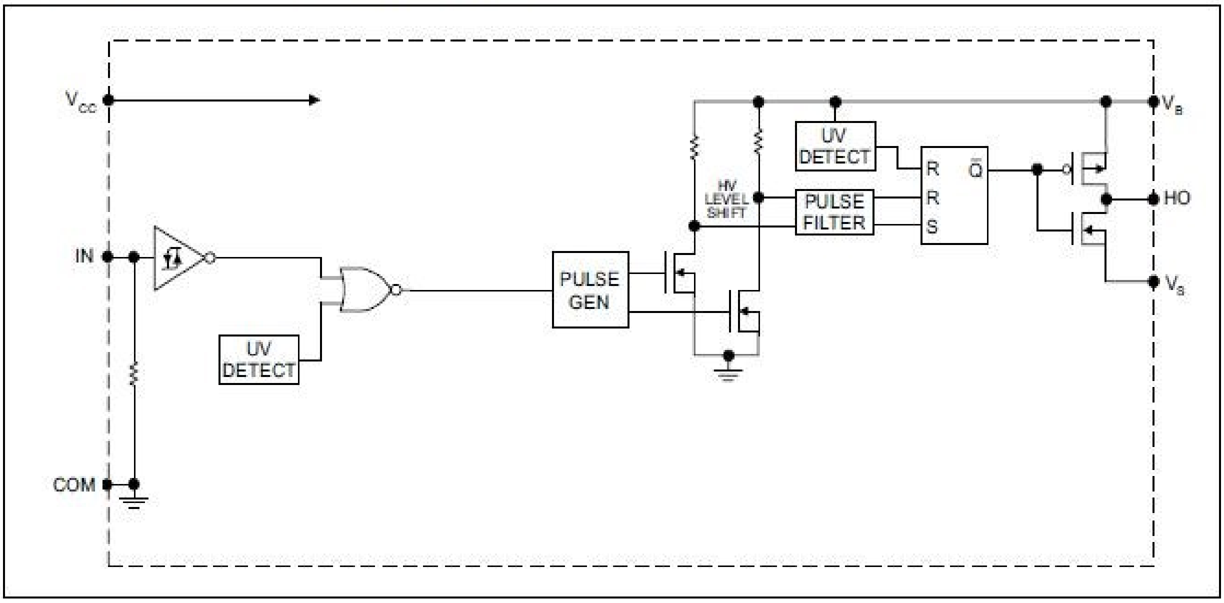

Functional Block Diagram (IR2118)

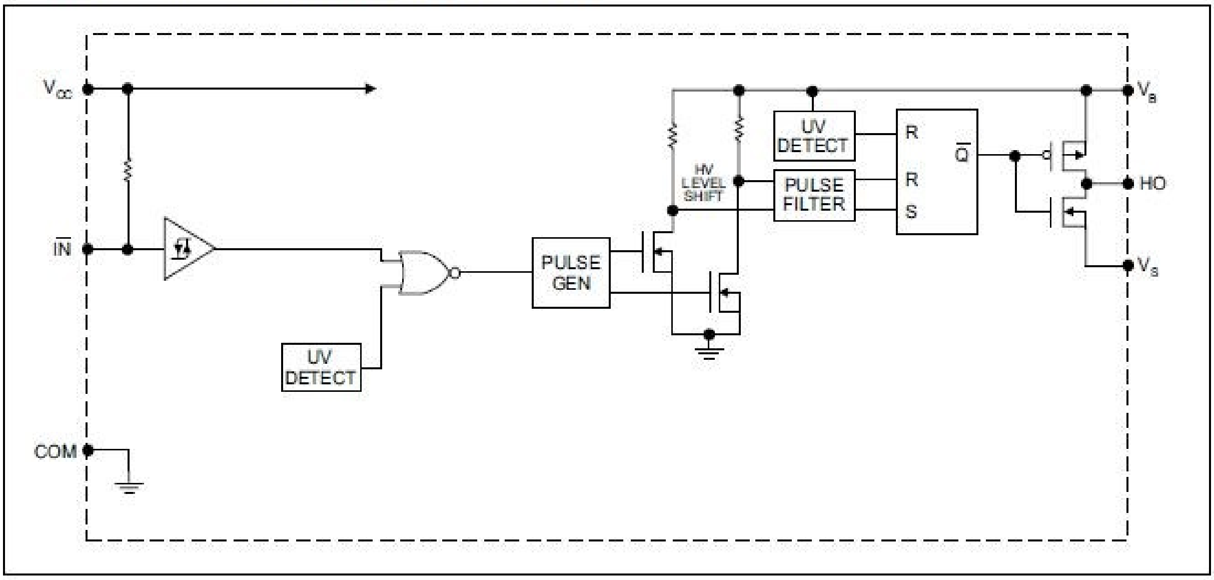

Lead Definitions

Symbol	Description
V_{CC}	Logic and gate drive supply
IN	Logic input for gate driver output (HO), in phase with HO (IR2117)
$\overline{IN}$	Logic input for gate driver output (HO), out of phase with HO (IR2118)
COM	Logic ground
V_B	High side floating supply
HO	High side gate drive output
V_S	High side floating supply return

Lead Assignments

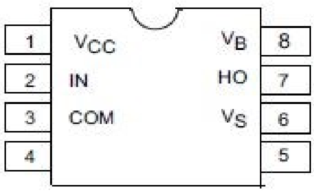

8 Lead PDIP

IR2117

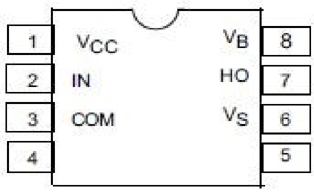

8 Lead SOIC

IR2117S

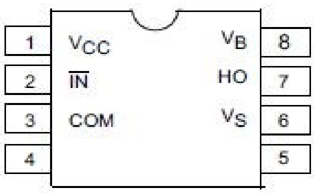

8 Lead PDIP

IR2118

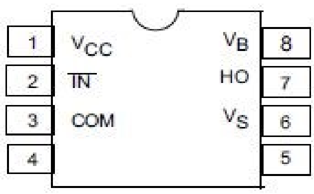

8 Lead SOIC

IR2118S

Appendix 6., 6N137 datas
heet catalog

6N137, VO2601, VO2611, VO2630, VO2631, VO4661

www.vishay.com

Vishay Semiconductors

High Speed Optocoupler, Single and Dual, 10 MBd

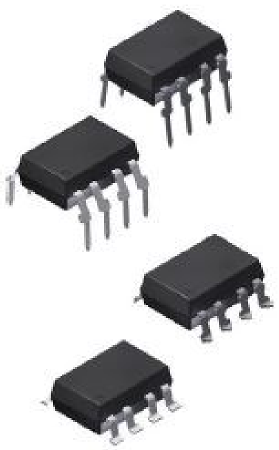

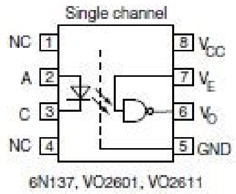

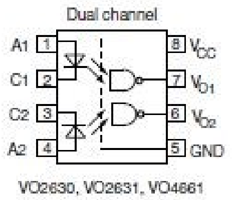

DESCRIPTION

The 6N137, VO2601, and VO2611 are single channel 10 MBd optocouplers utilizing a high efficient input LED coupled with an integrated optical photodiode IC detector. The detector has an open drain NMOS-transistor output, providing less leakage compared to an open collector Schottky clamped transistor output. The VO2630, VO2631, and VO4661 are dual channel 10 MBd optocouplers. For the single channel type, an enable function on pin 7 allows the detector to be strobed. The internal shield provides a guaranteed common mode transient immunity of 5 kV/µs for the VO2601 and VO2631 and 15 kV/µs for the VO2611 and VO4661. The use of a 0.1 µF bypass capacitor connected between pin 5 and 8 is recommended.

FEATURES

- Choice of CMR performance of 15 kV/µs, 5 kV/µs, and 1000 V/µs
- High speed: 10 MBd typical
- +5 V CMOS compatibility
- Pure tin leads
- Guaranteed AC and DC performance over temperature
- Meets IEC 60068-2-42 (SO_2) and IEC 60068-2-43 (H_2S) requirements
- Low input current capability of 5 mA
- Material categorization: for definitions of compliance please see www.vishay.com/doc?99912

RoHS COMPLIANT

APPLICATIONS

- Microprocessor system interface
- PLC, ATE input / output isolation
- Computer peripheral interface
- Digital fieldbus isolation: CC-link, DeviceNet, profibus, SDS
- High speed A/D and D/A conversion
- AC plasma display panel level shifting
- Multiplexed data transmission
- Digital control power supply
- Ground loop elimination, noise isolation

AGENCY APPROVALS

- UL1577
- cUL
- DIN EN 60747-5-5 (VDE 0884-5) available with option 1
- BS EN 60950-1
- CQC GB8898-2011, GB4943.1-2011

ORDERING INFORMATION

V O 2 6 0 1 - X 0 # # T

PART NUMBER — PACKAGE OPTION — TAPE AND REEL

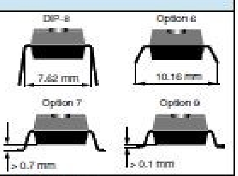

AGENCY CERTIFIED/PACKAGE	CHANNELS 1 CMR (V/µs)			CHANNELS 2 CMR (V/µs)		
BSI, UL, cUL	**1000**	**5000**	**15 000**	**1000**	**5000**	**15 000**
DIP-8	6N137	VO2601	VO2611	VO2630	VO2631	VO4661
DIP-8, 400 mil (option 6)	6N137-X006	VO2601-X006	VO2611-X006	VO2630-X006	VO2631-X006	VO4661-X006
SMD-8 (option 7)	6N137-X007T	VO2601-X007T	VO2611-X007T	VO2630-X007T	VO2631-X007T	VO4661-X007T
SMD-8 (option 9)	6N137-X009T	-	-	VO2630-X009T	-	-
VDE, BSI, UL, cUL	**1000**	**5000**	**15 000**	**1000**	**5000**	**15 000**
DIP-8, 400 mil (option 6)	-	VO2601-X016	VO2611-X016	-	VO2631-X016	-
SMD-8 (option 7)	-	VO2601-X017T	VO2611-X017T	-	VO2631-X017T	-

TRUTH TABLE (positive logic)		
LED	**ENABLE**	**OUTPUT**
On	H	L
Off	H	H
On	L	H
Off	L	H
On	NC	L
Off	NC	H

ABSOLUTE MAXIMUM RATINGS (T_{amb} = 25 °C, unless otherwise specified)				
PARAMETER	**CONDITIONS**	**SYMBOL**	**VALUE**	**UNIT**
INPUT				
Average forward current (single channel)		I_F	20	mA
Average forward current (per channel for dual channel)		I_F	15	mA
Reverse input voltage		V_R	5	V
Enable input voltage		V_E	V_{CC} + 0.5 V	V
Enable input current		I_E	5	mA
Surge current	t = 100 µs	I_{FSM}	200	mA
Output power dissipation (single channel)		P_{diss}	35	mW
Output power dissipation (per channel for dual channel)		P_{diss}	25	mW
OUTPUT				
Supply voltage	1 min maximum	V_{CC}	7	V
Output current		I_O	50	mA
Output voltage		V_O	7	V
Output power dissipation (single channel)		P_{diss}	85	mW
Output power dissipation (per channel for dual channel)		P_{diss}	60	mW
COUPLER				
Storage temperature		T_{stg}	-55 to +150	°C
Operating temperature		T_{amb}	-40 to +100	°C
Lead solder temperature	for 10 s		260	°C
Solder reflow temperature			260	°C

Note

- Stresses in excess of the absolute maximum ratings can cause permanent damage to the device. Functional operation of the device is not implied at these or any other conditions in excess of those given in the operational sections of this document. Exposure to absolute maximum ratings for extended periods of the time can adversely affect reliability.

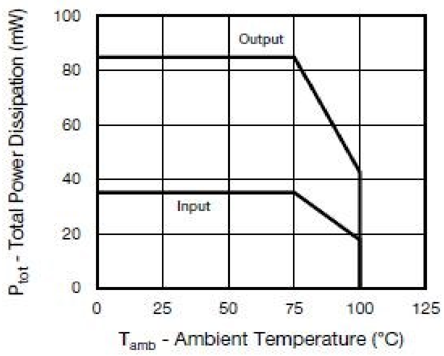

Fig. 1 - Total Power Dissipation vs. Ambient Temperature (single channel)

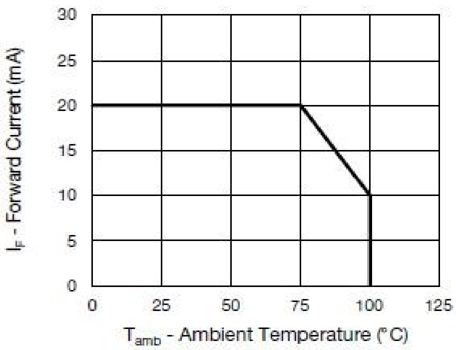

Fig. 3 - Forward Current vs. Ambient Temperature (single channel)

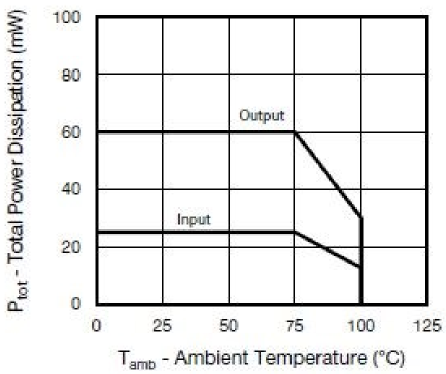

Fig. 2 - Total Power Dissipation vs. Ambient Temperature (dual channel)

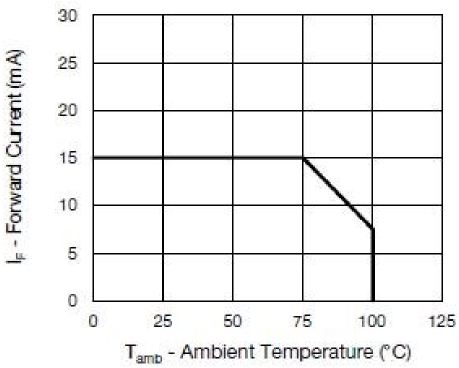

Fig. 4 - Forward Current vs. Ambient Temperature (dual channel)

RECOMMENDED OPERATING CONDITIONS					
PARAMETER	**TEST CONDITION**	**SYMBOL**	**MIN.**	**MAX.**	**UNIT**
Operating temperature		T_{amb}	-40	100	°C
Supply voltage		V_{CC}	4.5	5.5	V
Input current low level		I_{FL}	0	250	µA
Input current high level		I_{FH}	5	15	mA
Logic high enable voltage		V_{EH}	2	V_{CC}	V
Logic low enable voltage		V_{EL}	0	0.8	V
Output pull up resistor		R_L	330	4K	Ω
Fanout	R_L = 1 kΩ	N	-	5	-

ELECTRICAL CHARACTERISTICS (T_{amb} = 25 °C, unless otherwise specified)

PARAMETER	TEST CONDITION	SYMBOL	MIN.	TYP.	MAX.	UNIT
INPUT						
Input forward voltage	I_F = 10 mA	V_F	1.1	1.4	1.7	V
Reverse current	V_R = 5 V	I_R	-	0.01	10	μA
Input capacitance	f = 1 MHz, V_F = 0 V	C_I	-	55	-	pF
OUTPUT						
High level supply current (single channel)	V_E = 0.5 V, I_F = 0 mA	I_{CCH}	-	4.1	7	mA
	V_E = V_{CC}, I_F = 0 mA	I_{CCH}	-	3.3	6	mA
High level supply current (dual channel)	I_F = 0 mA	I_{CCH}	-	6.5	12	mA
Low level supply current (single channel)	V_E = 0.5 V, I_F = 10 mA	I_{CCL}	-	4	7	mA
	V_E = V_{CC}, I_F = 10 mA	I_{CCL}	-	3.3	6	mA
Low level supply current (dual channel)	I_F = 10 mA	I_{CCL}	-	6.5	12	mA
High level output current	V_E = 2 V, V_{CC} = 5.5 V, I_F = 250 μA	I_{OH}	-	0.002	1	μA
Low level output voltage	V_E = 2 V, I_F = 5 mA, I_{OL} (sinking) = 13 mA	V_{OL}	-	0.2	0.6	V
Input threshold current	V_E = 2 V, V_{CC} = 5.5 V, I_{OL} (sinking) = 13 mA	I_{TH}	-	2.4	5	mA
High level enable current	V_E = 2 V	I_{EH}	-	-0.6	-1.6	mA
Low level enable current	V_E = 0.5 V	I_{EL}	-	-0.8	-1.6	mA
High level enable voltage		V_{EH}	2	-	-	V
Low level enable voltage		V_{EL}	-	-	0.8	V

Note

- Minimum and maximum values are testing requirements. Typical values are characteristics of the device and are the result of engineering evaluation. Typical values are for information only and are not part of the testing requirements.

SWITCHING CHARACTERISTICS

PARAMETER	TEST CONDITION	SYMBOL	MIN.	TYP.	MAX.	UNIT
Propagation delay time to high output level	R_L = 350 Ω, C_L = 15 pF	t_{PLH}	20	48	75 (1)	ns
		t_{PLH}	-	-	100	ns
Propagation delay time to low output level	R_L = 350 Ω, C_L = 15 pF	t_{PHL}	25	50	75 (1)	ns
		t_{PHL}	-	-	100	ns
Pulse width disortion	R_L = 350 Ω, C_L = 15 pF	$\|t_{PHL} - t_{PLH}\|$	-	2.9	35	ns
Propagation delay skew	R_L = 350 Ω, C_L = 15 pF	t_{PSK}	-	8	40	ns
Output rise time (10 % to 90 %)	R_L = 350 Ω, C_L = 15 pF	t_r	-	23	-	ns
Output fall time (90 % to 10 %)	R_L = 350 Ω, C_L = 15 pF	t_f	-	7	-	ns
Propagation delay time of enable from V_{EH} to V_{EL}	R_L = 350 Ω, C_L = 15 pF, V_{EL} = 0 V, V_{EH} = 3 V	t_{ELH}	-	12	-	ns
Propagation delay time of enable from V_{EL} to V_{EH}	R_L = 350 Ω, C_L = 15 pF, V_{EL} = 0 V, V_{EH} = 3 V	t_{EHL}	-	11	-	ns

Notes

- Over recommended temperature (T_{amb} = -40 °C to +100 °C), V_{CC} = 5 V, I_F = 7.5 mA unless otherwise specified. All typicals at T_{amb} = 25 °C, V_{CC} = 5 V.

(1) 75 ns applies to the 6N137 only, a JEDEC® registered specification

Appendix 7., MOSFET datasheet catalogue

VISHAY

IRFP064, SiHFP064

Vishay Siliconix

Power MOSFET

PRODUCT SUMMARY		
V_{DS} (V)	60	
$R_{DS(on)}$ (Ω)	V_{GS} = 10 V	0.009
Q_g (Max.) (nC)	190	
Q_{gs} (nC)	55	
Q_{gd} (nC)	90	
Configuration	Single	

TO-247AC

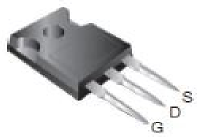

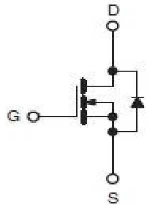

N-Channel MOSFET

FEATURES

- Dynamic dV/dt Rating
- Repetitive Avalanche Rated
- Ultra Low On- Resistance
- Very Low Thermal Resistance
- Isolated Central Mounting Hole
- 175 °C Operating Temperature
- Fast Switching
- Compliant to RoHS Directive 2002/95/EC

Pb Available
RoHS*
COMPLIANT

DESCRIPTION

Third generation Power MOSFETs from Vishay provide the designer with the best combination of fast switching, ruggedized device design, low on-resistance and cost-effectiveness.

The TO-247AC package is preferred for commercial-industrial applications where higher power levels preclude the use of TO-220AB devices. The TO-247AC is similar but superior to the earlier TO-218 package because its isolated mounting hole. It also provides greater creepage distances between pins to meet the requirements of most safety specifications.

ORDERING INFORMATION	
Package	TO-247AC
Lead (Pb)-free	IRFP064PbF
	SiHFP064-E3
SnPb	IRFP064
	SiHFP064

ABSOLUTE MAXIMUM RATINGS (T_C = 25 °C, unless otherwise noted)

PARAMETER			SYMBOL	LIMIT	UNIT
Drain-Source Voltage			V_{DS}	60	V
Gate-Source Voltage			V_{GS}	± 20	
Continuous Drain Current[e]	V_{GS} at 10 V	T_C = 25 °C	I_D	70	A
		T_C = 100 °C		70	
Pulsed Drain Current[a]			I_{DM}	520	
Linear Derating Factor				2.0	W/°C
Single Pulse Avalanche Energy[b]			E_{AS}	1000	mJ
Repetitive Avalanche Current[a]			I_{AR}	70	A
Repetitive Avalanche Energy[a]			E_{AR}	30	mJ
Maximum Power Dissipation	T_C = 25 °C		P_D	300	W
Peak Diode Recovery dV/dt[c]			dV/dt	4.5	V/ns
Operating Junction and Storage Temperature Range			T_J, T_{stg}	- 55 to + 175	°C
Soldering Recommendations (Peak Temperature)[d]	for 10 s			300	
Mounting Torque	6-32 or M3 screw			10	lbf · in
				1.1	N · m

Notes

a. Repetitive rating; pulse width limited by maximum junction temperature (see fig. 11).
b. V_{DD} = 25 V, starting T_J = 25 °C, L = 69 μH, R_g = 25 Ω, I_{AS} = 130 A (see fig. 12).
c. $I_{SD} \le$ 130 A, dI/dt $\le$ 300 A/μs, $V_{DD} \le V_{DS}$, $T_J \le$ 175 °C.
d. 1.6 mm from case.
e. Current limited by the package (die current = 130 A).

* Pb containing terminations are not RoHS compliant, exemptions may apply

IRFP064, SiHFP064

Vishay Siliconix

VISHAY.

THERMAL RESISTANCE RATINGS				
PARAMETER	**SYMBOL**	**TYP.**	**MAX.**	**UNIT**
Maximum Junction-to-Ambient	R_{thJA}	-	40	°C/W
Case-to-Sink, Flat, Greased Surface	R_{thCS}	0.24	-	
Maximum Junction-to-Case (Drain)	R_{thJC}	-	0.50	

SPECIFICATIONS (T_J = 25 °C, unless otherwise noted)						
PARAMETER	**SYMBOL**	**TEST CONDITIONS**	**MIN.**	**TYP.**	**MAX.**	**UNIT**
Static						
Drain-Source Breakdown Voltage	V_{DS}	V_{GS} = 0 V, I_D = 250 µA	60	-	-	V
V_{DS} Temperature Coefficient	$\Delta V_{DS}/T_J$	Reference to 25 °C, I_D = 1 mA	-	0.048	-	V/°C
Gate-Source Threshold Voltage	$V_{GS(th)}$	V_{DS} = V_{GS}, I_D = 250 µA	2.0	-	4.0	V
Gate-Source Leakage	I_{GSS}	V_{GS} = ± 20 V	-	-	± 100	nA
Zero Gate Voltage Drain Current	I_{DSS}	V_{DS} = 60 V, V_{GS} = 0 V	-	-	25	µA
		V_{DS} = 48 V, V_{GS} = 0 V, T_J = 150 °C	-	-	250	
Drain-Source On-State Resistance	$R_{DS(on)}$	V_{GS} = 10 V; I_D = 78 A[b]	-	-	0.009	Ω
Forward Transconductance	g_{fs}	V_{DS} = 25 V, I_D = 78 A[b]	38	-	-	S
Dynamic						
Input Capacitance	C_{iss}	V_{GS} = 0 V, V_{DS} = 25 V, f = 1.0 MHz, see fig. 5	-	7400	-	pF
Output Capacitance	C_{oss}		-	3200	-	
Reverse Transfer Capacitance	C_{rss}		-	540	-	
Total Gate Charge	Q_g	V_{GS} = 10 V; I_D = 130 A, V_{DS} = 48 V, see fig. 6 and 13[b]	-	-	190	nC
Gate-Source Charge	Q_{gs}		-	-	55	
Gate-Drain Charge	Q_{gd}		-	-	90	
Turn-On Delay Time	$t_{d(on)}$	V_{DD} = 30 V, I_D = 130 A, R_g = 4.3 Ω, R_D = 0.22 Ω, see fig. 10[b]	-	21	-	ns
Rise Time	t_r		-	190	-	
Turn-Off Delay Time	$t_{d(off)}$		-	110	-	
Fall Time	t_f		-	190	-	
Internal Drain Inductance	L_D	Between lead, 6 mm (0.25") from package and center of die contact 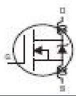	-	5.0	-	nH
Internal Source Inductance	L_S		-	13	-	
Drain-Source Body Diode Characteristics						
Continuous Source-Drain Diode Current	I_S	MOSFET symbol showing the integral reverse p - n junction diode 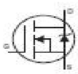	-	-	70[c]	A
Pulsed Diode Forward Current[a]	I_{SM}		-	-	520	
Body Diode Voltage	V_{SD}	T_J = 25 °C, I_S = 130 A, V_{GS} = 0 V[b]	-	-	3.0	V
Body Diode Reverse Recovery Time	t_{rr}	T_J = 25 °C, I_F = 130 A, dI/dt = 100 A/µs[b]	-	160	250	ns
Body Diode Reverse Recovery Charge	Q_{rr}		-	0.9	1.7	µC
Forward Turn-On Time	t_{on}	Intrinsic turn-on time is negligible (turn-on is dominated by L_S and L_D)				

Notes

a. Repetitive rating; pulse width limited by maximum junction temperature (see fig. 11).
b. Pulse width ≤ 300 µs; duty cycle ≤ 2 %.
c. Current limited by the package (die current = 130 A).

CURRICULUM VITAE

Ilyass Abdillahi Aden was born in 1992, DJIBOUTI-DJIBOUTI. He received his University Diploma of Technology in Industrial Engineering and Maintenance, and B.Sc applied in industrial maintenance from University of Djibouti, in 2013 and 2014 respectively. He is currently graduate student pursuing M.Sc. degree in the Department of Electrical and Electronics Engineering in Karadeniz Technical University, Trabzon-TURKEY. In 2014, he got Turkish Government Scholarship and came to Turkey to do Master in Karadeniz Technical University. During his master he has written papers, those are published in Turkey. Mr Ilyass also loves to travel and learn new cultures and languages. He travelled more than 11 countries in Europe and know 5 International languages except his mother tongue. He knows French, English, Turkish, Polish and Arabic. His stay in Turkey brought him a lot of opportunities to know many important persons around the world. During Master he went to Poland achieving Erasmus Scholarship and studied in A.G.H. University of Science and Technology which is one of the most prestigious universities in Europe. He attended International Conferences ICADET in 2017. His research interests include power electronics and renewable energy.